PREPARATION AND CHARACTERIZATION OF CHITOSAN-ALGINATE NANOPARTICLES FOR TRANS-CINNAMALDEHYDE ENTRAPMENT

A Thesis

by

ANDRE STEFANO LOQUERCIO

Submitted to the Office of Graduate and Professional Studies of
Texas A&M University
in partial fulfillment of the requirements for the degree of

MASTER OF SCIENCE

Chair of Committee,	Elena Castell-Perez
Committee Members,	Carmen Gomes
	Matthew Taylor
	Rosana Moreira
Head of Department,	Stephen Searcy

December 2014

Major Subject: Food Science and Technology

ABSTRACT

Trans-cinnamaldehyde incorporated chitosan and alginate nanoparticles were synthesized using the ionic gelation and polyelectrolyte complexation technique. Alginate, chitosan, calcium chloride, and *trans*-cinnamaldehyde at predetermined concentrations were complexed electrostatically to optimize size and loading efficiency (i.e. preliminary study). A final extrapolated methodology using optimized processing parameters (e.g. stirring, homogenization, and equilibration time; droplet size) was developed and utilized for controlled release, morphological, thermal, antioxidant, and antimicrobial studies. The best working alginate to chitosan mass ratio was determined to be 1.5:1 at a pH dispersion of 4.7. Particle size (166.26 nm) and encapsulation efficiency (73.24%) were further optimized at this mass ratio using an alginate:calcium chloride mass ratio of 4.8:1, alginate:*trans*-cinnamaldhyde mass ratio of 37.5:1, 18 gauge syringe needle, stirring times of 90 minutes, 15 minutes of homogenization, and equilibration time of 24 hours. Optimized nanoparticles showed increased shelf life (6 weeks) and translucency in solution. Release tests showed *trans*-cinnamaldehyde release from loaded nanoparticles best followed the bioexponential model; a burst release function (32.5% cumulative release) followed by a sustained release function (62.31% final cumulative release). Differential scanning calorimetry confirmed inclusion of oil into nanoparticles by indirectly comparing thermal stability of free *trans*-cinnamaldehyde with loaded *trans*-cinnamaldehyde in the inclusion complex. Nanoparticles resembled a spherical shell and core type arrangement (i.e. spherical,

distinct, and regular) and were in the size range of 10-100 nm. The final radical scavenging effect of loaded particles in apple juice was 62% and *trans*-cinnamaldehyde was just as available to react in free form as it was in inclusion complexes. Minimum inhibitory concentration values (MIC) for *trans*-cinnamaldehyde loaded nanoparticles was 7,031.25 μg/ml for *Escherichia coli* O157:H7 and 14,062.5 μg/ml for *Listeria monocytogenes*. The concentration of *trans*-cinnamaldehyde in the inclusion complexes corresponded to a MIC of approximately 730 and 1,4062 μg/ml of free *trans*-cinnamaldehyde for *E. coli* O157:H7 and *L. monocytogenes*, respectively. Results indicated that *L. monocytogenes* was more tolerant to the inhibition by *trans*-cinnamaldehyde inclusion complex in comparison to *E. coli* O157:H7. Overall, results suggest that the application of antimicrobial polymeric nanoparticles optimized for essential oil loading in food systems may be effective at inhibiting specific pathogens.

DEDICATION

To my parents, thank you for you love and support.

ACKNOWLEDGEMENTS

I would like to acknowledge the following people for their contributions to my research. Their support and assistance was instrumental to the success of this research project.

I would like to thank my committee chair, Dr. Castell, and my committee members, Dr. Gomes, Dr. Taylor, and Dr. Moreira for their guidance and support throughout the course of this research. Without the instruments and labs they provided me, I would have been unable to pursue and complete this study. I would like to thank Dr. Castell for allowing me the opportunity to work on my master‘s degree under her leadership and supervision. Her guidance and encouragement was essential in my growth as a student, researcher, and man. I would like to thank Dr. Gomes for sharing her expertise in the nanotechnology field and her continuous support in all facets of my academic career. I would like to thank Dr. Taylor for allowing me to use his microbiology lab, thus allowing me to complete my studies in a timely manner. Finally, I would like to thank Dr. Moreira for pushing me to be a better student and researcher through her candor and challenging me in the classroom. Working as a teaching assistant and undergraduate student mentor in the lab, I did my best to emulate these professors and teach with the passion, intelligence, humor, and elegance that they imparted upon me.

Thanks also go to my friends and colleagues and the department faculty and staff for making my time at Texas A&M University a great and unique experience.

Specifically, I want to thank Laura Hill, for her technical contributions to this study. I wish to extend my gratitude to Paulo Silva, Alex Puerta, Basri Omac, Keila Perez, Songsirin Ruengvisesh, and Mustafa Guzel which provided me with the friendly environment and support group to succeed every day.

Finally, thanks to my mother and father for their encouragement and financial contributions and also to my fiancée for her patience and love.

NOMENCLATURE

AG	Aginate
AntiMO	Antimicrobial
ATCC	American Type Culture Collection
CAG	Calcium-alginate
C-A	Chitosan-alginate
CFU	Colony forming unit
CMC	Critical micelle concentration
CS	Chitosan
DLS	Dynamic light scattering
DPPH	1,1-Diphenyl-2-picrylhydrazyl
DSC	Differential scanning calorimetry
EE	Encapsulation efficiency
FW	Formula weight
G	Guluronic acid unit (G block)
GRAS	Generally Recognized As Safe
h	Hour
HCl	Hydrochloric acid
ID	Internal diameter
IG	Ionotropic gelation
IG-PEC	Ionic gelation and polyelectrolyte complexation

In vitro	Taking place outside the living body
In vivo	Taking place in the living body
L	Liter
LCA-NP	*Trans*-cinnamaldehyde loaded chitosan-alginate nanoparticle
kDa	Kilodalton
kV	Kilovolt
M	Mannuronic units (M block) or Molar
mA	Milliamp
MBC	Minimum bactericidal concentration
MIC	Minimum inhibitory concentration
min	Minute
ml	Milliliter
mTorr	Millitorr
N	Normal
NaOH	Sodium hydroxide
nm	Nano-meter
NNI	National Nanotechnology Initiative
NP	Nanoparticle
PBS	Phosphate buffered saline
PEC	Polyelectrolyte complexation
psi	Pounds per square inch
PW	Peptone water

RPM	Rotations per minute
s	Second
SEM	Scanning electron microscopy
TC	*Trans*-cinnamaldehyde
TEM	Transmission electron microscopy
TSA	Tryptic soy agar
TSA-YE	Tryptic soy agar with yeast extract
TSB	Tryptic soy broth
TPB	Tryptose phosphate broth
ULCA-NP	Unloaded chitosan-alginate nanoparticle
UV-Vis	Ultraviolet visible
w/v	Weight/volume
°C	Degree Celsius
°F	Degree Fahrenheit
µg	Microgram
µl	Microliter
µm	Micrometer
µM	Micromolar
2XTSB	Double strength TSB
2XTPB	Double strength TPB

TABLE OF CONTENTS

Page

LIST OF FIGURES

Page

LIST OF TABLES

Page

1. INTRODUCTION

1.1 Background

Nanotechnology has received significant interest in the agricultural, medical, pharmaceutical, and biotechnology sectors in the past two decades. Nanotechnology is best described as the science and technology that has enabled the study of phenomena at the nanometer scale. This includes the design, manipulation, production, characterization, and application of nano-level structures and devices by controlling particle size in the range of 1 to 100 nm (Tiwari and Takhistov 2012).

Analytical tools have become available allowing the field of nanotechnology to develop into a multi-billion dollar industry. Recent technological advances in nanomedicine and nanomaterials in parallel with the food industries ambition to discover new and alternative solutions has created a new sector in the food industry where nanotechnology is emerging as a new solution to quality and safety assurance of foods. Most advances in the field of nano-sized carriers are a result of drug development strategies as well as the desire of pharmaceutical companies to create and patent new drugs (Thies 1996; Pray and Yaktin 2009). Food scientists have adopted the medical concept of targeted drug delivery and are extrapolating these intervention strategies for use in food applications.

Nanotechnology related fields have impacted billions of dollars across the global economy in the past decade, including the United States federal budget calling for $1.8

billion to be invested into the National Nanotechnology Initiative (NNI 2012). The National Nanotechnology Initiative, or NNI, is a central point of communication, cooperation, and collaboration for all federal agencies that participate in nanotechnology research and allows the expertise in this field to be consolidated.

Nanotechnology will provide new ways of controlling and structuring foods with greater functionality and value. Food technology experts have identified the following major applications of nanotechnology in the food industry: improved delivery of micronutrients and bioactive food components, controlled release of bioactive compounds, product traceability, food safety intervention using nanosensors, detection of zoonotic diseases, and development of new packaging materials. Nanomaterials being researched due to their potential food applications include microemulsions and nanoemulsions, solid lipid nanoparticles, nanofibers, liposomes, micelles, and polymeric nanoparticles with entrapment capabilities. These nanosystems are all being utilized to add functionality, nutrient delivery, and increase overall value of food (Anal and Stevens 2005; Mohanraj and Chen 2006; Pray and Yaktin 2009).

Nanoparticles are a form of nanotechnology which can be described as particulate dispersions ranging in size from 10 to 1000 nm and can consist of polymeric materials in which an active substance is dissolved, entrapped, encapsulated, absorbed, or chemically bound to a polymer matrix (Caban and others 2014). The small size of nanoparticles increasingly allows for the ability to cross biological barriers as well as increased cellular uptake and transport (Jong and Borm 2008). Nanoparticles are being developed to advance current food safety interventions and improve food quality. These

systems, when added to a food, can have antimicrobial and antioxidant effects and also improve quality parameters in raw, fresh, or ready to eat foods. Encapsulation can be described as the process of enclosing particles of solids, droplets of liquids, or gasses in an inert shell which in turn isolates and protects them from the external environment (Ghosh 2006). Encapsulation offers the following potential benefits to an active encapsulant: protection from environmental stressors and deteriorative reactions, high processing ability, odor masking, enzyme and microorganism immobilization, specific controlled release, and diffusion mechanisms. Encapsulation systems require a drug or active compound to be released at a rate required for a specified treatment to be effective. Many current nanoencapsulation systems apply biodegradable, biocompatible, and natural polymers (Anal and Stevens 2005). Nanotechnology in combination with encapsulation provides a viable solution to create controlled release systems with desired properties. Depending upon the method of preparation, nanospheres or nanocapsules can be obtained. These polymeric nanoparticles in the scale of 50 to 300 nm have begun to attract much interest in food applications technology and will be emphasized in this research.

A variety of materials have been used to entrap hydrophilic and hydrophobic substances including and not limited to polysaccharides, dendrimers, synthetic and natural polymers, lipids, proteins, and peptides (Ghosh 2006). Naturally occurring polysaccharides such as chitosan and sodium alginate are considered safe for human consumption and have been utilized by pharmaceutical companies for entrapment studies. The distinct advantages of using these polysaccharide matrices are the ability to

control the release of the encapsulated material, prevent encapsulant degradation, and size control (Thwala 2012).

1.2 Problem Statement

The food industry is the largest manufacturing sector in the world; with an annual turnover approximating US $4 trillion (FoodDrinkEurope 2013). However, most of what has been done with nano-sized food materials has occurred in a largely uncontrolled way, and there is still a lot to be learned about the natural nano-structure of foods. Nanotechnology holds tremendous promise to provide benefits not just within food products but also around food products. Nanotechnology can be used to structure new food ingredients and also build new types of packaging, quality detection tools, and other types of measurement and delivery systems (Pray and Yaktin 2009). Food safety and quality are of extreme importance in the food industry. Drug delivery systems offer an innovative approach for the food industry to keep foods safe and assure quality. Although improvements in nanoencapsulation have been significant, minor drawbacks include: low bioavailability, inability to target harmful agents, poor aqueous solubility, side effects of entrapped compound, and compound instability when entrapped (Thwala 2012). The major limitations associated with nanotechnology are the small size leading to gastrointestinal tract uptake which could have potential toxicity concerns, as well as lipophilic and hydrophilic compound‘s poor solubility, and difficulty to be entrapped with hydrophilic systems (Bergin and Witzmann 2013; Jong and Borm 2008). Thus, design flaws accompanied by potential toxicity concerns have been limiting nanoparticle

systems from becoming commercialized. It is important to consider potential toxicity and metabolic effects of nanoparticles *in vitro* and *in vivo*.

Current antioxidant and antimicrobial delivery systems are being developed primarily as large hydrophilic systems. Disadvantages of using polysaccharides in these systems include the poor solubility of active lipophilic compounds. This creates a major barrier for the hydrophobic molecules absorption, bioavailability, and clinical efficacy *in vivo* as well as entrapment *in vitro*. Thus, encapsulating hydrophobic or lipophilic actives is difficult and problematic. Lipophilic active compounds are often prepared in an emulsion with a surfactant to be entrapped in hydrophilic nanosystems. Poor solubility, stability, efficacy, and cost are often the downfall of these systems. The use of surfactants to solubilize oils can cause cloudiness and turbidity which leads to decreased shelf life due to increased volatility and poor stability (Thwala 2012).

Particle size and entrapment efficiency must also be optimized to assemble nanoparticles with highest payload capacity, increased cellular uptake, good mechanical strength, proper permeability and diffusion characteristics, faster drug release, as well as handling ease (Sinjan and Robinson 2003). Proper size and payload will allow for more significant characterization as well as efficacy in antimicrobial and antioxidant applications. Chitosan and alginate nanoparticles final particle size and entrapment efficiency can be improved as concentration dependence on biopolymers relates to particle size (Gupta 2011). Additional processing parameters such as droplet size, and homogenization rate will affect size of chitosan and alginate particle size and entrapment efficiency.

1.3 Justification of Study

Assembling and characterizing *trans*-cinnamaldehyde loaded chitosan-alginate nanoparticles will help pave the way for understanding the advantages and limitations of their potential use in food applications. This understanding will enable more precise manipulation of these molecules for the design of safer, healthier, and tastier food products. Characterization will allow for future optimization of the delivery systems as well as the development of improved taste, color, flavor, and shelf life stability of foods containing nanoparticles.

The development of novel nanoparticulate drug carriers is a main focus of food safety and food quality research. Nanoencapsulation has the potential to limit or inhibit microbial growth and also prevent oxidation in food products. Also, nanoencapsulation can improve the solubility of lipophilic compounds and protect labile molecules from the biological environment. Nanoencapsulation systems include oily drugs in liposomes, dendrimers, micelles, lipophilic and polymeric nanoparticles, cyclodextrins, and hydrogels.

Nanoscale delivery systems are being formulated with biodegradable, biocompatible, safe, non-toxic, naturally occurring and cost effective polymers. Specifically, biopolymers with hydrophilic surfaces have been utilized as building blocks of nanosystems in many studies. Alginate and chitosan are two prime examples of these hydrophilic colloids. Their high availability, low cost, and simplicity of handling makes these polymers unique and attractive choices when choosing nanoparticle building blocks (Sinjan and Robinson 2003). Similar to proteins, peptides,

and polynucleotides, chitosan and alginate work synergistically to protect entrapped active molecules from oxidation and enzymatic degradation. These polymers also help enhance the chemical stability of compounds that are photosensitive or prone to hydrolysis. Chitosan and alginate contain hydroxyl, amino, and carboxyl groups. These chemical groups form non-covalent bonds and allow for bioadhesion which has been shown to help increase the solubility and residence time of lipophilic molecules in a nanoparticulate system (Thwala 2012). Ionic interactions between active drug molecules and matrix materials have been shown to increase drug loading for small molecules (Caban and others 2014; Mohanraj and Chen 2006). Chitosan and alginate are unique in that their chemical and physical properties can be manipulated and enhanced in comparison to bulk materials (Sahoo and Labhasetwar 2003). The surface area to volume ratio of chitosan-alginate nanoparticles allows for formulation improvements of nanosystems (Caban and others 2014). With improved formulations, nanoparticle systems can release lipophilic molecules at their full potential. Thus, it is important to develop a standard formulation method and optimize processing parameters of loaded chitosan-alginate nanoparticles with hydrophobic compounds.

Characterization will allow for optimization of antimicrobial and antioxidant delivery systems as well as the development of improved taste, color, flavor, texture, consistency, shelf life stability, safety, and processability. Ideally, characterizing chitosan-alginate nanoparticles with an entrapped lipophilic compound will assist in future utility in post-processing and food applications such as the stabilization of flavoring agents, inhibitory and bactericidal capabilities, as well as the reduction of

unpleasant odors and tastes due to oxidation. *Trans*-cinnamaldehyde (3-phenylprop-2-enal) is an essential oil with antimicrobial and antioxidant properties that may degrade microbial membranes to cause cell death, but can also scavenge free radicals and prevent oxidation in food products. It is volatile and chemically labile as a result of oxidation, chemical interactions, or volatilization. Characterization will also help determine how well protected *trans*-cinnamaldehyde is when entrapped. Encapsulation of lipophilic compounds into aqueous-soluble nanoparticle systems could provide solutions to several problems in the food industry by improving solubility of active and providing a controlled way to deliver and release drug payload with full potential.

This research is important in determining if it is feasible to entrap lipophilic compounds in hydrophilic systems. Subsequently, this study will also show if the antimicrobial compounds have potential for improving the effectiveness and efficiency of delivery in food systems. Characterization of the system can allow for the understanding of the release mechanisms and the antimicrobial efficiency which could allow food manufactures to design smart food systems for delivery applications. This research is different from previous studies in that two new and unique polymers are used in the fabrication of nanoparticles. *Trans*-cinnamaldehyde was explored as an antimicrobial and antioxidant compounds. No current literature utilizes chitosan and alginate biopolymers with the essential oil *trans*-cinnamaldehyde as a combination for the assembly of a nano-sized food carrier. Additionally, characterization methods used in this study are commonly used methods that are easily repeatable and modifiable for use in future studies. This study is unique in that it improves and optimizes a synthesis

methodology (e.g. processing parameters and design constrains) followed by several characterization studies. Current literature does not attempt to optimize physical characteristics (e.g. size and entrapment efficiency) of particles prior to characterization studies.

1.4 Objectives of Study

This study aimed to explore combinations of alginate and chitosan as an entrapment matrix for the essential oil *trans*-cinnamaldehyde which is poorly soluble in aqueous media. This goal was attained by addressing the following specific objectives:

i. Determine a method to optimally synthesize chitosan-alginate nanoparticles with entrapped trans-cinnamaldehyde using the ionic gelation and polyelectrolyte complexation technique.
ii. Determine the physical and thermal characteristics of fully optimized nanoparticles.
iii. Test the optimized nanoparticle antioxidant activity on apple juice.
iv. Test optimized nanoparticle inhibitory and bactericidal capability on Escherichia coli O157:H7 and Listeria monocytogenes.

2. LITERATURE REVIEW

2.1 Introduction

The development of a working nanoparticle delivery system is crucial to obtain efficacy in food applications. Researchers are currently looking for solutions to entrap poorly soluble drugs, actives, and proteins. The following offers a review of relevant drug delivery systems, synthesis techniques, and characterization assays as well as essential information about the polymers, active compounds, preparation methods, and characterization methods used in this study.

2.2 Nanosystems for Drug Delivery

2.2.1 Polymeric Nanoparticles

Major food grade structural components that can be utilized to construct delivery systems for food applications include lipids, surfactants, and polymers. Polymeric nanoparticles are synthesized by a variety of materials such as proteins, lipids, polysaccharides, and synthetic polymers to obtain nanospheres or nanocapsules. Matrix materials are dependent on the size of nanoparticles required, active encapsulant properties and release profile, surface characteristics, charge, permeability, biodegradability, and toxicity (Mohanraj and Chen 2006). Nanocapsules represent vesicular systems where a drug is entrapped in a cavity surrounded by polymer membrane while nanospheres are solid colloidal particles in which an active can be entrapped, encapsulated, chemically bound, or absorbed by a polymer matrix (Figure 2.1). They have hydrophobic surface characteristics and mucoadhesive properties

(Sinjan and Robinson 2003; Caban and others 2014). Lipophilic compounds can be incorporated into the oily core of nanocapsules or solubilized in nanospheres while hydrophilic compounds can be adsorbed on the surface.

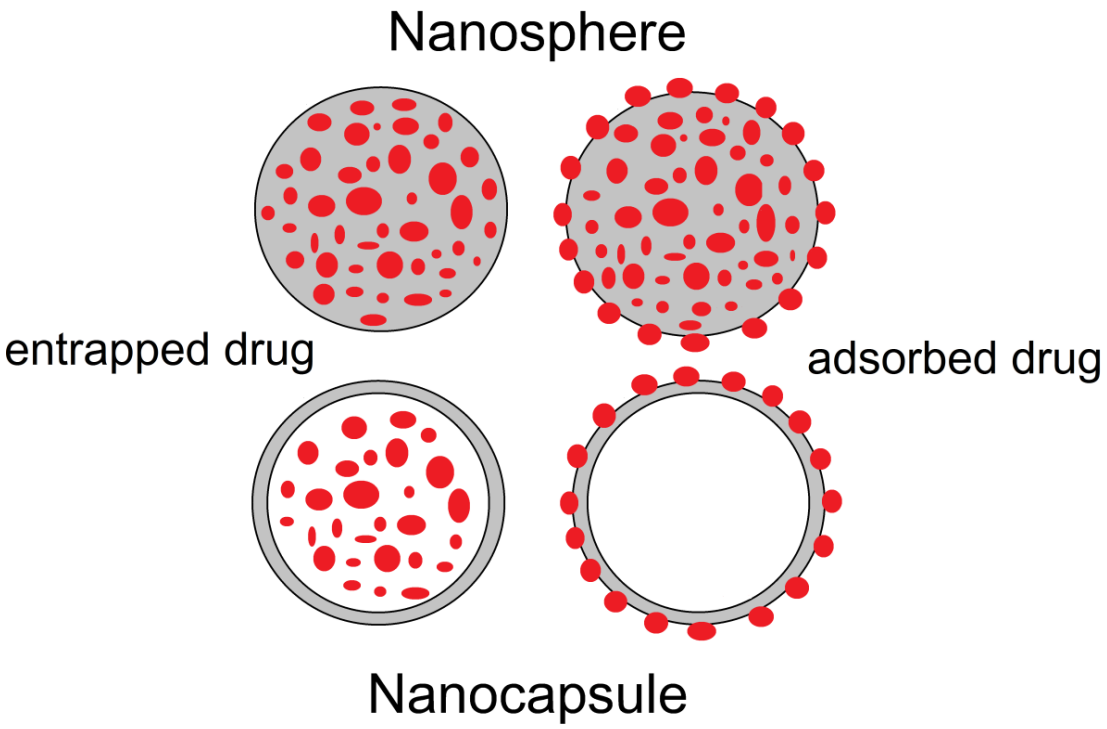

Figure 2.1. Nanospheres versus nanocapsules, entrapped versus adsorbed drug. Adapted from Thwala (2012).

The goals in designing a nanoparticle system are to control particle size, surface properties, and release mechanisms to provide good mechanical strength, minimize average particle size, and maximize active payload capacity. The advantages of

polymeric nanoparticles include small size, sustained drug release, site specific targeting, cheaply fabricated via large quantity and several methods, and engineered for specific functionality. Nanoparticles have high surface to volume ratio which allows control of particle size and surface characteristics, ability to sustain controlled release of encapsulant via pH, ion, biodegradation, and temperature treatments, as well as site specific targeting (Thwala 2012). However, this also leads to limitations such as particle aggregation, difficult handling procedures with potential limited drug loading and burst release (Jong and Borm 2008; Mohanraj and Chen 2006).

The biodegradability that leads to sustained drug release is an advantage over solid lipid nanoparticles and nanosuspensions. In comparison to liposomes, these polymeric nanoparticles are more stable *in vivo* and in storage (Tiwari and Takhistov 2012). However, disadvantages include entrapment capabilities that depend on the products water solubility as well as potential polymer related toxicity, organic residues, and scaling up difficulties (Tiwari and Takhistov 2012; Mohanraj and Chen 2006). Particle aggregation also makes physical handling of nanoparticles difficult in both liquid and dry form (Jawahar and Meyyanathan 2012).

2.2.1.1 Biodegradable Polymers

Polymers containing one or more functional group that have the ability to be hydrolyzed are biodegradable polymers. Examples of biodegradable polymers include biopolymers, polysaccharides, and synthetic polymers. These types of polymers are effective for use in controlled release studies due to their ability to sustain release of active drug molecules (Jawahar and Meyyanathan 2012). Nanoparticles synthesized via

polymers are superior to other delivery vehicles such as liposomes and micelles due to high shelf life stability, storage stability, site specific targeting abilities, reduced mobility leading to less loss of entrapped molecule, and ability to functionalize through coating of particle surface (Thwala 2012).

2.2.1.2 Synthetic Polymers

Polymers that can be constructed and built with specific functionality are considered synthetic polymers. Synthetic polymers can be used to fabricate nanoparticles that can be conjugated with functional groups and ligands to change the functionality of the particle (Ruo 2012). Polyethylene glycol (PEG) is a common example. PEG can be covalently attached to a synthetic polymer. Benefits of attachment include reduced immunogenicity and antigenicity while also increasing the size of the particle. PEGylation allows for increased water solubility of hydrophobic active molecules, increased active stability, reduced toxicity, as well as changing physiochemical properties such as conformation and electrostatic binding ability (Davis 2002).

Synthetic polymers and copolymers examples include poly(cyanoacrylate), poly(lactic acid) (PLA), poly(glycolic acid) (PGA), polycaprolactone (PCL), poly(alkylcyanoacrylate) (PACA), and poly(lactic-co-glycolic acid) (PLGA). Synthetic polymers have the advantage of having high purity and reproducibly over natural polymers. The polyester family which includes PLA, PCL, PLGA, and PGA are of significant interest to the food industry due to their biocompatibility and biodegradability. PLGA has even been approved for human therapy (Anderson and Shive 1997). Limitations of synthetic polymers include scale up difficulties, bulk

erosion, acidic environment within PLGA matrix, hydrophobicity, immune response to foreign bodies, potential toxicity, complicated storage and redispersibility, and high cost (Avgoustakis and Konstantinos 2004).

PLGA and PLA have broad uses in food applications due to their established safety profiles. PLGA has low toxicity, low immunogenicity, good mechanical properties, and predictable biodegradation mechanisms. PLGA was successfully utilized by Gomes and others (2011) to entrap cinnamaldehyde and eugenol for the inhibition of *Salmonella* and *Listeria* (Hill and others 2013b). PLA has been successfully used as an antimicrobial delivery vehicle for Nisin (Abdollahi and Lotfipour 2012). PLA helped to overcome the stability and solubility problems associated with Nisin loading. PCL has been effectively used as a delivery vehicle for antioxidant applications through the encapsulation of α-tocopherol (Byun and others 2011). PLGA nanoparticles have been used in poultry meat systems to deliver benzoic acid and inhibit the growth of *Salmonella* Typhimurium and *Listeria monocytogenes* (Hettiarachchy and Ravichandran 2012).

2.2.1.3 Natural Polymers

Natural polymers are widely used in food grade applications due to their stability, safety, high number of reactive groups, high abundance in nature, and low cost. Their unique characteristics include wide range of molar masses, molecular conformation, varying chemical composition and electropotential, hydrophobicity, and flexibility (Huang and others 2009). Natural polymers used in food delivery applications are proteins, non-ionic polysaccharides, and ionic polysaccharides. Specifically, polymers

such as gelatin, albumin, pectin, starch, chitosan, and sodium alginate have been extensively used to assemble food grade nanoparticles.

Polysaccharides are cost effective, form integral parts of numerous food systems, occur in a wide range of polymeric sizes, and have physical properties such as solubility, melting, and phase change that are advantageous in encapsulation applications (Lakkis 2007). They are stable, safe, non-toxic, and hydrophilic. The ability to control particle size using polysaccharides is advantageous. The size of nanoparticles will change as pH and concentration of solution is changed due to free end groups being available for ionic bonding and particle formation. Lower concentrations yield fewer interactions, thus less particle formation. Gupta and others (2011) found that particle size of a nanosystem is dependent on concentrations of the polysaccharides used.

Ionic polysaccharides can undergo electrostatic interactions which are largely dependent on solution pH conditions (Benita 1998). Also of importance are hydrophobic interactions among food constituents. Hydrophobic interactions allow for non-polar groups to aggregate with other non-polar groups. Hydrophobic interactions can be controlled by altering temperature or changing the polarity of the aqueous solution through the addition of a polar solvent. This is important in entrapment procedures where hydrophobic or lipophilic constituents need to be entrapped (Li and others 2008; McClements 2009). Nanoparticles made from polysaccharides are bioadhesive and can increase the absorbance of loaded drugs as well as improve the dissolution rate of poorly soluble drugs and control their release.

A number of studies have been completed using natural polymers. Animal based polymers such as chitosan, albumin, and gelatin have been used to assemble nanoparticles with the following food applications: enhance mechanical and thermal stability of fruit puree and carboxymethylcellulose films (Martelli and others 2013; de Moura and others 2011), reduce the bacterial count of uncoated psychrophilic bacteria coliform bacteria, and proteolytic bacteria on fish fingers coated with commercial edible coatings (Abdou and others 2012), encapsulate quercetin to improve antioxidant properties for use in manufacturing of functional foods (Marthyna and others 2014), and improve the stability of anthocyanins under neutral conditions (Chen and others 2014). Algal based polymers such as alginate have been used to assemble nanoparticles with the following food applications: encapsulate iron and zinc to be released and enrich ice cream without changing sensory effects (Armoon and others 2013), and encapsulate zinc oxide to have potential antibacterial properties (Bajpai and others 2012). Plant based polymers such as pectin and cellulose have been used in to assemble nanoparticles that can entrap lipids in a core-shell matrix by electrostatic deposition of pectin onto protein aggregates (Santipanichwong and others 2008), entrap hydrophobic zein (Dhanya and others 2012), and entrap ascorbic acid (Liu 2014). Cyclodextrins, or cyclic oligosaccharides enzymatically derived from starch, have been utilized as a delivery vehicle in the entrapment of black pepper oleoresin, and essential oils for antimicrobial applications (Hill and others 2013a; Kamimura and others 2014; Teixeira and others 2013). Cyclodextrins are active carrier materials due to how easily they can form inclusion complexes in solution and in solid state. Within the inclusion complex,

molecules are protected from the hydrophobic environment in the cyclodextrins cavity. This leads to greater delivery potential due to the enhancement of the physical, chemical, and biological properties of entrapped molecule (Thwala 2012). Cyclodextrins can also be combined with polymers to offer enhanced delivery systems.

2.2.2 Liposomes

Liposomes are spherical shaped vesicles produced by phospholipids and cholesterol with size from 30 nm to several microns. An aqueous volume is surrounded by this phospholipid bilayer. Liposome properties are controlled by lipid composition, size, surface charge, and method of preparation. The biocompatibility of liposomes as well as their amphiphilic character and small size make them promising delivery systems. Liposomes are easy to modify, are biodegradable, and encapsulate a wide variety of active molecules with limited toxicity (Tiwari and Takhistov 2012). Liposomes can entrap both hydrophilic and hydrophobic molecules which leave the phospholipid bilayer through diffusion. Limitations of liposomes include interaction with lipoproteins, difficulty encapsulating aqueous ingredients, difficulty improving stability of entrapped active, limited physical stability, aggregation during storage, and lipase degradation destroying the encapsulated material (Thwala 2012). In the food industry liposomes have been used to deliver food flavors, enzymes, and nutrients as well as delivery antimicrobial compounds for protection against spoilage and pathogenic microorganisms (Taylor and others 2005; Mozafari and others 2008). Antimicrobial peptides have been successfully entrapment into liposomes for food application (da Silva Malheiros and others 2010).

2.2.3 Micelles

Micelles are spherical aggregates of surfactant molecules dispersed in liquid colloid. Micelles have unique amphiphilic properties with a core-shell like structure with size of 10 to 100 nm. The inner core of a micelle is hydrophobic and can dissolve lipophilic drugs. The outside of micelles is hydrophilic. Micelles can enhance solubility as well as increase bioavailability of hydrophobic active molecules. Another advantage of using micelles for entrapment of active molecules is the ability to modify the surface in order to improve site specific targeting. Micelles can self-assemble due to large solubility differences in optimal solvent media (Thwala 2012; Ruo 2012).

Encapsulation by micelles is a technique that can enhance the solubility of slightly soluble active molecules. This technique involves the simple entrapment of a hydrophobic active in a hydrophilic shell material thus making the particle soluble in aqueous media. The micelle serves as a nanocontainer that allows active to be released by diffusional processes. Critical micelle concentration (CMC) is the minimum polymer or surfactant concentration required to form a micelle. CMC is unique to micelles in that the lower the CMC, the greater the thermodynamic stability of micelles in solution. However, this can cause limitations in drug delivery such as dose dumping, or the dilution of micelles in solution leading to spontaneous disassembly (Hatefi and Amsden 2002). Micelle use is limited due to physical and thermodynamic stability (Thwala 2012). Micelles have been used in food application to improve antioxidant capacity of curcumnoids via entrapment (Yu and others 2011), enhance solubility of curcumin for

entrapment in beta-casein-micelle nanovehicle (Esmaili and others 2011), and incorporate mustard oil in food-grade micelles (Kirchner and others 2009).

2.2.4 Hydrogels

Hydrogels are hydrophilic structure networks formed chemically or physically through crosslinking of polymer chains with covalent bonds, hydrogen bonds, Van der Waals interaction, and physical entangling. They must be functionalized to improve biodegradability, drug loading capacity, and drug release. Drug molecules can be loaded by their porous structure which is advantageous over polymeric delivery systems which require biocompatible drug to matrix. Hydrogels structure can be controlled through pH and temperature changes. This is often referred to as a stimuli-responsive drug delivery system (Figure 2.2). Hydrogels can also be prepared from the hybrids of a synthetic polymer and a biopolymer, two different biopolymers, or two different synthetic polymers. Advantages include the mimicking of structure and functionality of biological tissue, improved functionality, improved stability, and biodegradability profile (Lin and others 2012). Hydrogel nanoparticles have been used for potential food applications to load curcumin (Dandekar and others 2010) as well as incorporate liposomes for antimicrobial delivery and inhibition of *Staphylococcus aureus* (Gao and others 2014).

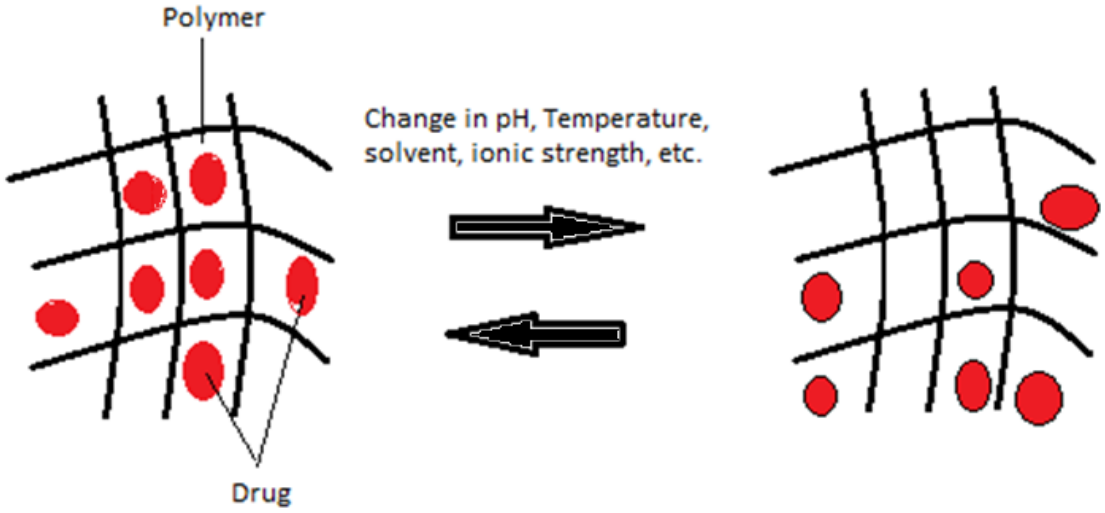

Figure 2.2. Hydrogel formation and stimuli-response for drug entrapment. Adapted from (Thwala 2012).

2.2.5 Dendrimers

Dendrimers are monodisperse symmetric macromolecules with highly branched structures around an inner core. They are three dimensional molecules with low polydisperity and high functionality. Dendrimers are built from a starting atom, or the central core, which in many cases is a nitrogen atom. Carbon or other elements are added to the nitrogen atom through a series of repeating chemical reactions that produce spherical branching structure (Holister and others 2003; Duncan and Izzo 2005) Dendrimers provide a number of advantages compared to other linear polymeric materials including high concentration of active entrapment, easier passage across biological barriers, and internal cavities which can be optimized in order to accommodate large or smaller molecules. Thus, encapsulation capacity can be tailored to

the molecule of interest in a dendrimer system while linear polymeric structures are random and internal cavities cannot be optimized. The ability to customize a dendrimer allows for the nanomaterial to be tailored to exact specifications for a food application and also allows the dendrimer to be ideal carriers for small molecules. This high level of control and the ability to change inner cavity to polar or nonpolar allows for entrapment of hydrophilic and hydrophobic drugs making them an attractive system for drug delivery (Astruc and others 2011). However, limitations of dendrimers include the multi-step chemical synthesis, poor entrapment of large bioactive molecules, and leaking of incorporated compounds from the branch structure (Thwala 2012).

2.2.6 Nanoemulsions

Nanoemulsions are non-toxic lipid droplets in the scale of 50 to 100 nm in continuous phase and fabricated from surfactants that are generally approved for human consumption. Nanoemulsions are synthesized by mixing two immiscible liquids with one of the liquids dispersed as a small spherical droplet in the other (Tiwari and Takhistov 2012). Nanoemulsions are stabilized by surfactants or alcohol. Lipophilic cores are separated from aqueous phase by a monomolecular layer of surfactant thus allowing for nanoencapsulation potential. Nanoemulsions are advantageous for food applications due their broad-spectrum antimicrobial activity against bacteria, fungi, protozoa and spores, as well as its lysing ability. The active ingredient and the high energy are essential for the antimicrobial mechanisms of action. Nanoemulsion particles are thermodynamically driven to fuse with lipid containing organisms. Upon fusion, energy from the emulsion is released into the pathogen with the active ingredient

destabilizing the lipid membrane (He and others 2011). Nanoemulsions are biocompatible, kinetically stable, increase bioavailability of lipophilic components, and can entrap hydrophobic active molecules. On the other hand, limitations include potential toxicity of certain fabrication components during long-term drug dose release, thermodynamic instability, and poor storage stability (McClements and Rao 2011; Tiwari and Takhistov 2012).

Current studies with potential food application include: nanoemulsion fabrication with proteins such as soybean isolate, whey isolate, and ß-lactoglobulin for delivery systems with poorly water-soluble drugs (He and others 2011), and nanoemulsions with basil oil incorporated using surfactants for antibacterial activity against *E. coli* (Ghosh and others 2013). Nanoemulsions fabricated from food-grade ingredients are being increasingly utilized in the food industry to encapsulate, protect, and deliver lipophilic functional components. These include ω-3 fatty acids, conjugated linoleic acid, lipophilic flavors, vitamins, and preservatives (McClements and Rao 2011).

2.2.7 Lipid and Solid Lipid Nanoparticles

Solid lipid nanoparticles consist of spherical particles with size of 10 to 100 nm dispersed in water or in an aqueous surfactant solution. They consist of a lipid core and have the ability to solubilize lipophilic molecules which is a fundamental problem in food nanotechnology (Ruo 2012). These particles are solid at room temperature and are very much like nanoemulsions, differing in lipid nature. Solid lipid nanoparticles are bioavailable, can incorporate lipophilic and hydrophilic molecules, avoid use of organic solvents, control drug release and drug targeting, and can be scaled up allowing for

functionality enhancement, site specific targeting, and low toxicity (Üner and Yener 2007). Solid lipid nanoparticles combine the advantages of lipid emulsion and polymeric nanoparticle systems while overcoming stability issues. Limitations include high pressure induced drug degradation, lipid crystallization, drug incorporation implied localization, coexistence of different lipid modifications and colloidal species, low drug loading capacity, storage stability difficulties, and particle burst concerns. Studies with potential relevance to food application include the solid lipid nanoparticles encapsulation of vitamin D_2 stabilized with Tween 20 (Patel and San Martin-Gonzalez 2012), synthesis of transparent dispersions of milk fat based solid lipid nanoparticles for delivery of beta-carotene bioactive (Zhang 2013). Disadvantages include cost and complexity (Tiwari and Takhistov 2012).

2.2.8 Inorganic Nanoparticles, Carbon Nanotubes, Nanocrystals

Inorganic nanoparticles consist of metal oxide particles or particles that are comprised of at least one metallic composition at the nanoscale. They have small particle size and have been used in drug delivery, controlled release studies, and as nanosensors for microorganism detection (Caban and others 2014; Safari and Zarnegar 2013). Biocompatible materials such as silica, alumina, and titanium have been formulated for ceramic nanoparticles with specific targeting moieties (Ruo 2012). Inorganic nanoparticles are suited for food packaging systems as well as water filtration systems. Inorganic particles in food applications silver nanoparticles have been incorporated in hydroxypropyl methylcellulose for food packaging applications and were antibactericidal against *E. coli* and *Staphylococcus aureus* (de Moura and others 2012).

Titanium dioxide nanoparticles have been used as effective antimicrobials against *Salmonella choleraesuis*, *Vibrio parahaemolyticus*, and *L. monocytogenes* (Kim and others 2003). Silver, gold and copper oxide nanoparticles have shown considerable antimicrobial activity against Gram negative bacteria as well as microbial detection and screening (Duncan 2011).

Carbon nanotubes are cylindrical carbon nanostructures with the size of approximately 1 to 50 nm. They have great mechanical strength, electrical, and surface properties. The advantage of using carbon nanotubes is the ability to functionalize and facilitate transmembrane penetration. Although carbon nanotubes can be used in drug delivery, their need to be functionalized and potential cytotoxicity create problems when being applied to food applications. Carbon nanotubes are currently being utilized in nanosensor applications. They have been shown to detect staphylococcal enterotoxin B, cholera toxin, and bind to the surface of the cyanobacteria toxin Microcystin-LR (Duncan 2011).

Nanocrystals are nanoparticles aggregates composed of atoms in a single or poly-crystalline arrangement synthesized via nanosuspensions. They are drug powder dispersed in aqueous surfactant solution. Nanocrystals are capable of entrapping poorly soluble drugs, increasing bioavailability, and improving solubility of hydrophobic active molecules (Tiwari and Takhistov 2012). Nanocrystals have been shown to be useful in rapid microorganism detection as fluorescent tags of *E. coli* (Duncan 2011).

2.3 Nanoparticle Synthesis Methodologies

Production of nanoparticles has been limited by the difficulties and complexities of preparation methods. Conventional approaches used to prepare nanoparticles have noteworthy disadvantages including: relative high cost, long synthesis time, scaling up difficulties; unknown toxicity of solvents and reagents used for fabrication; rigorous processing such as interfacial polymerization, high torque mechanical shearing, and homogenization which may be damaging to entrapped molecules; inability to easily reproduce stable particles; and low encapsulation efficiency of many types of drugs.

Various materials and methods have been utilized for nanoencapsulation purposes, as no individual encapsulation method is adaptable to all product applications or core materials (Table 2.1 and Table 2.2). Different nanoparticle preparation methods will result in particles of different size, shape, and morphology. Selection of the proper technique is based on the physical and chemical properties of the wall and core materials, as well as the desired functional properties of the nanoparticles. Nanoparticles with electrostatic potential are prepared most frequently by three methods: dispersion of preformed polymers, polymerization of monomers, and ionic gelation complex coacervation of hydrophilic polymers (Mohanraj and Chen 2006). Methods of preparing polymeric nanoparticles generally includes two main steps; the preparation of an emulsification system followed by the precipitation or gelation of the polymer or copolymers (Thwala 2012). Ionic gelation followed by polyelectrolyte complexation (IG-PEC) of hydrophilic polymers was utilized in this research. The goal of this method is to form polyelectrolyte complexes by interactions of molecules that carry oppositely

charged ionizable groups. This method was chosen over emulsion evaporation methods due to its simplicity, reproducibility, and mild nature. Additionally, crosslinking by electrostatic interactions avoids toxicity that would otherwise result from chemical bonding. The emulsion cross linking method has several drawbacks which include overall tedious procedures and harsh cross linking agents which can induce chemical reactions with active agents. Additionally, complete removal of the unreacted cross linking agent can also be difficult (Agnihotri and others 2004).

The ionotropic gelation method should develop stable, nontoxic complexes of ionic cross linked chitosan-alginate nanoparticles. One of the key factors in encapsulating *trans*-cinnamaldehyde in a chitosan-alginate matrix is the hydrophobicity of *trans*-cinnamaldehyde. The ionotropic gelation technique can help overcome this obstacle (Thwala 2012; Li and others 2008).

Table 2.1. Polymeric nanoparticles: Advantages and Limitations of Preparation Methods. Adapted from Pinto Reis and others (2006).

Method	Simplicity of Procedure	Need for Purification	Facility Scaling-up	EE (%)	Compound Safety
Polymerization of monomers	-	-	-	-	-
Emulsion polymerization	-	-	-	-	-
Organic	Low	High	-	Low	Low
Aqueous	High	High	High	High	Medium
Interfacial Polymerization	Low	High	Medium	High	Low
Preformed Polymers	-	-	-	-	-
Synthetic	-	-	-	-	-
Emulsification Evaporation	High	Low	Low	Medium	Medium
Solvent Displacement	High	-	-	High	Medium
Salting Out	High	High	High	High	Low
Solvent Diffusion	Medium	Medium	High	High	Medium
Preformed Polymers	-	-	-	-	-
Natural	-	-	-	-	-
Albumin	NR	High	-	Medium	Low
Gelation	NR	High	-	Medium	Low
Alginate	High	Medium	High	High	High
Chitosan	High	Medium	High	High	High
Agarose	Medium	High	-	-	High
Preformed Polymers	-	-	-	-	-
Desolvation	-	High	-	Low	Low

Table 2.2. Examples of Preparative Methods, Polymers, and Encapsulants. Adapted from Pinto Reis and others (2006).

Polymer	Encapsulant	Size [nm]
Interfacial polycondensation	α-Tocopherol	< 500
Solvent Evaporation	-	-
Poly(lactic acid)	Albumin	100 or 120
Poly(lactic acid)-poly(glycolic acid) copolymer	Cyclosporin A	~300
Solvent Displacement	-	-
Poly(lactic acid)-poly(glycolic acid) copolymer	Doxorubicin	274
	Insulin	~105-170
Poly(lactic acid)	Vitamin K	~270
Interfacial Deposition	-	-
Poly(lactic acid)	Indomethacin	230
Salting Out	-	-
Poly(lactic acid)	Savoxepin	<1000
Emulsion/Solvent Diffusion	-	-
Poly(lactic acid)-poly(glycolic acid) copolymer	Doxorubicin	<1000
Poly(lactic acid)	DNA	<300
Nanoparticles Produced From Natural Macromolecules	-	-
Serum Albumin	Doxorubicin	200-1500
Gelatin	Mitomycin C	280
Polysaccharides	Oligonucleotides	<1000
	Insulin	<1000
	Doxorubicin	<1000

2.3.1 Ionotropic Gelation Polyelectrolyte Complexation

Ionotropic gelation (IG) is based on the ability of polyelectrolytes to cross link in the presence of counterions to form hydrogels or spherical particles that can undergo precipitation. Polysaccharides are first dissolved in weak acidic solutions to form ionic solutions. An anionic solution is cross-linked with a counterion (e.g. calcium chloride) to form a hydrogel (IG step). Polyelectrolyte complexation (PEC) consists of dropping an aqueous solution of polyvalent cations into a drug loaded anionic polymeric solution (i.e. hydrogel) to form PEC. The cations will diffuse into the drug-loaded polymeric drops forming lattice structures of ionically cross linked moieties (Berger and others 2004). This is the stage of fabrication where nanoparticles are formed (Figure 2.3)

Ionotropic gelation and polyelectrolyte complexation (IG-PEC) should develop stable, nontoxic complexes of ionic cross linked chitosan-alginate with entrapped *trans*-cinnamaldehyde (TC). Ideally, a calcium-alginate core will be bounded by a membrane which itself is surrounded by a complexed layer of precipitated chitosan.

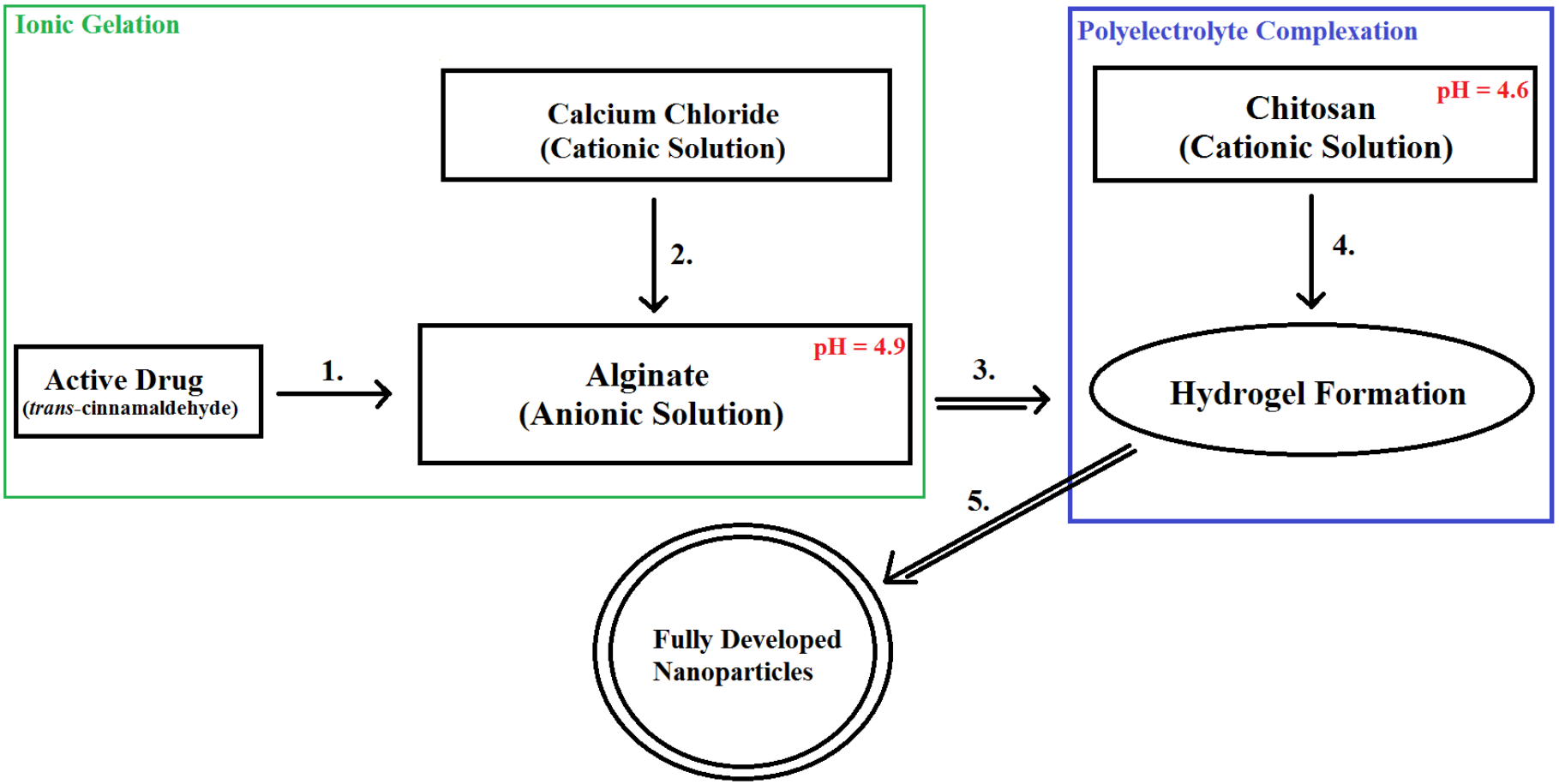

Figure 2.3. Schematic representation of the ionic gelation and polyelectrolyte complexation method.

2.3.1.1 Ionotropic Gelation (IG)

There are two IG methods, external and internal. In external IG, the cross linking cation is positioned externally while in the internal IG method the cross linking cation is incorporated within the polymer solution (Figure 2.4). External cross-linking produces nanoparticles with greater matrix strength, encapsulation efficiency, and slower active release (Ahirrao and others 2013, Ruo 2012). The quality and mechanical strength of hydrogel beads prepared by ionotropic gelation method can be improved by PEC technique (Patil and others 2012). For instance, addition of polycations to the IG pre-gel allows a membrane of polyelectrolyte complex to form on the surface of alginate beads (Patil and others 2010).

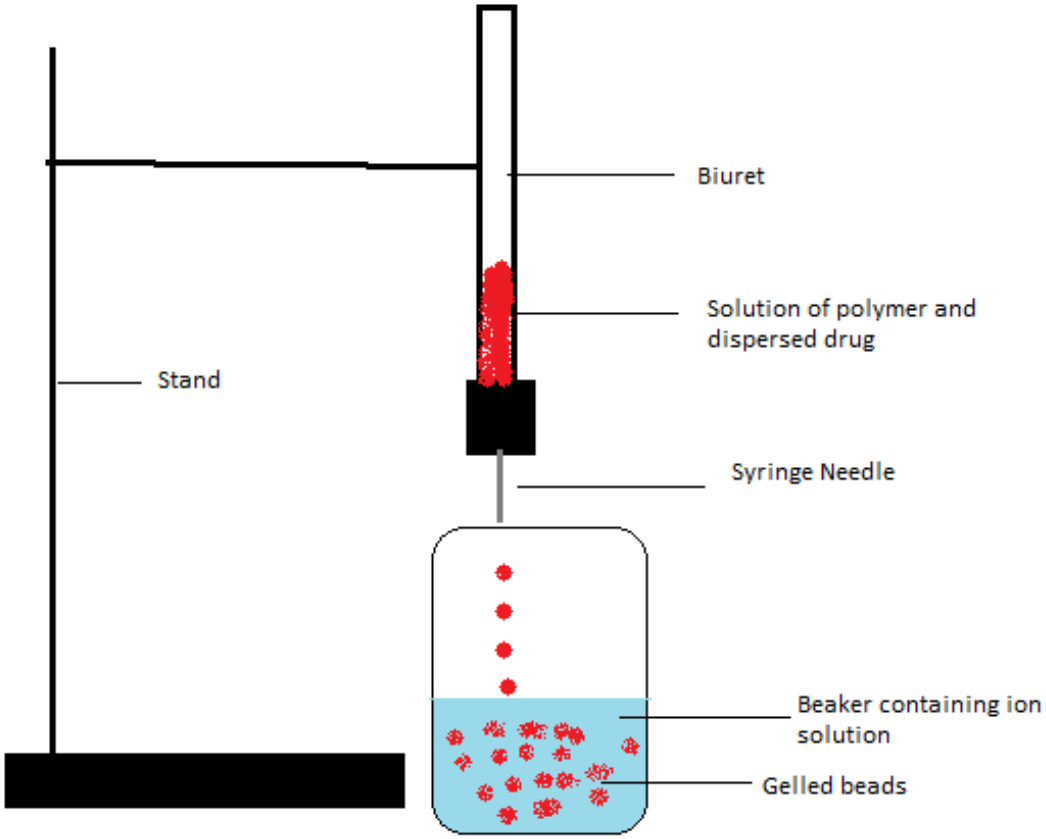

Figure 2.4. External Ionotropic Gelation Technique. Adapted from Ahirrao and others (2013).

2.3.1.2 Polyelectrolyte Complexation (PEC)

The driving force of PEC is the strong electrostatic interactions between oppositely charged polyelectrolytes which leads to inter-polymer ionic condensation and formation of aggregates in the nanosized range called nanospheres (Challa and others 2005). PEC is due to the carboxyl residues of alginate and the amino groups of chitosan ionically interacting (Figure 2.5 (a) and Figure 2.5 (b)). PEC reduces porosity of alginate beads and decrease leakage of encapsulated drug (Thwala 2012).

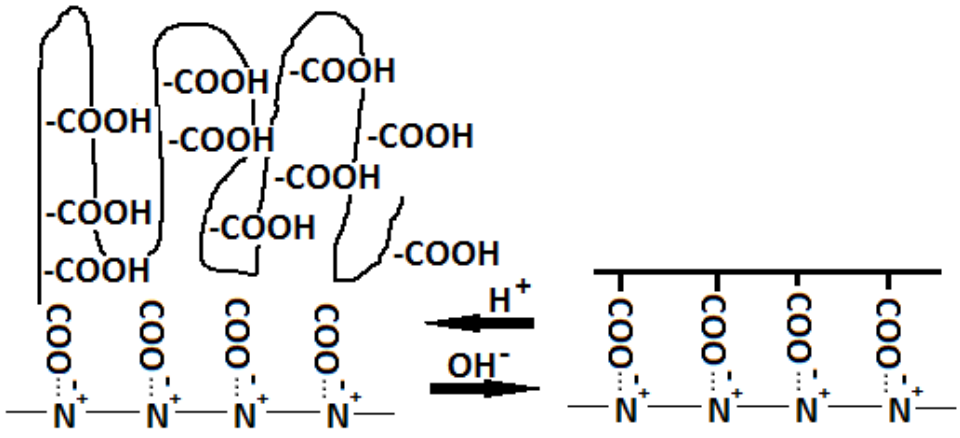

Figure 2.5 (a). Representation of oppositely charged poly-ions interacting to form a PEC. Adapted from Thwala (2012).

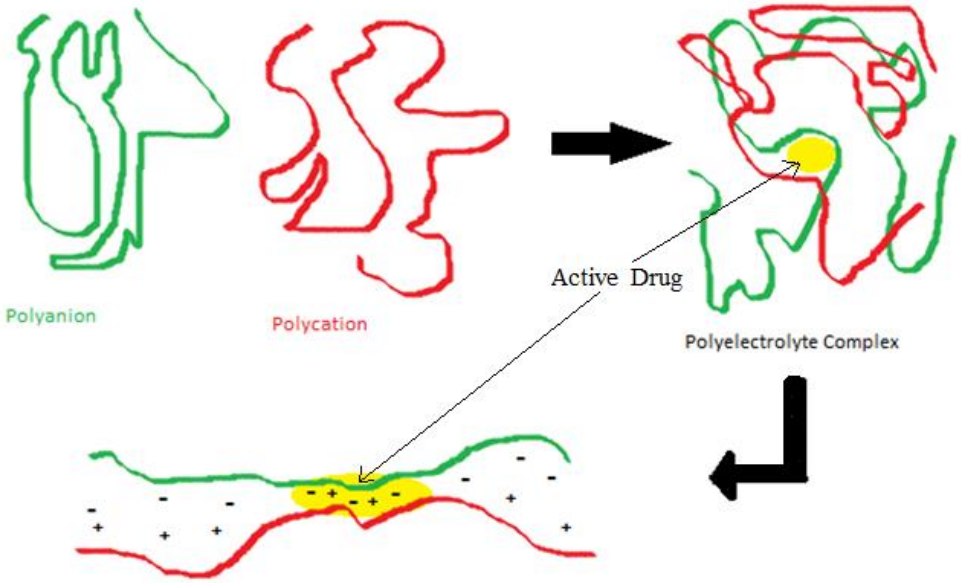

Figure 2.5 (b). Additional representation of PEC formation. Adapted from Thwala (2012).

2.3.1.3 Application to Research

IG-PEC is a two stage procedure. The first stage is the preparation of calcium-alginate pre-gel via ionotropic gelation followed by cross linking with CS via PEC. In the first stage polyguluronate units of alginate molecules form a chelated structure with the cation calcium chloride thus packing into spherical structures. Calcium ions have unequal affinity for the guluronic (G) and mannuronic units (M) of alginate and will form an egg box structure (Figure 2.6) with the repeating G units of alginate. Any additional calcium ions will interact with unreacted G and M acid residues forming a stacked calcium-alginate complex in a planar two dimensional manner (Sinjan and Robinson 2003). Upon stacking of G groups, the alginate chains will dimerize with other chains and form a gel network. The ability of alginates G acid residues to complex with divalent ions such as calcium allows the pre-gel to form (Racovita and others 2009). Continuous stirring of this state results in formation of a pre-gel and avoids the gelling point (Leonard and others 2004; Sarmento and others 2006).

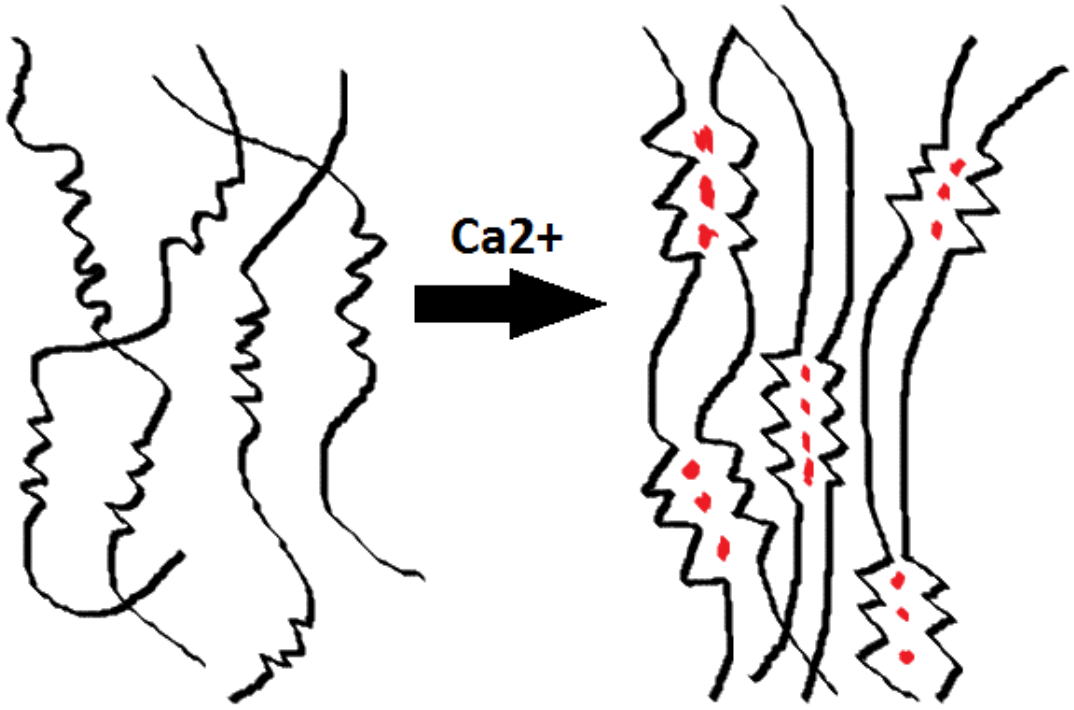

Figure 2.6. Egg-box structure of an alginate gel formed by chelating of calcium chloride ions. GG blocks represented by zig-zag portions and MM and MG blocks represented by smooth parts of polymer chains. Adapted from Thwala (2012).

The second stage of the process is PEC. This is the addition of aqueous chitosan solution. Upon chitosan addition the pre-gel is stabilized and PEC is formed into sponge like particles. A nanoparticle matrix is created with a core composed of complexed calcium-alginate segments while any unreacted polymer in the PEC are segregated in the outer shell. This increases colloidal stabilization of particles thus reducing potential coagulation and aggregation (Leonard and others 2004; Thwala 2012). Under acidic

conditions the ionizable amino group in chitosan molecules are protonated and have affinity for the deprotonated carbonyl groups of alginate. Thus, carbonyl residues of alginate undergo ionic interactions with the amino groups of chitosan to form nanoparticles. Essentially, chitosan stabilizes the calcium-algiante pre-gel nucleus into individual sponge-like nanoparticles.

2.3.2 Emulsification-Solvent Evaporation

Emulsification evaporation is the process where polymer solutions are dissolved in volatile solvents and emulsions are formulated with a stabilizer. Emulsions are formulated with polymer solutions prepared in volatile solvents such as dichloromethane, chloroform, and ethyl acetate. The evaporation of the polymer solvent through diffusion of the continuous phase converts the emulsion into a nanoparticle suspension under vacuum (Thwala 2012). Emulsions can be prepared via single-emulsions or double emulsions and utilize homogenization, ultrasonication, and solvent evaporation. Thus, each emulsion droplet forms one polymer particle when the solvent is removed. The advantages of this technique include the obtaining of small nanoparticles with high encapsulation efficiency, reproducibility, and incorporation of lipophilic active molecules. Limitations include the use of ultrasonication which can induce chemical reactions, scaling difficulties, and harsh solvent use (Nagavarma and others 2012).

2.3.3 Emulsification-Solvent Diffusion

Emulsification diffusion is similar to emulsification evaporation with the caveat that extraction of the polymer solvent from the emulsion occurs in milliseconds leading

to nanoparticles. The encapsulating polymer is partially dissolved in a water soluble solvent and saturated with water to ensure thermodynamic equilibrium. This organic phase is then emulsified in an aqueous solution containing a stabilizer leading to solvent diffusion to the external phase thus forming nanoparticles (Nagavarma and others 2012). The solvent is then eliminated through evaporation or filtration. Nanoparticles are formed because of a physicochemical instability produced by solvent transport. The diffusion of the solvent carries molecules into the aqueous phase from supersaturated regions where new polymer aggregates form. Once stabilized, nanoparticles are formed following diffusion of the solvent. The advantages of this technique include high encapsulation efficiencies, no homogenization, reproducibility, ease of scaling up, simplicity, and narrow size distribution. Limitations include high volumes of water to be eliminated from the suspension, leakage of water-soluble molecules into the saturated-aqueous external phase, and the process cannot be freeze-dried because of the presence of residual benzyl alcohol (Mohanraj and Chen 2006; Pinto Reis and others 2006).

2.3.4 Complex Coacervation

Coacervates from complex coacervation are formed as a result of electrostatic interactions between two aqueous phases whereas ionic gelation involves the material undergoing transition from liquid to gel due to ionic interactions at room temperature (Nagavarma and others 2012). Complex coacervation is a liquid/liquid phase separation that occurs when two oppositely charged polyelectrolytes are mixed under suitable conditions forming enclosed solid particles. Thus, PEC is formed. In complex coacervation two liquid phases are formed which include the coacervate phase and the

supernatant phase. The coacervate phase is the phase where the capsule forms. Capsules or particles are often held together by hydrophobic forces. The supernatant phase is a dilute polymer solution that acts as the continuous phase where capsule formation occurs. Core materials that are suitable for complex coacervation include water-insoluble actives that will not dissolve in the aqueous phase. Coacervation offers high payload potential and is versatile and adaptable (Astete and others 2009; Nagavarma and others 2012).

2.3.5 Salting Out

Salting out is a technique based on the separation of a water-miscible solvents from an aqueous solution. The salting out procedure can be considered a modification of the emulsification evaporation and diffusion processes. Acetone is commonly chosen as the water-miscible solvent due to its solubilizing properties and its separation from aqueous solutions by salting out with electrolytes. The encapsulating polymer and the active drug are dissolved in acetone and emulsified in aqueous gel containing a salting agent and a colloidal stabilizer (Nagavarma and others 2012). Electrolyte salting agents include magnesium acetate or magnesium chloride. The selection of the salting out agent is important due to the effect on encapsulation efficiency of the drug. The emulsion is then diluted with sufficient water increasing the diffusion of acetone into the aqueous phase. The diffusion of acetone from the droplets is the most important step. This diffusion, which takes place on dilution with excess water, can generate interfacial turbulence leading to polymer aggregation in the form of nanoparticles. This signifies the formation of nanoparticles. The solvent and salting out agent can then be eliminated.

Advantages of salting out include high incorporation of drug, high yield, protection of heat susceptible molecules, and ease of scaling up for industrial manufacturing. Limitations of this technique are that it is limited to lipophilic drugs, high processing times, extensive purification to remove salting agents, and potential salting without precipitation (Rodriguez and others 2004; Nagavarma and others 2012)

2.3.6 Nanoprecipitation

Nanoprecipitation, or solvent displacement, is the precipitation of a polymer from an organic solution and the diffusion of that organic solvent in the presence or absence of a surfactant. A polymer is dissolved in a water miscible organic solvent and added to an aqueous solution in which the organic solvent diffuses. As the solvent diffuses out, the polymer precipitates and the organic solvent is typically evaporated with the help of a vacuum. Nanoparticle formation is spontaneous due to the polymer precipitating in the aqueous environment. Diffusion and surface tensions at the interface of the organic solvent and the aqueous phase cause abruptions, which form small particles containing the polymer. Surfactants or stabilizers can modify the size and the surface properties of nanoprecipitate particles as well as ensure the stability of the nanoparticle dispersion (Nagavarma and others 2012; Fessi and others 1989).

Advantages of this method include its simplicity, no homogenization, ability to enhance encapsulation by changing pH, and ease of scale up. However, drawbacks of this technique include difficulty in choosing the active molecule to be entrapped, polymer building blocks, and solvents in delivery system. Other disadvantages include poor encapsulation efficacy of hydrophilic drugs, because the drug can diffuse to the

aqueous outer phase during polymer precipitation (Fessi and others 1989; Rodriguez and others 2004).

2.4 Assembly Components of Loaded Chitosan-Alginate Nanoparticles

The selection of nanoparticle wall materials, synthesis methods, and characterization methods in published research has be made primarily through empirical knowledge, processing conditions and advantages (Table 2.3), as well as a general trial and error basis (Zuidam and Nedović 2009). Polymeric wall materials can be used independently or in combination. Combining wall materials enhances stability and increases functionality (Forssell 2004; Liu 2014). Cost and toxicity are two parameters to consider when choosing wall materials. Risks of toxicity can be minimized by using naturally occurring dietary polysaccharides such as chitosan and alginate, which is particularly important for food applications (Liu 2014)

Table 2.3. Properties of common used wall materials for encapsulation process. Adapted from Fang and Bhandari (2012).

Wall Material		Properties
Carbohydrates	Hydrolyzed starches: corn syrup solids, maltodextrins, etc.	Good oxygen barrier, low viscosity at high solids; no/limited emulsion stabilization; economical
	Modified starches: acetylated starch, monostarch phosphate, etc.	Good emulsion stabilization; sometimes varying quality; not universally usable; economical
	Gums: agar, Arabic gum, sodium alginate, etc.	Good emulsions; good retention of volatiles; varying quality; price depends on availability; some impurities
	Cyclodextrins: α-, *β*- cyclodextrins	Good inclusion of volatiles; excellent oxygen barrier; relatively expensive
Proteins	Milk Proteins: whey protein caseinates skim milk powders, etc.	Good emulsions; being dependent on other factors such as pH and ionic strength; allergenic potential; expensive
	Other Proteins: soy protein, egg proteins, etc.	
Lipids	Food fats: milk fat, soybean oil, cocoa butter, etc.	Good colloidal stability, rheological properties and moisture barrier properties; economical
	Polar Lipids: monoglycerides, phospholipids, glycolipids, etc.	Amphiphilic properties; good surface activity and emulsion stability; self-assembly behavior; expensive
	Waxes: Beeswax, carnauba wax, etc.	Excellent moisture barrier properties; ideal for spray cooling or chilling (melting > 45°C); low viscosity at melt state; economical

2.4.1 Chitosan

Chitosan is a polysaccharide, hydrophilic colloid, and a product of the N-deacylated chitin (Figure 2.7). Commercially available chitosan has an average molecular weight of 3,800 to 20,000 Daltons and is 66 to 95% deacylated. It has a similar chemical structure to 2-aminocellulose. Chitosan is composed of linear beta-(1-4)-linked monosaccharaides (Figure 2.13). These monosaccharaides include 2-amino-2-deoxy-beta-D-glucan in combination with glycosidic linkages (Risch and Reineccius 1995; Bansal and others 2012).

Chitosan is protonated at acidic conditions making it a good candidate for coacervation and ionic gelation reactions. At acidic pH ranges, amino groups undergo protonation thus becoming soluble in water. Thus, chitosan is a cation which allows for unique bonding characteristics due to its electrostatic potential. Chitosan has a ridged crystalline structure built through inter- and intra-molecular hydrogen bonds. The cationic nature of chitosan in acidic solution allows chitosan to adhere to negatively charged molecules such as alginate (Agnihotri and others 2004). This is a key point as chitosan can be manipulated to be useful in food pH ranges. Solubility of chitosan depends on the free amino and N-acetyl group distribution. Literature shows that 1-3% acetic acid is sufficient to solubilize chitosan in solution (Sinjan and Robinson 2003; Sarmento and others 2006; Li and others 2008).

Recent advances in nanoparticle research has proposed chitosan to be used in gel forming systems with multivalent anionic counterions like polyphosphate and sodium alginate by ionic cross linking methods, coacervation, or ionic gelation methods

(Agnihotri and others 2004). Chitosan nanoparticles prepared via ionic gelation have been examined in the past decade as delivery media for drugs with low molecular weight (Koukaras and others 2012). Chitosan is efficient in the entrapment of drugs and has been shown in literature to reinforce nanoparticle structure by creating impermeability and preventing rapid diffusion out of particle (Risch and Reineccius 1995). Chitosan allows nanoparticles to enlarge their surface area via swelling to compensate for osmotic differences between interior and exterior nanoparticle environments (Ruo 2012).

Chitosan is advantageous for use in nanoparticle systems due to its ability to control the release of active agents, nontoxic nature, ability to avoid use of organic solvents, readily available free amine groups for cross linking, and good electropotential (Agnihotri and others 2004). Chitosan also possesses antimicrobial properties, good adhesive properties, coagulation abilities, and absorbs toxic metals (Berger and others 2004; Kong and others 2010). Chitosan is also effective in releasing water soluble drugs and enhancing the bioavailability of poorly water soluble compounds (Peniche and others 2003). This is a key issue as the active encapsulant in this research, *trans*-cinnamaldehyde (TC), is hydrophobic.

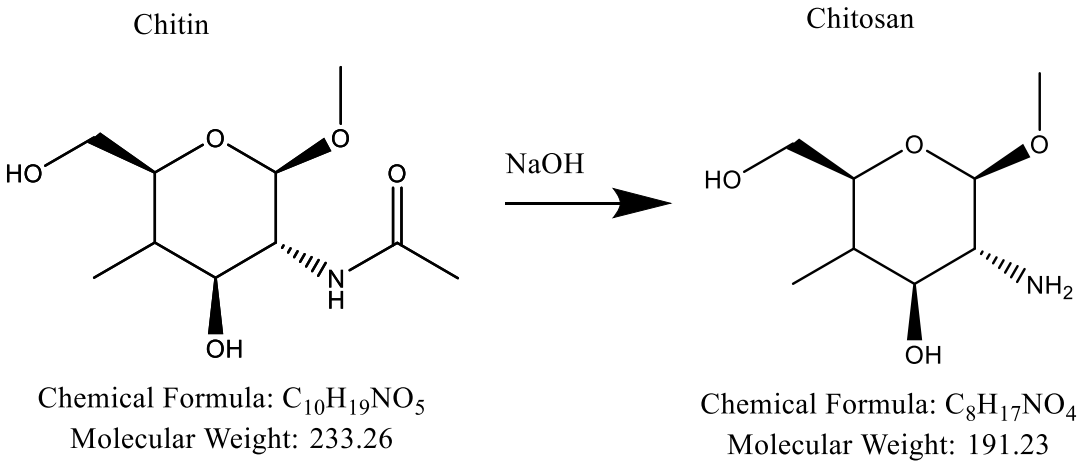

Figure 2.7. Conversion of chitin to chitosan. Adapted from Ahirrao and others (2013).

2.4.2 Alginate

Sodium alginate is an anionic polysaccharide and hydrocolloid which forms ionic mediated gels. Alginates are widely used natural polymers in the preparation of micro and nanoparticles with sustained release dosage. Alginates are obtained primarily from *Laminaria hyperborean*, *Ascophyllum nodosum*, and *Macrocystis pyrifera* species of brown algae. They are widely abundant in nature and can easily form nanoparticles due to its ability to form hydrogels upon cross-linking. This ability to gel under mild conditions makes alginate the polymer of choice in food applications (Peniche and others 2003; Thwala 2012). Alginate has the unique property of forming water insoluble gels through IG. Formation of alginate gel is simple, mild, and eco-friendly with the main function of entrapping active molecules rapidly (Ahirrao and others 2013; Peniche and others 2003).

Sodium alginate is water soluble sodium salt of alginic acid (Figure 2.8). Alginic acid is a linear unbranched copolymer composed of D-mannuronic acid (M) and L-guluronic acid (G). The M and G monomers are 1, 4 linked by glycosidic bonds, forming homopolymeric M or G blocks and heteropolymeric MG blocks (Figure 2.13). The functional properties of alginate are strongly associated with the composition and sequence of M and G acids. Alginates polyanionic character is a result of carboxyl groups along its polymeric chain. Every sugar on the chain contains a carboxyl group. The degree of ionization of carboxyl groups is a function of pH and decreases as the pH decreases. Alginate maintains a negative charge under acidic conditions which is ideal for forming complexes with polyvalent cations such as chitosan, calcium, or aluminum. The cations act as bridges between the anionic polymer chains, constituting junction zones, forming a hydrogel network (Daemi and Barikani 2012).

Advantages of using sodium alginate include the ability to encapsulate lipophilic drugs, utilized in a multiplicity of techniques, high stability, simplicity, non-toxicity, biocompatibility, and low cost. Also, alginate has the highest mucoadhesive strength compared to other natural and synthetic polymers (Thwala 2012). Drawbacks of use are that the porous structure without addition of membrane coating to reduce permeability as well as the low viscosity of alginate solutions cause lack of mechanical and physical stability. Therefore, the use of alginate is limited due to its low physical stability and subsequent degradation at acidic pH ranges causing faster release of entrapped active ingredients. In order to add mechanical strength to alginate, coating alginate beads with

polycations has been suggested in literature. Chitosan can be utilized in this fashion (Sinjan and Robinson 2003; Thwala 2012; Patil and others 2010).

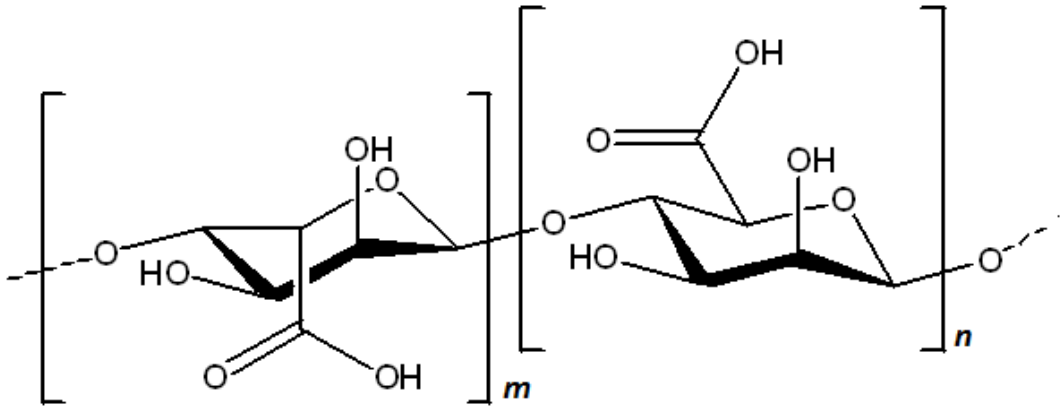

Figure 2.8. Structure of alginic acid. Adapted from Ahirrao and others (2013).

2.4.3 Calcium-Alginate Complex

Calcium chloride plays a key role in nanoparticle synthesis in the pre-gelation step. Calcium chloride is a commonly used cross-linker that interacts with G blocks of alginate due to structurally favorable chelation sites to form insoluble meshwork pre-gels (Figure 2.9 and Figure 2.10)(Ahirrao and others 2013). Calcium chloride was chosen for this study because it has been highly reported to be optimal for encapsulation efficiency of several active drugs with high mechanical strength and low toxicity (Khazaeli and others 2008; Thwala 2012; Joshi and others 2012). Literature shows that the pre-gel state is essential in enabling ionic interaction between calcium-algiante and chitosan in the

PEC step. Thus, stability of the *trans*-cinnamaldehyde loaded chitosan-alginate nanoparticles (LCA-NP) can be increased by incorporating calcium chloride in the gelation of alginate step. As the concentration of calcium chloride increases the rate of chitosan binding increases (Patil and others 2012). Sinjan and Robinson (2003) found the optimal mass ratio of alginate to calcium chloride to chitosan to be 100:17:10. Many researchers have reported calcium cross linked alginate beads for different controlled release applications and delivery applications (Thwala 2012; Daemi and Barikani 2012; Mumper and others 1994; Rajaonarivony and others 1993). These studies use the calcium–alginate cross-linking step as a cross-linking step and not as a final nanoparticle formation step.

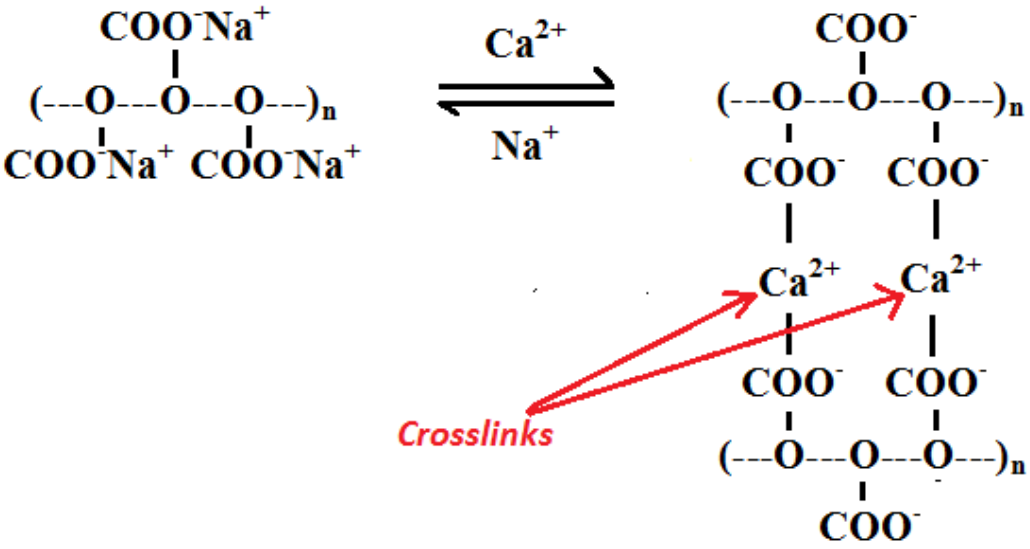

Figure 2.9. Electrostatic interaction between carboxyl groups of alginate and calcium ions. Adapted from Ahirrao and others (2013).

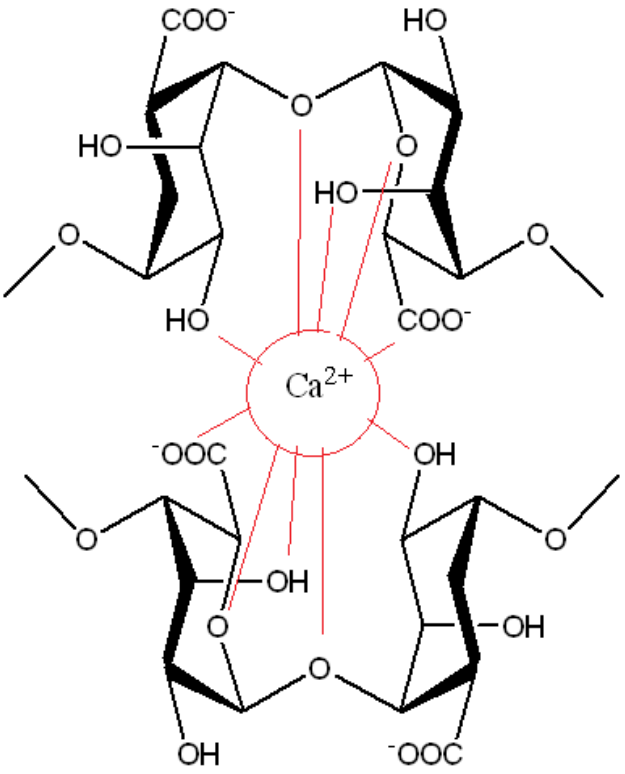

Figure 2.10. Cross linked structure of sodium alginate and calcium ions. Adapted from Ahirrao and others (2013).

2.4.4 *Trans*-cinnamaldehyde (TC)

Active encapsulants or molecules can include flavors, antimicrobial agents, nutraceuticals, vitamins, minerals, colors, nutrients, enzymes, cross-linking agents, and yeast among many others (Figure 2.11). Core materials are normally in the form of either solid, liquid, or gas and are used in the form of a solution, dispersion, or emulsion. Size of the core material effects permeability, diffusion, and controlled-release applications. Hydrophobicity is one of the critical attributes that play a significant role in determining encapsulants entrapment efficiency as well as controlled release into a food

system. The major problem in this research was determining the correct method to encapsulate hydrophobic TC with two hydrophilic polymers; chitosan and alginate.

Trans-cinnamaldehyde (Figure 2.12) or cinnamic aldehyde (3-phenyl-2-propenal) is a component in cassia oils, cinnamon bark oils, and is also a Generally Recognized as Safe substance based on 21 CFR part 172.515 (CFR 2009). It is a cyclic terpene alcohol with low water solubility (Gomes and others 2011). It is viscous, liquid, organic compound that is responsible for the flavor and odor associated with cinnamon and naturally present in the bark of cinnamon trees. It is an essential oil with great antimicrobial and antioxidant properties which makes it ideal for the use in food systems (Chia-Wen and others 2009; Yen and Chang 2008; El-Baroty and others 2010; Kong and others 2010). TC has been shown to be one of the most effective antimicrobials against foodborne pathogens and also shows more inhibitory action in comparison to purified oils (Gomes and others 2011; Beuchat 1994). Although it has low solubility in water, entrapping TC can prevent loss of volatility and improve solubility of the oil, thus improving delivery to an aqueous system. Water soluble polymers have been used in pharmaceutical research to increase drug solubility. The polymers can interact with drug molecules via electrostatic bonds such as ion to ion, dipole to dipole, or other forces such as Van der Waal and hydrogen bridges. These interaction participate in drug-polymer complex formation (Thwala 2012).

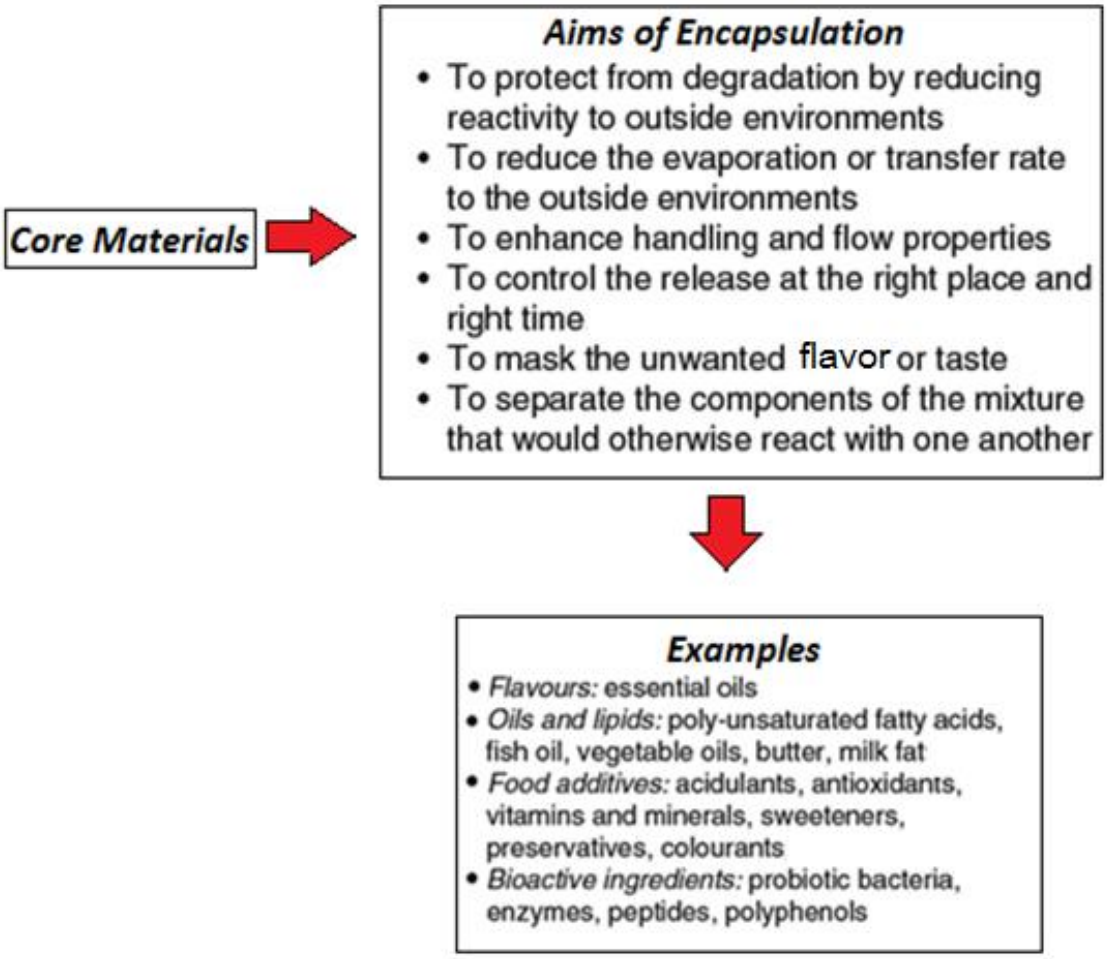

Figure 2.11. A brief illustration of the aim of encapsulation along with some examples of core materials. Adapted from Fang and Bhandari (2012).

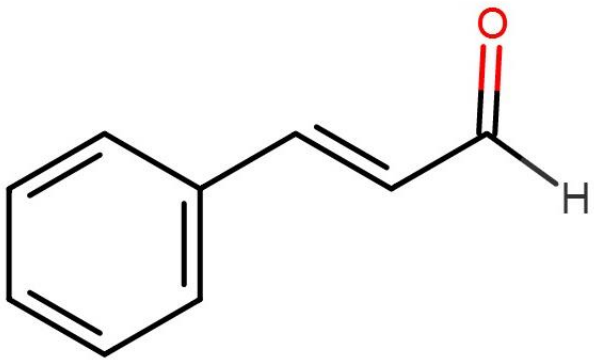

Figure 2.12. Structure of *trans*-cinnamaldehyde. Adapted from ColeParmer (2014).

2.4.5 Active Molecule Entrapment

Entrapment is the trapping of active encapsulant molecules within or throughout a matrix. Encapsulation with semi-permeable membranes has been used to attain slow and prolonged release of active molecules. A successful nanoparticle system should have a high active substance loading capacity (Ruo 2012). Various methods of loading have been developed to improve the efficiency of loading which is dependent on the method of preparation as well as the physical properties of the drug and the polymer. Active-substance loading is normally achieved by two methods: incorporation or absorption. In these systems the drug is physically embedded into the matrix or adsorbed onto the surface. Incorporation is the loading of active molecules at the time of nanoparticle production. Absorption is loading of drug after formation of nanoparticles by incubating the carrier with a concentrated drug. Incorporation gives a low initial burst effect and better sustained release characteristics in comparison to absorption methods. The

biopolymer membrane layer will control the diffusion out of the nanoparticle while also protecting the particle from environmental stressors (Mohanraj and Chen 2006; Patil and others 2012).

Maximum loading can be achieved through incorporation. Ford and others (1999) found that hydrophobic peptides dissolved in water miscible organic solvents can be precipitated in the aqueous phase as discrete spherical particles. Li and others (2008) also found the same precipitation to occur by dissolving a hydrophobic drug in a mixture of dehydrated alcohol and water before the addition of calcium chloride. This resulted in the Tyndall effect, or light scattering by particles in a colloid or fine suspension. This procedure can be used to allow for *trans*-cinnamaldehyde entrapment (Sarmento and others 2007; Sarmento and others 2006; Gupta and others 2011; Li and others 2008; Thwala 2012).

2.4.6 Chitosan-Alginate Complexation

Alginate has been mixed with other polymers to form PEC to solve problem of drug leaching and instability. Likewise, chitosan will form nanoparticles on its own but the matrix is often to permeable. Alginate shrinks in low pH and dissolves in high pH ranges while chitosan dissolves in low pH and is insoluble at high pH ranges. The high solubility of chitosan at low pH ranges is prevented by the alginate network due to alginate being insoluble in the low pH range. Similarly, dissolution of alginate at high pH is prevented by stable chitosan at high pH. Thus, complexation of oppositely charged polyelectrolytes has been used to strengthen alginate particles and reduce porosity (Leonard and others 2004).

The strong electrostatic interaction of the amine groups (NH_2^+) of chitosan with the carboxyl groups (COO^-) of alginate in acidic pH ranges leads to the formation of chitosan-alginate nanoparticles (Figure 2.13). Amino groups on chitosan become protonated and carboxyl groups on alginate become ionized leading to chitosan binding onto the surface of alginate. As chitosan solution is dropped into alginate solution, the spreading of alginate particles decreases as the chitosan viscosity increases. This leads to decreased maneuverability and freedom resulting in the production of small and uniform particles. Alginate‘s function is to entrap TC while chitosan‘s function is to add mechanical strength to the nanoparticle (Thwala 2012; Sezer and Akbuga 1999; Mumper and others 1994). Chitosan-alginate complex nanoparticles are stabilized through Brownian motion, or the thermal motion of particles in the colloidal size range. Gravitational forces normally would cause particles to sediment. However, Brownian motion and gravitational forces oppose each other, but at small particles sizes Brownian forces dominate leading to suspended particles (Abdelwahed and others 2006).

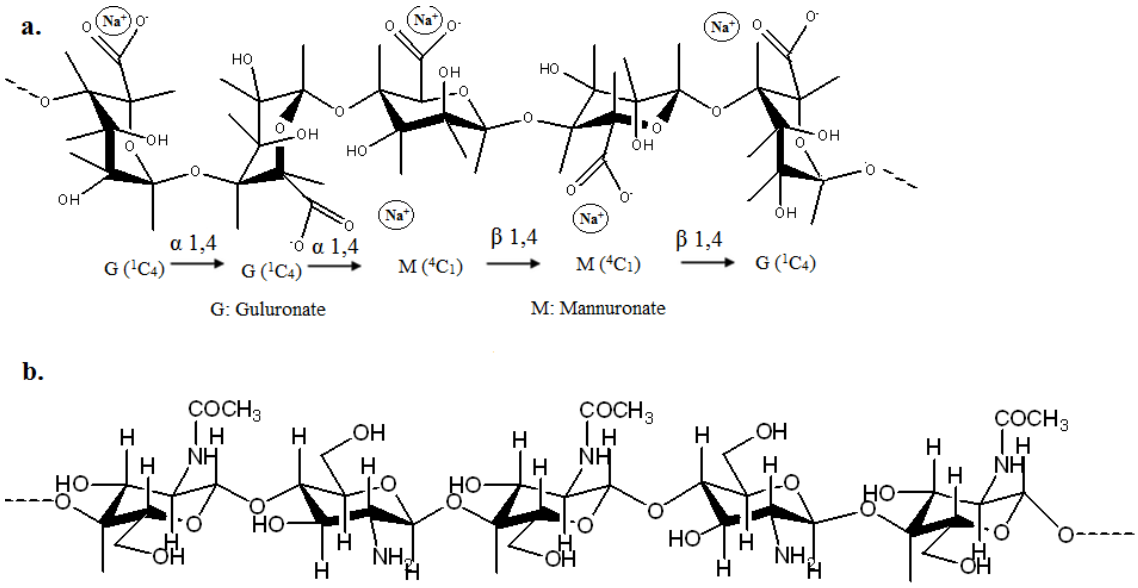

Figure 2.13. (a) Representative structure of sodium alginate with G unit residues, and M unit residues, and glycosidic linkages (b) Representative structure of chitosan. Adapted from Lertsutthiwong and others (2009) and Wang and others (2006).

2.4.7 Surfactant Choice

Essential oils can be emulsified in an ~~"o~~il in water" emulsion using surfactants. Surfactants are compounds having active hydrophilic and lipophilic reactive groups on the same surfactant molecule. Thus, surfactants are able to arrange themselves to lower interfacial tension leading to formation of water based emulsion. Tween 20 (Polysorbate 20) is a non-ionic and food permitted solubilizing agent.

Surfactants such as Tween 20 may bind strongly to both hydrophilic and hydrophobic sites of polymers, forming high energy links between chains. These links can be formed in C-A polyelectrolyte complexation where the stronger and tighter structures lead to smaller particle size. Li and McClements (2013) showed that mean

droplet diameters in –oil in water" emulsions prepared using a homogenizer were considerably larger if polymer is used without combination of a surfactant. Edris and El-Galeel (2010) presented that the best surfactant to solubilize large amounts of cinnamon oil in a surfactant water system was Tween 20. The study also showed Tween 20 would solubilize more pure cinnamic aldehyde and cinnamon oil at different surfactant to water ratios in comparison to Tween 80. Tween 20 has a lower hydrophilic-lipophilic balance (HLB value) versus Tween 80 meaning that Tween 20 has higher strength of the lipophilic groups of the surfactant molecule hence stronger lipophilic nature. If an essential oil and a surfactant have similar polarity or HLB, maximal solubilization takes place (Edris and El-Galeel 2010). The HLB value of Tween 20 is 16.7 which in the HLB region appropriate for solubilization of oils. Tween 20 is also a simple, economical, and feasible solution to create an emulsion for the solubilization of TC in this study.

2.4.8 Solvent Choice

The selection of organic solvent is important in developing a successful nanoparticulate formulation. The miscibility of the solvent with water and its ability to dissolve the chitosan, alginate, and entrapped TC impacts overall encapsulation efficiency of TC and particle size. Generally, solvent should have low solubility in water to yield a more stable emulsion and formulate high-quality nanoparticles (Bala and others 2004). Other important aspects of solvent choice are toxicity and purification method. Acetonitrile was chosen for this study due to its polar, aprotic nature (i.e. solvent that will dissolve many salts but lacks an acidic hydrogen, thus can accept hydrogen bonds). It is a medium polarity solvent which is miscible in

water. Acetonitrile is more polar than common solvents used in nanoparticle formulation such as acetone and ethyl acetate. In a study by Galanakis and others (2011) it was found that cinnamic aldehyde generally solubilized easiest in polar aprotic solvents such as dichloromethane and acetone. The dielectric constant of TC is 16.9 while the dielectric constant of acetonitrile is 37, higher than that of acetone (i.e. 20.7). Thus, acetonitrile should allow higher dissolution of TC.

2.5 Nanoparticle Treatment Post Assembly

2.5.1 Introduction

Nanoparticles should be free from impurities and the degree of purification depends upon the final purpose of the formulation developed. All impurities were attempted to be removed in this study through the use of filtration. The most commonly used procedures in literature are gel filtration, ultracentrifugation, centrifugal filtration, dialysis, and cross-flow filtration.

2.5.2 Stability

Homogenization and sonication are utilized to reduce particle size and aggregation as well as improve uniformity of nanoparticles. Homogenization is a fluid mechanical process that involves shearing of particles to create a stable evenly distributed dispersion or emulsion. Increasing shear or energy input can reduce size of particles and disrupt aggregates (Harte and Venegas 2012). A reduction in the mean diameter of the particles increases the number of individual particles. This leads to a reduction of the average particle diameter and increases the particle surface area. Ahmed and others (2012) found that increasing homogenization speed produced smaller solid

lipid nanoparticles with a small polydisperity index and homogenous distribution of particle size. However, downfalls of homogenization include tearing and stretching of nanoparticles.

Sonication is the act of applying ultrasonic frequencies to agitate particles in a sample to speed up dissolution by breaking intermolecular interactions and prevent aggregation of particles. In addition, sonication is useful for evenly dispersing nanoparticles in liquids. A study by Al-Kaysi and others (2005) demonstrated that sonication provides an approach to exert control over particle size, morphology, and colloidal stability. Sonicators are commonly used for dispersing, deagglomerating, particle size reduction, particle synthesis, precipitation, and surface functionalization applications (Qsonica 2014).

2.5.3 Purification

A rotary evaporator is utilized to remove any remaining volatile solvents. This instrument can remove acetonitrile under evaporation at reduced pressure. Removal of solvent is essential to eliminate toxicity concerns and interference during freeze drying. By lowering the pressure of the nanoparticle solution, the boiling point of incorporated acetonitrile is lowered allowing for simple extraction. The boiling point of acetonitrile is 179.6°C. Thus, lowering the pressure of the acetonitrile solution reduces the boiling temperature.

2.5.4 Filtration

Tangential filtration, also called cross flow filtration is utilized to filter nanoparticles and remove excess aggregates, unreacted polymer, or foreign materials. In

tangential filtration, the sample being filtered travels tangentially across the surface of the filtration membrane, and two exiting streams are generated. The permeate stream is the portion of the fluid that passes through the membrane. This filtered fluid will contain some percentage of soluble and/or insoluble components from the initial feed stream that are smaller than the membrane removal rating (50 kDa cutoff). The remainder of the feed stream, which does not pass through the membrane, is the retentate stream (Koros and others 1996; Pall 2013).

Advantages of using tangential filtration include ability to set molecular weight cutoff, a higher overall liquid removal rate, and continuous operation at relatively high solid loads without blinding due to trapped particles on the filter surface to be rubbed off. Membrane filters can have pore sizes between 0.001 and 0.1 microns. Tangential filtration has greater throughput capacity compared to traditional cartridge direct flow filtration. Limitations include long processing times, difficult cleaning procedures, short membrane life, and pH and temperature sensitive membranes (Pall 2013).

2.5.5 Lyophilization

Lyophilization, or freeze-drying, is a process used to preserve and improve storage stability of nanoparticles that would normally degrade or become contaminated in suspension by microorganisms. Lyophilization works through the freezing of a material and reducing pressure to allow sublimation of ice to gas. Essentially, the solvent is removed from the system. In the case of nanoparticle assembly, the solvent is commonly water as harsh solvents are removed via evaporation. Freeze drying is a commonly accepted method to remove water from nanoparticles formulations (Hirsjärvi

2008). Freeze drying is affected by freezing rate, temperature, pressure, cryoprotectant use, and changes in pH or ionic strength. Ideally, nanoparticles should be easily resuspended after lyophilization without physical changes.

Nanoparticles are normally isolated by freeze-drying using cryoprotective agents such as trehalose or mannitol. Trehalose, utilized in this research, will help protect the physical integrity of purified nanoparticles and from any freeze drying and desiccation related stresses. Trehalose aids in the redispersibility of nanoparticles and helps prevent aggregation of nanoparticles during the freeze-drying process (Liu 2014). Trehalose is best utilized in a trehalose to polymer mass ratio of 1:1 (Abdelwahed and others 2006). The protective mechanism of trehalose is due to its amorphous matrix. Protection arises when the amorphous matrix forms hydrogen bonds with the nanoparticles. Trehalose will act as a substitute to water inhibiting the destructive effect of ice crystals. Thus, the use of trehalose enables a wider temperature scale for drying (Hirsjärvi 2008; Abdelwahed and others 2006). Trehalose is a preferred cryoprotectant compared to other sugars due to its low hygroscopicity, absence of internal hydrogen bonds which allows for more flexible formation of hydrogen bonds with nanoparticles, low chemical reactivity, and high glass transition temperature (Abdelwahed and others 2006; Astete and others 2009).

Advantages of freeze drying nanoparticles include improved reconstitution and redispersibility characteristics, reduced foreign matter, and enhanced sterility. In comparison to spray drying, freeze drying is accomplished at low temperatures and is less destructive to nanoparticles. Disadvantages of the process include cost, high purity

of solvents needed, difficult handling procedures, and potential aggregation in lag time before nanoparticles are dry (Hirsjärvi 2008).

2.6 Design Constraints and Processing Parameters

2.6.1 Introduction

Processing parameters such as stirring time, droplet size, and equilibration time affect the formation of nanoparticles thus affecting particle size, shape, size distribution, and entrapment efficiency. The average size and uniformity of nanoparticles impacts the encapsulation ability and release kinetics.

2.6.2 Processing Parameters

Optimization of nanoparticle size during assembly is an important phase of this research in regards to assembling a delivery system with optimal TC entrapment. To do this, processing parameters must be optimized. Processing parameters include stirring time, homogenization time, sonication time, equilibration time (time elapsed from post-assembly to freezing), and concentration of drug to polymer. Gupta (2011) optimized stirring rate at 800 RPM and optimal stirring time at 90 minutes. In the same study, the optimal drug to polymer mass ratio was determined to be 5:75 for TC:alginate and 5:50 for TC:chitosan. The optimal concentration of cross linking agent used was determined to be 2 ml. With optimal parameters considered, the entrapment efficiency was on average 91% while particle size was 245 nm. Droplet size of chitosan and alginate as well as homogenization rate and time, and sonication time will affect the size of loaded chitosan alginate nanoparticles. A number of studies use differing processing parameters, thus it is important to consolidate these methods into one standard method

(Thwala 2012; Sarmento and others 2007; Gupta 2011; Li and others 2008; Rajaonarivony and others 1993).

2.6.3 Particle Size

Particle size and size distribution are critical characteristics of nanoparticle systems. The average size and uniformity of nanoparticles impacts the mechanical stability, permeability, handling ease, encapsulation ability, and diffusion kinetics. Smaller particles have larger surface area to volume ratio therefore most of the encapsulant material is located near or at the particle surface leading to faster drug release (Li. and others 2008). Although small particles have greater risk of aggregation and gelation, small particles form faster leading to higher entrapment efficiency. Larger particles have larger cores and the encapsulant can diffuse out of nanoparticles over longer formation times. Larger particles also degrade and erode at a more rapid rate than smaller particles (Berkland and others 2004; Ghosh 2006).

Chitosan molecular weight has a direct effect on properties of nanoparticles. In a study by Honary (2009) involving low, medium, and high molecular weight chitosan, it was found that increasing molecular weight of chitosan decreased the diameter of particles. It was also determined that higher concentration chitosan solution formed larger size particles. Thus, polymer molecular weight and concentration has a direct effect on size and encapsulation potential. Fortunately, chitosan and alginate‘s final particle size is easily changed as concentration dependence on biopolymers relates directly to particle size.

2.7 Characterization of Assembled Nanoparticles

2.7.1 Particle Size Analysis

The most routine and current method for determining particle size is through the use of dynamic light scattering (DLS). DLS has been a vital probe into the structure and dynamics of nanoscale materials. Results from DLS can be verified though the use of transmission electron microscopy (Mohanraj and Chen 2006). Laser diffraction sizing is highly efficient and repeatable compared to other sizing methods.

DLS relies on the superposition of a scattered light field. Nanoparticles exist in aqueous suspension and are not stationary. These particles are undergoing Brownian motion which brings upon frequency and phase changes of scattered light. Nanoparticles block a laser beam that the DLS instrument emits. A scattered wave is generated from the path that is blocked and reaches the DLS detector at a fixed position. Thus, the detector accumulates the signal and the superimposition of the electrical field is calculated. Each particle in solution carries its own phase determined by its relative position. The intensity, angular distribution, and polarization of the scattered light carry data about the particles size, shape, and electrical character.

2.7.2 Encapsulation Efficiency

Encapsulation efficiency, also known as drug loading efficiency, is a measure of the amount of entrapped active compound in nanoparticles. It is expressed throughout literature as the amount of active compound entrapped relative to the initial active compound amount. In this study, encapsulation efficiency is the amount of TC entrapped relative to the initial TC added during incorporation into alginate solution.

Encapsulation efficiency is one of the critical properties of nanoencapsulation and its applications. Nanosystems with high loading efficiency often use less wall material and need less net amount of encapsulated compound to deliver the required amount of core material (Liu 2014).

Generally, steps for encapsulation efficiency include completely dissolving resuspended lyophilized nanoparticles and determining concentration of active compound via spectroscopy methods or high-performance liquid chromatography.

2.7.3 Cumulative Controlled Release

Controlled release is the modification of the rate or place at which an active substance is released. This modification can be made using materials with certain barrier properties for manipulating the release of an active substance to provide sensory or functional benefits (Lakkis 2007) . Functional benefits could include antioxidant, antimicrobial, or nutrient properties.

Controlled release can be broken down into two modes: delayed release or sustained release. Delayed release is the release of an active substance being delayed to a point where the release is favored. Sustained release is designed to release an active and maintain constant concentration of that active to the target site. Release of TC from *trans*-cinnamaldehyde loaded chitosan-alginate nanoparticles (LCA-NP) in this research will be initiated through the use of phosphate buffered saline (PBS) stressor at pH 7.4. Stressors can include temperature, moisture, pH, enzymes, and shear (Li and others 2008). The release profiles are expected to show two phases. The first phase is from the initial burst release followed by a second phase of uniform controlled release. This

effect is primarily based on the fact that a large concentration of TC may be attached close to the surface of the particle allowing for rapid release as well as permeability of thin polymeric membrane coating. The second release phase, uniform release, is due to the diffusion of the drug molecules from the inner compartment and core. In the first several hours of the release phase, higher pH levels should correlate with a higher concentration of TC release (Sinjan and Robinson 2003).

In vitro release testing is one of the most important analyses to assure the functionality of an encapsulated ingredient due to the estimation of the behavior of nanoparticles in actual applications, by using similar environmental conditions. Controlled release also evaluates the sensitivity of the diffusion release mechanism. Release tests are referred to as release profiles where cumulative concentration or percentage release of the TC is plotted against time, as in this study. The release rate of the TC in this study is dependent on its solubility, nanoparticle morphology, size, pH of media, polarity, density of the particulate system, desorption of any surface-bound active, active diffusion through the nanoparticle matrix, and the combination of erosion and diffusion processes (Mohanraj and Chen 2006; Liu 2014; Wise 2000).

The pH dependent behavior of alginate and chitosan allows for the modification of release profiles (Thwala 2012). The release medium used in this research is PBS. PBS is an isotonic water based buffer solution containing sodium phosphate and sodium chloride. Over time, PBS degrades LCA-NP to release TC. This release involves the following three steps: PBS penetration into loaded nanoparticle system, swelling of the matrix, conversion of the glassy polymer into a rubbery matrix, and diffusion of the drug

from the rubbery matrix (Liu 2014). If the diffusion of TC out of nanoparticle is faster than matrix erosion, the mechanism of release is primarily diffusion. The membrane polymer acts as a barrier to release and is therefore the most important parameter in active substance release. The diffusion mechanism of controlled release acts to limit the release of TC by controlling the diffusion of TC from its location in the particle to the surface of the particle. Diffusion is controlled by the solubility of a component in the matrix and the permeability of the component through the matrix. The true driving force for diffusion is the activity or chemical potential as related to the vapor pressure on each side of the membrane(Mohanraj and Chen 2006; Liu 2014; Wise 2000).

Literature shows drug release kinetics as being primarily first order as well as swelling and erosion being the main causes of drug release. Based on work done by Li and others (2008), it is expected that the mechanism of active release may follow non-Fickian behavior after initial burst release. Other controlled release methods found in literature include side-by-side diffusion cells with an artificial or biological membrane, dialysis bag method, ultracentrifugation, and centrifugal ultrafiltration (Jawahar and Meyyanathan 2012).

2.7.4 Spectroscopy

Ultraviolet spectroscopy will be utilized in this study as a quantitative analysis method to determine the concentration of TC in solution as a result of encapsulation efficiency and *in vitro* release tests (Rajaonarivony and others 1993). Ultraviolet radiation interacts with matter causing electrons to move from a grounded state to a high energy state. The ultraviolet region falls in the range of 190-380 nm. UV absorption

spectroscopy measures the radiation that is absorbed by a compound at that wavelength. Absorption is dependent on the compound, concentration, and molecular structure. TC absorbs radiation at 280 nm (Čeppan and others 1993; Gomes and others 2011). Beer's Law can be utilized to find the unknown TC concentration from absorbance readings at 280 nm. This is done through the use of a standard curve, where TC concentrations are accurately known and experimental absorbance is read.

2.7.5 Differential Scanning Calorimetry

Differential scanning calorimetry (DSC) will be utilized as a thermal characterization tool for *trans*-cinnamaldehyde loaded chitosan-alginate nanoparticles (LCA-NP). Thermal characterization assists in understanding structural properties, hydrophilic properties, and associate state of nanoparticles. A complete thermal profile will also validate thermal oxidative stability, loss of water in polymers, depolymerization at high temperature, and confirm inclusion of active compound in nanoparticle formation (Hill and others 2013a; Thwala 2012). This information is used to characterize materials, design products, predict performance, optimize processing conditions, and improve quality. Shifts in endothermic and exothermic peaks show polymer-polymer interactions as well as active compound-polymer interactions.

DSC works on the thermodynamic concept of heat flow differences between sample and a reference. Thus, calorimeters measure the amount of heat absorbed or released during material transformation (Thwala 2012). DSC outputs a plot of heat flow as a function of temperature. Heat flow is determined by measuring the temperature

difference over an accurately known thermal resistance. The difference of heat flow of reference to the heat flow of the sample is final heat flow.

DSC will be used to study complex formation between TC and LCA-NP (Sarmento and others 2006; Hill and others 2013a; Kamimura and others 2014). TC is liquid at room temperature and can be confirmed to be included in the inclusion complex indirectly by comparing the thermal stability of the free TC with the encapsulated TC. The boiling point of TC should disappear in the LCA-NP thermogram confirming that TC has been included into the nanoparticle inclusion complex. The energy change associated with water loss and depolymerization at high temperatures along with exothermic and endothermic peak shifts will help indicate interaction of entrapped TC with the wall forming biopolymers chitosan and alginate.

DSC diagrams should show two peaks. It was expected that an endothermic peak would arise at 80ºC to 120ºC and an exothermic peak would arise at 146°C. The first peak should be attributed to the loss of water from the nanoparticles while the second peak attributed to the partial crystallization of TC after the loss of water at 120ºC (Honary 2009). DSC curves should show a broad endothermic peak as the nanoparticle becomes anhydrous as well as exothermic region at high temperatures corresponding to depolymerization and decarboxylation of polymers. The broader endotherm is associated with the loss of bound water.

The advantages of DSC include rapid measurements, both solids and liquid can be tested, programmability, and functionality. Hermetically sealed aluminum pans with a pinhole for pressure reduction are used to incinerate samples. Aluminum pans allow for

a highly conductive capsule distributed in a thin layer reducing internal resistance of the sample. This allows for superior temperature control and maximized heat transfer (Elmer 2014).

2.7.6 Transmission electron microscopy

Surface characteristics will be evaluated using transmission electron microscopy (TEM). An electron beam will be transmitted through an ultra-thin nanoparticle specimen under vacuum and will interact as it passes through the sample. An image is formed from the transmitted electrons to a phosphorescent screen or camera. The TEM will interact with nanoparticles through transmission rather than absorption. This test will also allow nanoparticle size to be estimated. TEM should confirm nanoparticle shape; spherical with smooth surfaces. TEM is a versatile sizing and morphology characterization method. However, TEM is limited by its stringent sample requirements as well as its laborious and time-consuming sample preparation. Advantages of TEM in comparison to a scanning electron microscope (SEM) include less electron interaction with specimen, cheaper and less sample contamination (Bala and others 2004; Thwala 2012).

2.8 Applications of Assembled Nanoparticles

2.8.1 Antioxidant Capacity

Free radical reactions are a common occurrence in food systems. Free radicals can be in the form of reactive oxygen and nitrogen species. Free radical production is initiated through oxidative stresses (Singh and others 2007). They are generated as a result of normal metabolic processes or from extraneous stressor. They can initiate

peroxidation or the accumulation of lipid peroxides. Polyunsaturated fats are easily oxidized by molecular oxygen and are a major cause of oxidative deterioration, nutritional loses, and sensory changes. Antioxidants have been used in the food industry to prolong shelf life of foods prone to oxidation. Antioxidants provide a way to scavenge these free radicals in food products thus maintaining sensory parameters of foods and increasing shelf life stability. Essential oils have potential to act as natural food preservatives. They are being increasingly used as antioxidants in food applications due to their safe status, acceptance by consumers, and high functionality (Chia-Wen and others 2009; Yen and Chang 2008). Cinnamon bark has been shown to have free radical scavenging potential (Singh and others 2007). Chia-Wen and others (2009) found cinnamon bark at 5 mg/ml showed highest DPPH free-radical scavenging activity of about 91.4%. TC is a large component of cinnamon bark and is an important antioxidant compound (Chia-Wen and others 2009; Shimada and others 1992; El-Baroty and others 2010). Cinnamon extracts in ethanol or methanol have been reported to show considerable antioxidant activities at a 1:1 mass ratio (Rao and Gan 2014).

Scavenging of DPPH free radical is the basis of a common antioxidant assay (Sharma and Bhat 2009). 2,2-Diphenyl-2-picrylhydrazyl (DPPH) (Figure 2.14) is a stable free radical with an unpaired valence electron at one atom of its nitrogen bridge. DPPH shows absorption at 517 nm on a spectrophotometer due to presence of hydrogen free radical. When it encounters proton radical scavengers, DPPH‘s innate purple color fades to a yellow. Thus, the concentration of DPPH lost gives an indication of scavenging power. Decreased absorbance of DPPH indicates increased rate of

antioxidant effect. This antioxidant test will determine the ability of LCA-NP to reduce oxidation, inhibit fatty acid oxidation, and lipid peroxidation *in vitro* with potential food application (Sharma and Bhat 2009; Chien and others 2007; Shimada and others 1992)

The DPPH assay is simple, rapid, inexpensive, and will yield a radical scavenging activity profile for nanoparticles. The DPPH method can be used for solid or liquid samples and is not specific to any particular antioxidant component. However, it applies to the overall antioxidant capacity of the sample. Measuring the total antioxidant capacity will determine functional properties of foods or in the case of this research the nanoparticles. Essentially, DPPH solution was added to apple juice containing LCA-NP. LCA-NP release TC where TC acts as an antioxidant scavenging free radicals. The antioxidant effect (%) = $(1\text{-Absorbance}_{\text{sample, 517nm}}/\text{Absorbance}_{\text{control, 517nm}})*100$.

Apple juice is an important food commodity because of its nutritional value and its ability to inhibit the oxidation of low density lipoprotein in humans. It is widely consumed in many countries and is a relatively cheap product (Chien and others 2007). Apple juice can also be purchased as a transparent medium which is convenient for spectrophotometric studies.

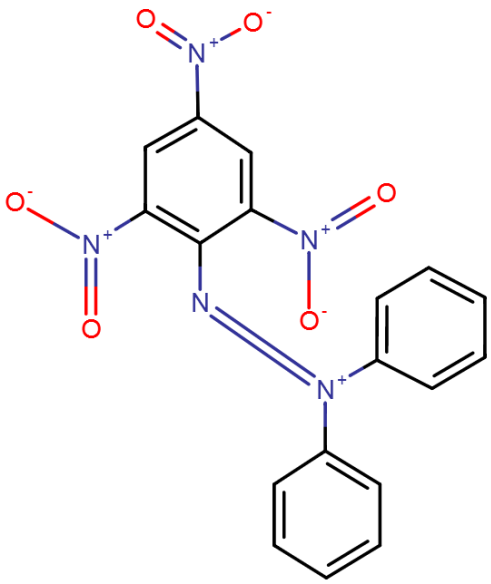

Figure 2.14. Structure of DPPH. Adapted from (Sharma and Bhat 2009).

2.8.2 Antimicrobial Effectiveness

2.8.2.1 Introduction

International and domestic outbreaks of pathogens such as *Listeria monocytogenes* and *Escherichia coli* O157:H7 justifies the continuous search for ways to inhibit these microorganisms and improve food safety without sacrificing quality. The majority of foodborne illness associated with fresh produce are caused by *Salmonella* enteritidis, *E. coli* O157:H7, *L. monocytogenes*, and *Campylobacter jejuni* (Kong and others 2010). *E. coli* O157:H7 and *L. monocytogenes* are of particular importance due to their detection in a high variety of foods as well as their ability to affect immunocompromised individuals. Increasing consumer demands for high-quality and

microbial safe foods paralleled with longer product shelf life are continuously forcing researchers to develop novel food preservative strategies (Jin and Zhang 2008).

Recently, natural antimicrobials such as essential oils have been of research interest due to low toxicity, biodegradability, and consumer perception (Kalemba and Kunicka 2003). Minimum inhibitory concentration and minimum bactericidal concentration analysis were used to determine effectiveness of LCA-NP on inhibiting the growth of *L. monocytogenes* and *E. coli* O15H7:H7. This section of the study aimed to show the potential for antimicrobial nanoparticles to inhibit the growth of two microorganisms that are of principal food safety concern. This data can not only provide a better idea of nanoparticle antimicrobial efficacy, but also may assist researchers bridging the gap between microbiological safety and stability of foods through the use of polymeric nanoparticles that encapsulate essential oils.

2.8.2.2 Microorganisms

Listeria monocytogenes and *Escherichia coli* O157:H7 are two common foodborne pathogens that are of concern in food safety. *L. monocytogenes* is Gram positive, facultative anaerobe, nonspore-forming, motile, rod-shaped bacterium. It is catalase positive and oxidase negative and expresses beta-hemolysin for the destruction of red blood cells (Mead and others 1999). It is capable of surviving in the presence or absence of oxygen. It is present in raw foods with ready to eat meats, poultry products, soft cheeses, and seafood commodities. *Listeria* can live in food processing plants and can grow at refrigeration temperatures (FoodSafety 2013). Listeriosis is the serious infection caused by *L. monocytogenes* and is associated with such conditions as

gastroenteritis, stillbirth, meningitis, septicemia, and death in immunocompromised individuals (Brandt and others 2010). *L. monocytogenes* can grow and replicate inside host cells and is considered one of the most virulent foodborne pathogen with 20-30% of clinical infections leading to death (Ramaswamy and others 2007). The CDC estimates approximately 1600 illnesses and 260 deaths due to listeriosis annually in the United States. This amounts to 0.29 cases per 100,000 people from 2009 to 2011 and is the third leading cause of death amongst foodborne bacterial pathogens (CDC 2014; Mead and others 1999). Recent domestic and international listeriosis outbreaks and death totals include: multistate outbreak in 2011 originating from whole cantaloupes in Colorado (33 total deaths), multistate outbreak linked to imported Ricotta Cheese in 2012 (2 deaths), and outbreaks linked to contaminated product lines in Ontario (6 deaths) (CDC 2014). The Food and Drug Administration (FDA), U.S. Department of Agriculture (USDA) (e.g. Food Safety Inspection Service (FSIS)) maintain a zero-tolerance policy for *L. monocytogenes* in ready to eat food products (FDA 2003).

Escherichia coli O157:H7 is an enterohemorrhagic serotype of *E. coli* and a major food safety concern. It is a Gram-negative, rod shaped bacterium. *E. coli* is a facultative anaerobe, is nonspore-forming, and is motile. It is catalase positive and oxidase negative. Many *E. coli* strains are harmless and can be found within the intestines of mammals. However, *E. coli* O157:H7 can produce a Shiga-like toxin and cause severe illness and even death. *E. coli* O157:H7 is often referred to as "Shiga toxin-producing" (STEC). Shiga-toxins are iron-regulated toxins that inactivate ribosomal subunits of eukaryotic cells which block mRNA production leading to

eventual cell death. Infection is progressive and could lead to gastroenteritis, hemorrhagic colitis, diarrhea, kidney failure, and possibly death. *E. coli* O157:H7 is often transferred via fecal to oral route through undercooked contaminated ground beef or ground pork (FDA 2013; Mead and others 1999). Recent domestic *E. coli* O157:H7 Shiga toxin-producing outbreaks and hemolytic uremic syndrome (HUS) totals include: multistate outbreak linked to ground beef (0 HUS), multistate outbreak linked to ready-to-eat salads (2 HUS), and multistate outbreak linked to frozen food products (2 HUS) (CDC 2013). The USDA declared a zero tolerance policy for *E. coli* O157:H7 in 1994. This bacterium is considered an adulterant if detected in raw ground beef, its components, and tenderized steaks (USDA 2011).

2.8.2.3 Minimum Inhibitory and Bactericidal Concentration

Agar dilution and broth dilution are the most commonly used techniques to determine minimum inhibitory concentration (MIC) and minimum bactericidal concentration (MBC) of antimicrobial compounds, including substances that kill (bactericidal) or inhibit the growth (bacteriostatic) of bacteria (Wiegand and others 2008). The broth dilution method was utilized in this study. Broth dilution uses a liquid growth medium containing LCA-NP antimicrobial, which is inoculated with *E. coli* or *L. monocytogenes*. Following incubation into a microplate well, the presence of turbidity or sediment (measured via optical density at 630 nm) indicates growth of microorganisms. A limitation of MIC/MBC is that it is a poor predicator of drug efficacy *in vivo*. The test does not give an indication of the mode of action (bactericidal or bacteriostatic) of the LCA-NP.

Minimum inhibitory concentration is the lowest concentration (mg/L) of an antimicrobial that will inhibit the visible growth of a microorganism after 24 h incubation at 35°C. MIC is important in analytic test to confirm resistance of microorganisms to LCA-NP and also to monitor the activity of new antimicrobial agents. A MIC is generally regarded as the most basic laboratory measurement of the activity of an antimicrobial agent against an organism (Burt 2004; Wiegand and others 2008).

The minimum bactericidal concentration (MBC) is the lowest concentration of an antibacterial agent required to kill a particular bacterium. It can be determined from broth dilution MIC tests by subculturing to agar plates that do not contain the test agent. The MBC is identified by determining the lowest concentration (mg/L) of antibacterial agent that reduces the viability of the initial bacterial inoculum by ≥ 3.0 $\log_{10}$ CFU/ml. MBC tests use colony-forming units (CFU) as a measure of bacterial viability. This means the test can be confounded by antibacterial agents which cause aggregation of bacterial cells (Wiegand and others 2008).

Previous studies with solubilized chitosan, chitosan nanoparticles, and copper loaded chitosan nanoparticles against *E. coli* showed MIC to be highest for solubilized chitosan and lowest for copper loaded chitosan particles (Kong and others 2010). MBC showed similar results. These conclusions should be reconfirmed in this study as components of loaded nanoparticles should work synergistically to inhibit microbial growth lowering MIC and MBC.

2.8.2.4 Antimicrobial Mechanisms

2.8.2.4.1 Chitosan

Small nanoparticles can penetrate through the cell wall of bacteria and combine with DNA to inhibit synthesis of mRNA and DNA transcription (El-Baroty and others 2010). Larger nanoparticles may interact with cell surfaces instead and alter cell permeability forming an impermeable layer around the cell which blocks the transport of essential solutes into the cell. Age of the cell can influence antimicrobial efficiency due to changes in cell surface electronegativity, leading to susceptibility of cells towards chitosan and other antimicrobials compounds. Once the cells lose their protection of the cell wall, the cell membrane is left unguarded with membrane permeability altered. Additional interactions will denature membrane proteins and initiate penetration into the phospholipid bilayer. Thus, increased membrane permeability leads to destabilization of cell membrane and leakage of intracellular substances and ultimately, death of cells. The sequence of events that leads to antimicrobial efficacy by chitosan and chitosan nanoparticles is as follows: adsorption onto the bacterial cell surface, diffusion through the cell wall, adsorption onto the cytoplasmic membrane, disruption of the cytoplasmic membrane, leakage of the cytoplasmic constituents, and cell death (Kong and others 2010).

Chitosan and its derivatives can act as antimicrobials against both Gram-negative and Gram-positive bacteria as well as fungi and yeasts (Sadeghi and others 2008; Kong and others 2010). Chitosan nanoparticle prepared by ionic gelation showed high antibacterial activity against Gram-positive organisms. Particularly, *E. coli* had the

highest MIC and MBC of all organisms at 0.25 μg/ml and 1 μg/ml, respectively (Qi and others 2004).

2.8.2.4.2 *Trans*-cinnamaldehyde

In vitro studies have demonstrated antibacterial activity of essential oils such as TC against *L. monocytogenes* and *E. coli* O157:H7. Overall, Gram-negative organisms are less susceptible than Gram-positive bacteria to essential oils having MICs of 0.05–5 μl/ml. Gram-negative organisms are less susceptible to antimicrobials due to their outer hydrophilic membrane surrounding the cell wall which limits diffusion of hydrophobic compounds through its lipopolysaccharide covering (Hyldgaard and others 2012). A higher concentration of antimicrobial is needed to achieve the same effect in foods. Studies with fresh meat, fish, dairy products, vegetables, and fruit have shown that the concentration needed to achieve a significant antibacterial effect is around 0.5–20 μl/g in foods and about 0.1–10 μl/ml in solutions for washing fruit and vegetables (Burt 2004). Cinnamon bark has also shown significant inhibitory activity against selected strains of bacteria and fungi with MIC from 20 to 120 μg/ml (El-Baroty and others 2010). Overall, the essential oil from cinnamon is more potent than other tested plant extracts, such as *Azadirachta indica* and *Syzygium aromaticum* (Rao and Gan 2014). Gomes and others (2011) found the MIC of PLGA-TC on *Salmonella* and *Listeria* to be 10 mg/ml and 20 mg/ml respectively. The test concentration per well ranged from 20,000 to 20 μg/ml of nanoparticle.

The mode of antibacterial action of TC likely involves action against several targets in the bacterial cell. The hydrophobicity of TC enables it to partition in the lipids

of the cell membrane and mitochondria, rendering them permeable and leading to leakage of cell contents. Extensive loss of cell contents or the exit of critical molecules and ions will lead to eventual death (Burt 2004).

Additional studies have shown that TC does not necessarily disintegrate the outer membrane or deplete the intracellular ATP pool. Thus, researchers believe the carbonyl group of TC may bind to proteins and prevent the action of amino acid decarboxylases in microorganisms. These reactive aldehyde groups will cross-link covalently with DNA and proteins through the amine groups disturbing normal function. Hyldgaard and others (2012) describe cinnamaldehyde‘s antimicrobial mechanism as inhibiting enzymes involved in cytokinesis and cellular functions, acting as an ATPase inhibitor, and perturbing cell membranes.

3. METHODOLOGY

3.1 Introduction

This chapter focuses on the methodologies used to synthesize and characterize *trans*-cinnamaldehyde loaded chitosan-alginate nanoparticles. Nanoparticles were optimized for smallest particle size and maximum encapsulation efficiency by evaluating several processing parameters in a "preliminary" stage study. Upon completion of this stage, a parent methodology was developed with optimized processing parameters and design constrains. *Trans*-cinnamaldehyde loaded chitosan-alginate nanoparticles (LCA-NP) were synthesized with this final methodology and further characterized.

3.2 Materials

The essential oil *trans*-cinnamaldehyde (TC) (93%) was of food grade quality and purchased from Sigma Aldrich Co. (St. Louis, MO). Low molecular weight chitosan (10-120 kDa, 90% deacetylation) and low viscosity sodium alginate (10-100 kDa, M/G = .6) were ordered from Spectrum Chemical (New Brunswick, NJ). Tryptic soy agar (TSA), tryptic soy broth (TSB), peptone water (PW), modified oxford medium (MOX), and tryptose phosphate broth (TPB) for bacterial growth and enumeration were ordered from Becton, Dickinson and Co. (Sparks, MD). 2,2-diphenyl-1-picrylhydrazyl (DPPH) for free radical scavenging potential tests was purchased from VWR (Chicago, IL). HPLC grade acetonitrile (99.8%, FW 41.05) was purchased from VWR (West Chester, PA). All other chemicals including Tween 20®, acetic acid, trehalose, calcium chloride,

sodium phosphate dibasic, sodium phosphate monohydrate**,** and sodium chloride were of analytical grade.

3.3 Preliminary Study

The framework used to build a final nanoparticle synthesis methodology was based primarily on observational stability testing, particle size analysis, and entrapment efficiency (EE) tests. Through these tests, the best overall processing parameters and design constraints were determined. All testing was carried out at varying concentrations and combinations of alginate, chitosan, and TC at different pH ranges to determine a base model formulation. All initial model parameters were adapted from existing literature (Gupta 2011; Manish and Kulkarni 2012; Mohanraj and Chen 2006; Rajaonarivony and others 1993; Sinjan and Robinson 2003). Once the base model for alginate to chitosan mass ratio was identified at the proper pH range (highest EE and lowest particle size), additional processing parameters such as syringe gauge size, homogenization time, equilibration time, calcium chloride concentration, and TC loading volume were improved and optimized (Das and others 2010).

3.3.1 Observational Stability Study

Observational tests were simple, rapid lab techniques used to determine stability of a nanoparticle sample. Observational methods were graded in three distinct categories: transparency, precipitation, and aggregation. Transparency was recorded as opaque (O), translucent (TL), or transparent (TP). A 5 mW laser was passed through samples in a dark room. Nanoparticle samples with good stability were recorded as translucent or some light being refracted through the sample. Nanoparticle samples with

poor stability were recorded as opaque or transparent (Li and others 2008). Aggregation (A) was considered to be white cloudiness or clumping of particles normally centralized in a sample. Precipitation (P) was considered the cloudy or clumped particles which had fallen out of suspension to the bottom of the sample solution. Any solution showing aggregation or precipitation was considered a poor working sample. Thus, in order for a nanoparticle sample to be considered stable and workable, the sample must have shown translucence and no signs of precipitation or aggregation at 0 and 24 h post synthesis. Laboratory trials showed that a stable and workable sample will have an increased shelf life, will not obstruct expensive filtration membranes, will not lose particles and entrapped TC during filtration, will have lower average particle size, and will have more homogenous morphology.

3.3.1.1 pH Testing

The first design parameter tested was the pH value of alginate and chitosan at varying mass ratios of alginate to chitosan. Initially, the pH of alginate was set to 5.5 while chitosan pH was set to 5.3 (Sinjan and Robinson 2003; Li and others 2008). Observations about clarity, precipitation, and aggregation of final nanoparticle solution helped to determine formulation stability. Stable nanoparticle (TL) formulations would continue to be optimized while nanoparticle formulations showing O, TP, P, or A would be eliminated from future synthesis. The pH of alginate and chitosan was changed to 4.9 and 4.6 respectively for varying mass ratios of alginate to chitosan to determine pH effect on stability (Gupta 2011; Thwala 2012; Sarmento and others 2007; Sarmento and others 2006). Observational tests were completed at this pH range. The three most

stable mass ratios (TL, no A, no P) were then tested for particle size and EE to determine the best overall mass ratio. This mass ratio formulation (smallest particle size/highest EE) was considered the most stable, workable formulation and would undergo further process modification and optimization (Figure 3.1).

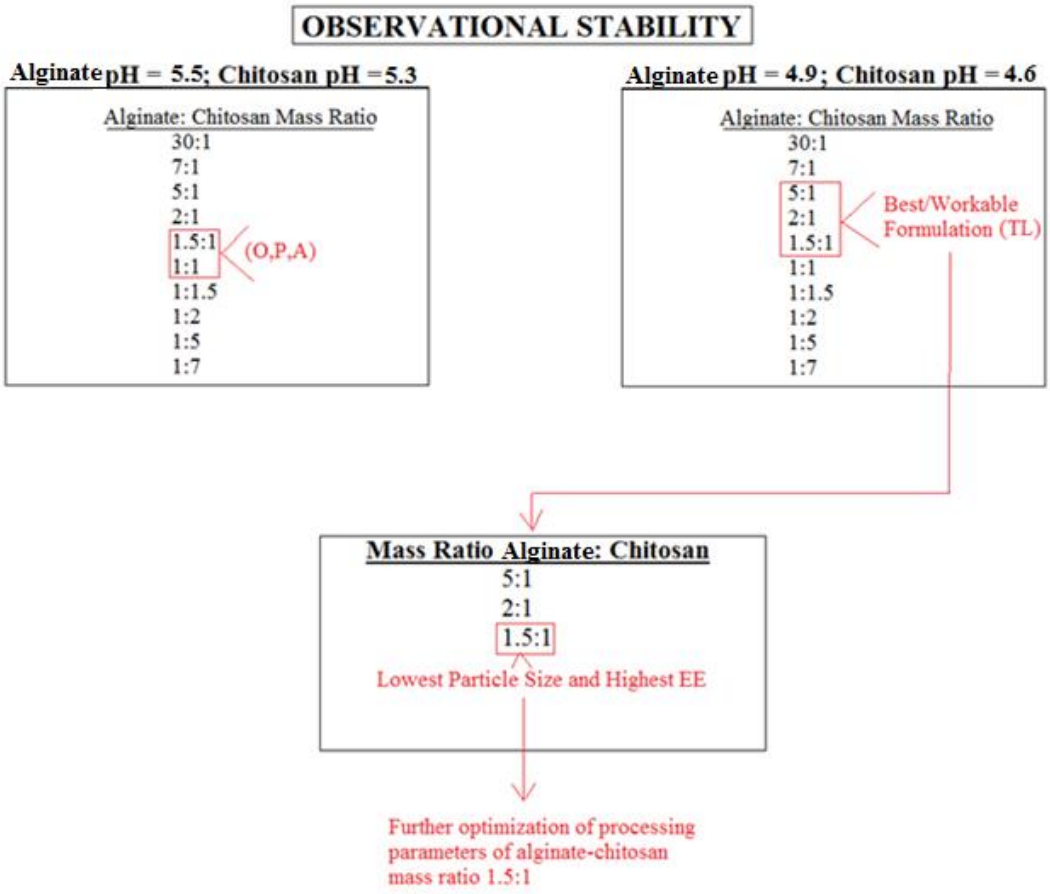

Figure 3.1. Example of observational stability roadmap to determine best combination of chitosan-alginate mass ratio at different pH ranges.

3.3.2 Processing Parameters

The following processing parameters were modified for the best working formulation from the observational stability and pH testing: (1) calcium chloride concentration, (2) TC encapsulant volume, (3) stirring time, (4) syringe size, (5) homogenization time, and (6) equilibration time. The initial methodology was adapted from Rajaonarivony and others (1993) and Sinjan and Robinson (2003). Only one variable was changed per formulation with all other processing constraints held constant (Figure 3.2). Changing one processing parameter yielded one unique nanoparticle formulation. Particle size and EE tests were carried out to compare formulations within batches. The best formulation from within a processing parameter batch (smallest particle size/highest EE) was considered an optimal formulation (Figure 3.3). All modified/optimized processing parameters from discrete batches were then consolidated and extrapolated into one final working formulation.

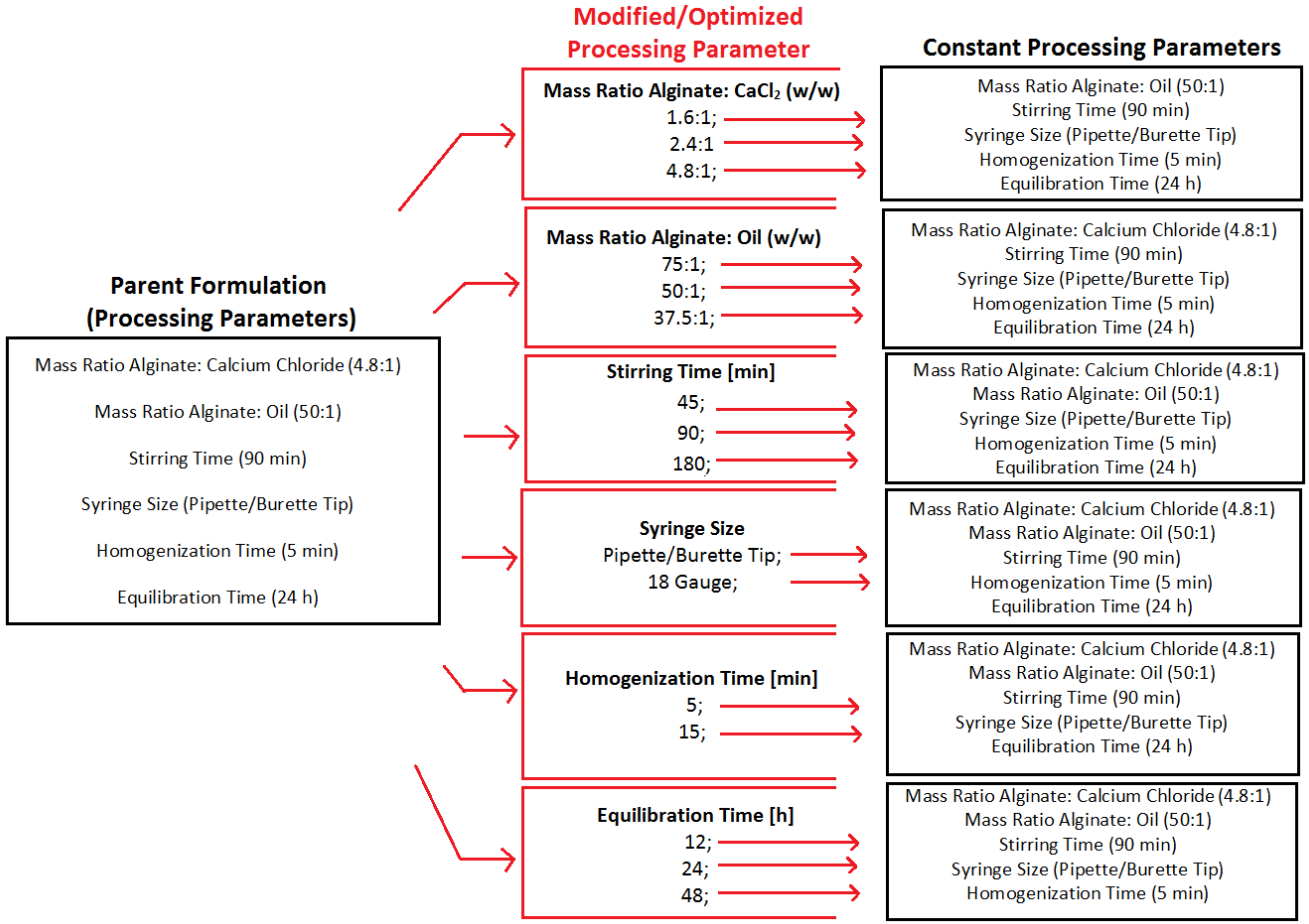

Figure 3.2. Schematic representation of processing parameter modification and optimization with respect to constant parent formulation.

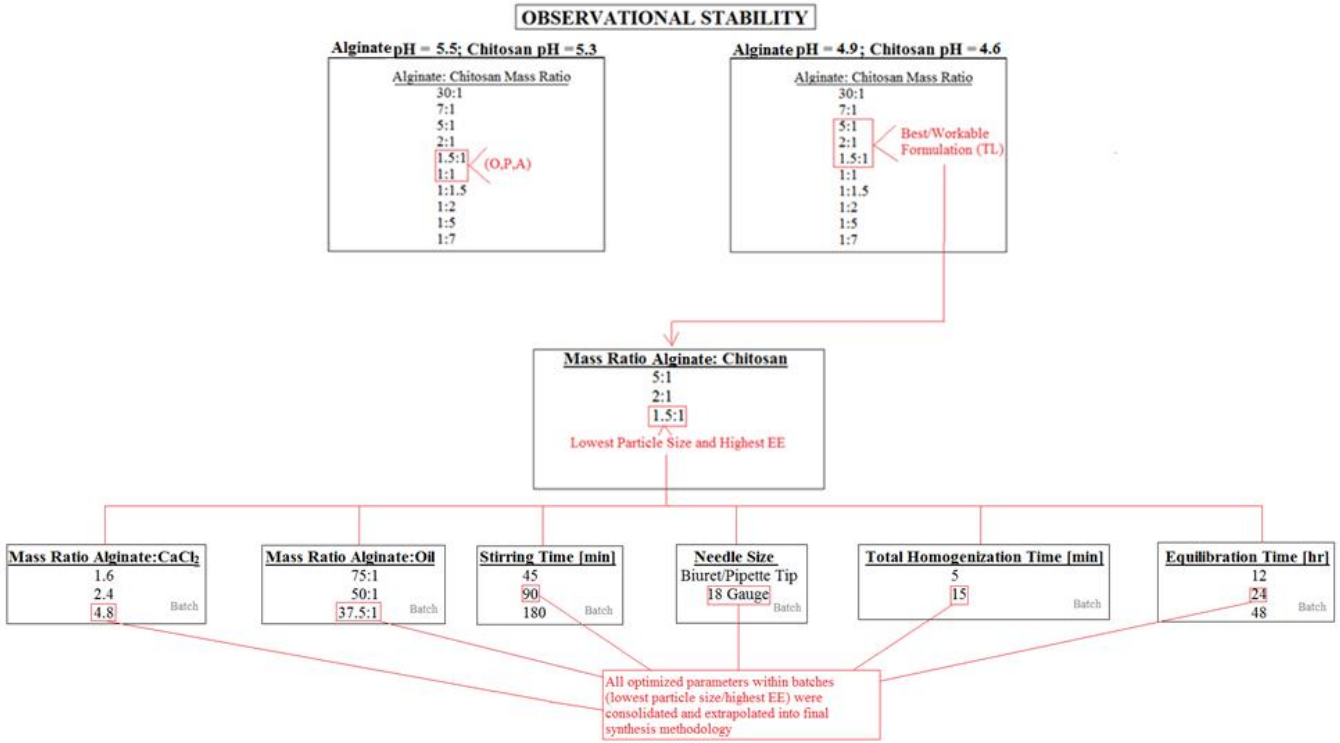

Figure 3.3. Example of observational stability/processing parameter roadmap to determine pH, alginate to chitosan mass ratio, and optimized processing parameters for use in final synthesis methodology.

3.4 Final Methodology

The following methodology was based on work from Sinjan and Robinson (2003), Rajaonarivony and others (1993), Gupta (2011), Li and others (2008), Das and others (2010) and modified accordingly (Figure 3.4).

3.4.1 Sample Preparation

3.4.1.1 Alginate 0.06% (w/v)

0.15 g of sodium alginate (Food Grade, $(C_6H_7NaO_6)_n$, low viscosity, M/G = .6) were added to 250 ml volumetric flask. Added slightly less than 250 ml of 0.2 µm filtered water (Nalgene Filtration Products, 50 mm filter) and stirred for 4-6 h until fully dissolved to obtain a 0.06% (w/v) alginate solution. Filtered sodium alginate solution using vacuum filtration unit (VWR, Filter Flask 1000 ml, 40/35 inner joint) and qualitative filter paper (VWR, Filter Paper 5.5 cm, 10 µm particle retention). Added approximately 1.25 ml of Tween 20® (Fischer Scientific, Polyoxyethylene-20 sorbitan monooleate) and stirred 4-6 h until solution appeared homogenous. Volume and pH were adjusted to 250 ml and 4.9, respectively, in volumetric flask by adding 4-8 drops (transfer pipette) of 0.5 N HCl and 0.2 µm filtered water. This method was a combination of methods as stated previously.

3.4.1.2 Chitosan 0.05% (w/v)

0.1 g of chitosan (Food Grade, $(C_6H_{11}NO_4)_n$, 90% deacetylated) were added to 200 ml volumetric flask. Added slightly less than 200 ml of 0.2 µm filtered water and stirred for 1 h to obtain a 0.05% chitosan solution. Added 0.952 ml acetic acid (Glacial, FW 60.05) and stir for 4-6 h. Filtered chitosan solution using vacuum filtration unit and

qualitative filter paper. Volume and pH were adjusted to 200 ml and 4.6 respectively in volumetric flask by adding 6-8 drops of 5N NaOH and 0.2 µm filtered water. This method was a combination of methods as stated previously.

3.4.1.3 Calcium Chloride 0.2% (w/v)

0.2 g calcium chloride (Food Grade, Anhydrous, FW 110.98) were added to 100 ml volumetric flask. Added 100 ml of 0.2 µm filtered water and stirred for 2-4 h to obtain 0.2% (w/v) calcium chloride solution. This method was a combination of methods as stated previously.

3.4.2 Ionotropic Gelation and Polyelectrolyte Complexation

Trans-cinnamaldehyde (93%, FW 132.16) was dissolved in an acetonitrile/water mixture (1:1, 2 mg/ml) and vortexed for 10-20 s (Das and others 2010; Zohri and others 2011; Li and others 2008). Two ml of this solution was added drop-wise with adapted burette-syringe (PrecisionGlide, 18 gauge syringe attached to 50 ml burette with stopper) into the previously prepared 250 ml pH adjusted (4.9) sodium alginate solution and stirred for 90 min. 15.625 ml of 0.2% (w/v) calcium chloride solution (i.e. previously prepared) was then added drop-wise with adapted burette-syringe into TC-incorporated sodium alginate to form pre-gel (ionotropic gelation) (Figure 3.4). Pre-gel was stirred for 90 min and sonicated (Cole Parmer 8890, Vernon Hills, Ill., USA) for three cycles of 5 min (Zohri and others 2011). 200 ml of pH adjusted (4.6) chitosan solution (i.e. previously prepared was added drop-wise with adapted burette-syringe into the TC-incorporated calcium-alginate pre-gel (PEC) (Figure 3.5). Resulting solution was stirred for 90 min (Figure 3.6).

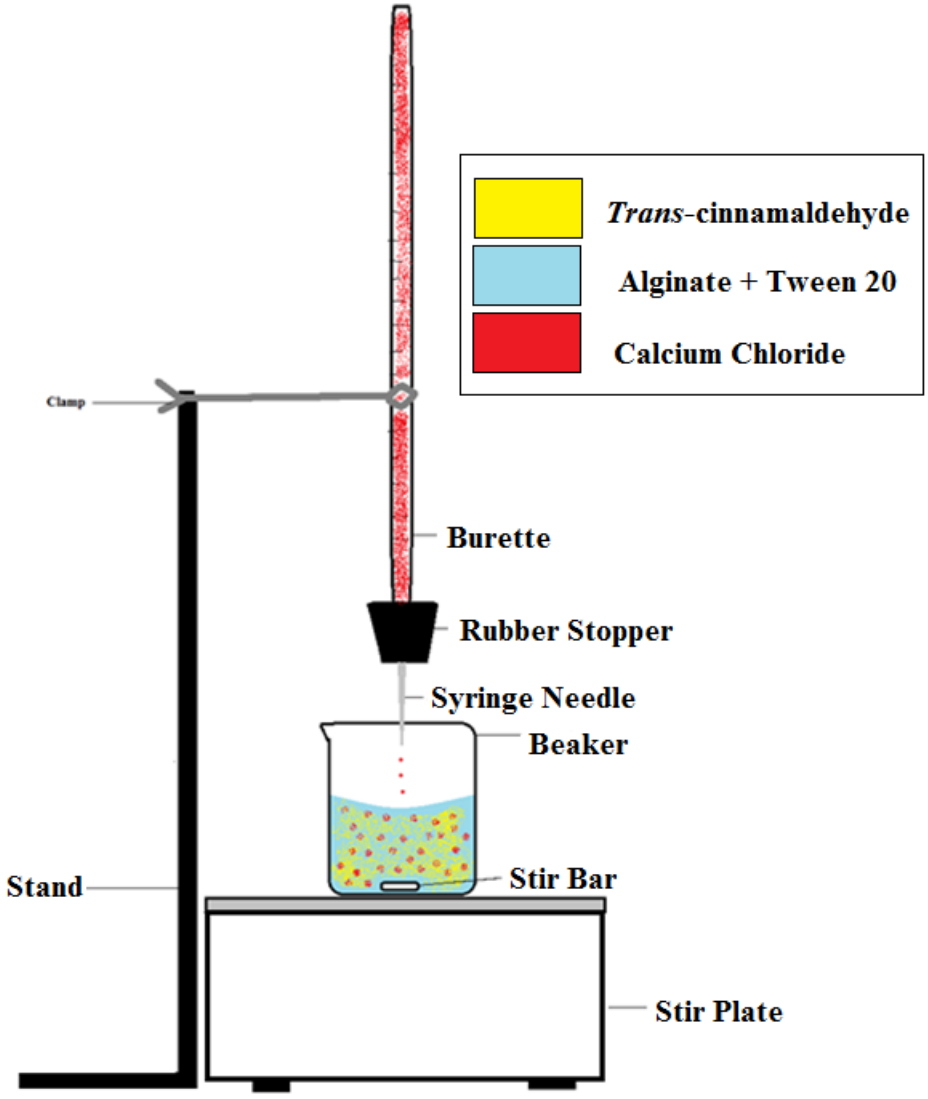

Figure 3.4. Diagram illustrating the preparation of calcium alginate pre-gel with incorporated *trans*-cinnamaldehyde by ionotropic gelation.

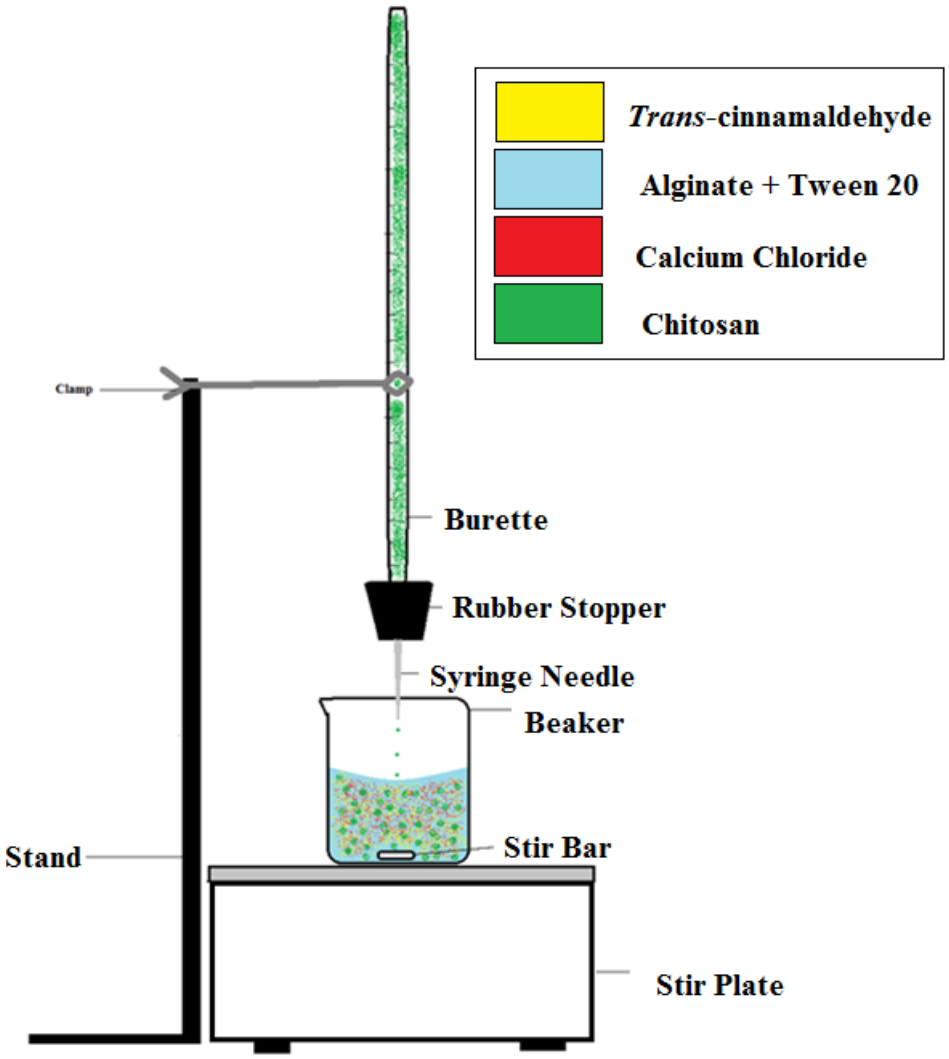

Figure 3.5. Diagram illustrating the addition of chitosan to calcium-alginate pre-gel with incorporated *trans*-cinnamaldehyde to form nanoparticles by polyelectrolyte complexation.

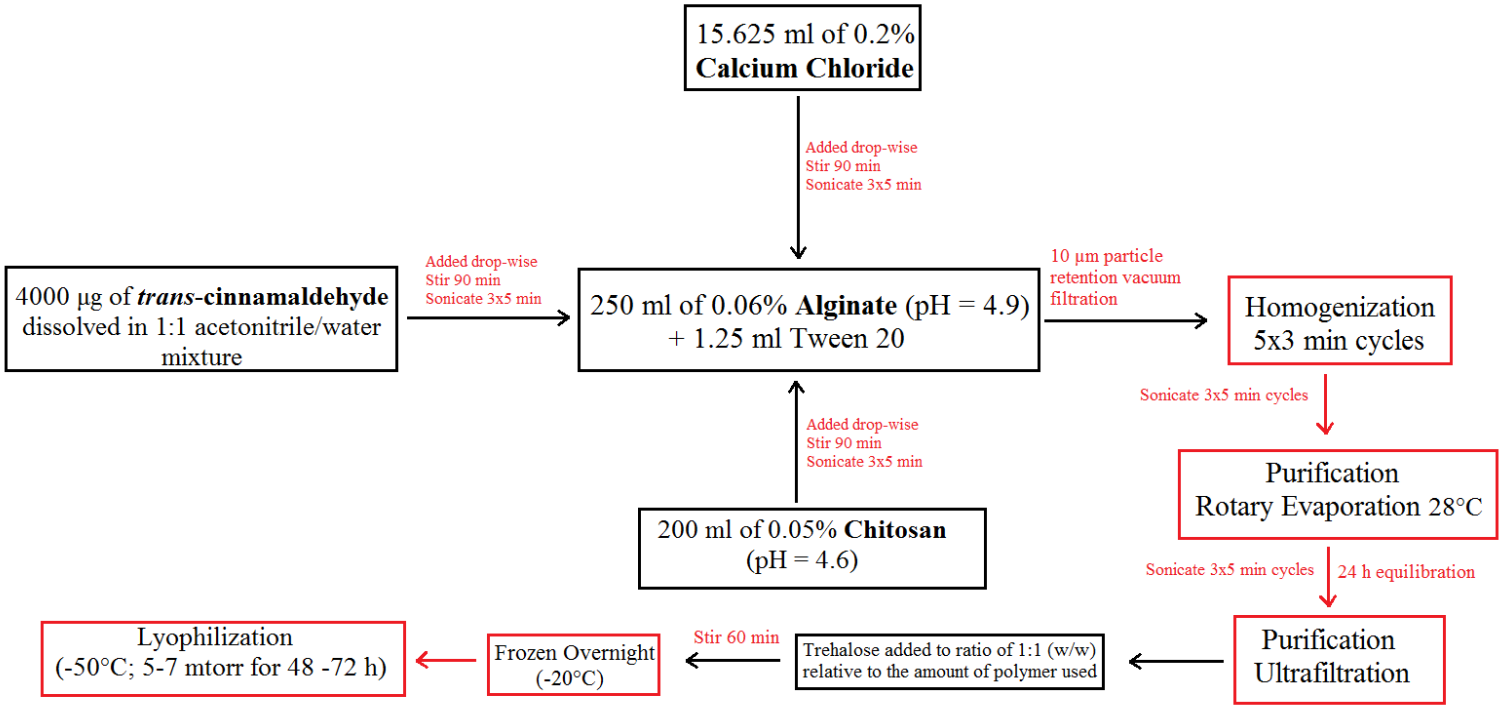

Figure 3.6. Schematic representation of final methodology.

3.4.3 Homogenization, Purification, and Filtration

Nanoparticles were homogenized at high RPM (21500 RPM, Ultra-Turrax T25 Basic IKA-Works Inc., Wilmington, NC) in five 3 min cycles to prevent suspension overflow due to shearing of Tween 20®. Any sample remaining on the homogenizer shaft was rinsed into sample using 0.2 μm filtered water. Sonicate sample for three cycles of five minutes using ultrasonic bath (Cole Parmer 8890, Vernon Hills, Ill., USA). Any trace acetonitrile was then removed from sample by a rotary evaporator. Nanoparticle suspension was heated to 28°C under vacuum (40-50 torr, Heidolph Laborota 4001 with Lauda K-4R Heating/Cooling System, Elk Grove Village, IL). Suspension was allowed to settle and equilibrate overnight allowing full PEC to take place (24 h).

Following volatile evaporation, nanoparticle suspensions were purified via ultra-filtration to remove excess of surfactant Tween 20®, large aggregates, and TC. Samples were sonicated in three cycles of 5 min prior to ultrafiltration. Sample volume to be filtered was recorded. A Millipore-Labscale™ TFF system equipped with a 50 kDa cutoff Pellicon XL-Millipore (Biomax 50, 50 cm^2 membrane, Millipore Co., Kankakee, Ill., U.S.A.) was used. Inlet pressure was 40 psi and outlet pressure was maintained below 10 psi. Ultrafiltration took place with an initial 300 ml volume and sample was collected when approximately 50 ml was remaining in the retentate column. Retentate was transferred to a 100 ml beaker and 0.2 μm filtered water was used to gather all remaining retentate in column. Trehalose (Calbiochem, Dihydrate, FW 378.3) was added to retentate nanoparticle suspension at a ratio of 1:1 (w/w) relative to the amount of

nanoparticles and stirred for 1 h. Sample was then transferred into a 250 ml glass Pyrex container and sealed with lid. Post ultrafiltration, nanoparticles were frozen overnight at -20°C in a freezer (Frigidaire FRT21, Electrolux Home Products, Augusta, GA) (Hill and others 2013a).

3.4.4 Lyophilization

After retentate was frozen, the Pyrex lid was replaced with permeable cloth and wrapped with an elastic band. Frozen retentate was placed into a freeze dryer (Labconco Freeze Dry-5, Kansas City, MO) at -50°C under 5-7 mtorr (9.67×10^{-5} psi) for 48 -72 h to sublimate all moisture from nanoparticles. Samples were removed from the freeze dryer and weighed out. Lyophilized samples were stored in an air tight container in a freezer (-20°C) (Frigidaire FRT21) until further use (Astete and others 2009; Hill and others 2013a).

3.5 Characterization Methodologies

3.5.1 Introduction

Food nanotechnology is an expanding field in which new technologies are being used to characterize nanostructures. Physical characterization such as visualization, scaling, and morphology are now possible due various techniques and instruments for imaging and detecting. Similarly, new and conventional thermal and chemical characterization techniques are available to characterize nanostructures. Thus, the advent of new techniques and instruments in tandem with new nanostructures makes the selection of these instruments and methods critical to allow for standardization of methods across this field (Tiwari and Takhistov 2012). The following tests were

conducted to physically characterize the LCA-NP: (1) particle size analysis, (2) physical yield percentage, (3) encapsulation efficiency, (4) thermal analysis, (5) a controlled release test, (6) and surface characterization.

3.5.2 Particle Size Analysis

Particle size measurements were obtained for LCA-NP by dynamic light scattering (DLS) in a Malvern Nanoseries ZetaSizer (Nano–ZS90, 633 nm He-Ne 200). For measurements, 200 µg of resuspended lyophilized LCA-NP in 2 ml of 0.2 µm filtered water was allowed 3-6 hours to fully dissolve large aggregates. Resuspended particles were vortexed for 20 s, sonicated for 15 min, vacuum filtered (10 µm particle retention), and sonicated again for 5 min immediately before transferring to plastic cuvettes (1 cm path length, disposable polystyrene) and placed in analyzer. Analysis was performed at a scattering angle of 90°, refractive index of 1.590, and temperature of 25°C. For each LCA-NP sample, the mean diameter and standard deviation of 100 iterations was performed in triplicate. Particle size was read in terms of z-average size (intensity) (Gomes and others 2011; Hill and others 2013a; Sinjan and Robinson 2003).

3.5.3 Yield Analysis

All nanoparticle samples were weighed after lyophilization. Physical percent yield (w/w) of nanoparticles was calculated from the weight of dried nanoparticles recovered (W_1) and the sum of the initial dry weight of starting materials (W_2). This yield of LCA-NP was determined according to the following equation (Dudhani and Kosaraju 2010):

$$Yield\ (\%) = \frac{W_1}{W_2} \times 100 \qquad (3.1)$$

3.5.4 Encapsulation Efficiency

For each nanoparticle sample, 5 mg of LCA-NP was dissolved in 5 ml of 95 g/100 ml acetonitrile and mixed thoroughly. The suspension was left for 48 h under constant agitation in dark area to allow for enough time for all entrapped TC to be available in solution. Samples were vortexed for 10 s, filtered with 0.2 µm membrane, and measured in a UV-Visible spectrophotometer (Genesys 10S UV-Vis, Thermo Scientific, Madison, WI) at 280 nm in triplicate. Encapsulation efficiency (EE) was determined according to the following equation (Gomes and others 2011; Hill and others 2013a):

$$EE\ (\%) = \frac{amount\ of\ active\ compund\ entrapped}{inital\ active\ compound\ amount} \times 100 \qquad (3.2)$$

where the ―amount of active compound entrapped" is the compound (TC) amount present in the particles and the ―initial active compound amount" indicates the compound (TC) amount initially used to manufacture the particles (Hill and others 2013a).

A standard calibration curve was obtained for TC between 0.93 µg/ml and 4.65 µg/ml and followed the equation y = 4.294x (R^2 = .975) (Appendix 1). ―Amount of

active compound entrapped" was determined by substituting the absorbance value of the LCA-NP read from the spectrophotometer into the x-value of the calibration equation. This yields the y-value (i.e., TC concentration). Samples were diluted with acetonitrile for proper spectrophotometric readings when necessary.

3.5.5 Controlled Release

0.15M phosphate saline buffer (PBS, .85% NaCl) was prepared by mixing two separate stock solutions. Solution 1 was dibasic composed of 21.3 g/L sodium phosphate dibasic (Na_2HPO_4, anhydrous, FW 141.96) and 8.5 g/L sodium chloride (NaCl, crystalline, FW 58.44) while solution 2 was monobasic composed of 20.7 g/L sodium phosphate monohydrate ($NaH_2PO_4*H_2O$, anhydrous, FW 137.99) and 8.5 g/L sodium chloride. Solution 2 was added to solution 1 until pH 7.4 was obtained.

36 mg of LCA-NP was weighed in a beaker and 36 ml of phosphate buffer (pH 7.4) was added. The suspension was stirred with a magnetic stirrer until homogenized. From this suspension, 1 ml was added to an eppendorf vial (in triplicate). Eppendorfs were placed in a 35°C bath with constant agitation. Eppendorfs were removed from the bath, vortexed for 10 s and filtered with 0.2 μm membrane measured in a UV-Visible spectrophotometer (model Genesys 10S UV-Vis, Thermo Scientific, Madison, WI) at 280 nm in triplicate at predetermined times of 15 min, 30 min, 45 min, 1 h, 1.5 h, 2 h, 4 h, 8h, 12 h, 24 h, 48 h, and 72 h. Samples were diluted with acetonitrile for proper spectrophotometric readings when necessary. Release at preset times was determined using the same calibration curve as entrapment efficiency testing (Appendix 1).

Cumulative release percentage was calculated using the equation below (Das and others 2010; Xing and others 2010):

$$Cumulative\ Release\ (\%) = \frac{Released\ TC}{Total\ TC} \times 100 \qquad (3.3)$$

3.5.6 Differential Scanning Calorimetry

Differential scanning calorimetry (DSC) was performed using a Perkin-Elmer DSC 6 with ISOTEMP 1028P (Fischer Scientific, Pittsburg, PA) with an integrated cooling system (Pyris 5 Software, Boston, MA). Lyophilized samples (~2 mg) and control samples (i.e. empty crimped pan) were weighed to the nearest 0.1 mg and were added into hermetically sealed and crimped 20 µl aluminum pans with one hole in the lid. Scanning of samples was completed at a rate of 10°C/min from 25°C to 350°C with temperature maintained for 1 min at 350 °C with nitrogen purging at 20 ml/min. An empty loosely covered aluminum pan was used as the reference or blank. Calibration was completed using zinc and indium metals prior to sample testing. Each sample was run twice (Sarmento and others 2006; Hill and others 2013a).

3.5.7 Transmission Electron Microscopy

Surface morphology of particles was visualized using a FEI Morgagni Transmission Electron Microscope (FEI Company, Hillsboro, OR) at the School of Veterinary Medicine and Biomedical Sciences at Texas A&M University (College Station, TX) using a negative staining technique. 100 µg of lyophilized nanoparticles were resuspended in 2 ml of 0.2 µm filtered water and sonicated for 10 min. Samples

were kept at 4°C for about 3 hours. 600 µl of this sample in ethanol was mixed with 600 µl water. 1.4 µl of suspension was applied directly to carbon film (300 mesh Cu/Ni grid filmed with carbon) and incubated for 4 min in humid area. Stains were cleaned with a 60 s glow at 5 mA. Excess fluid was wicked off slowly with filter paper. 180 µl of 2% phosphotungstic acid (pH 7, FW 2880.05) or 0.2% uranyl acetate (FW 424.14, EMS, Hatfield, PA) was dripped onto grid surface tilted at 45°. Excess stain was wicked off slowly with filter paper and grids were air dried. Backs of grids were washed off with water, wicked again, and dried a final time. Viewing took place at 2,200 to 140,000 x magnification, 32 to 2024 pixels per µm, and 80 kV (Astete and others 2009; Hill and others 2013a; Hill and others 2013b; Dudhani and Kosaraju 2010).

3.5.8 Antioxidant Capacity in Apple Juice

The method used to measure antioxidant capacity in this study was the 1,1-Diphenyl-2-picrylhydrazyl (DPPH) test (Chien and others 2007; Fathi and others 2013)**.** Clear, ultra-high-temperature processed, shelf stable apple juice with no additional preservatives was purchased from a local retailer (HEB, College Station, TX). 5 ml of resuspended LCA-NP was added to 45 ml of apple juice in a 250 ml Erlenmeyer flask to obtain working concentrations of 0.1 to 1 g/L of LCA-NP in apple juice. A control flask was prepared using 5 ml of water instead of LCA-NP or ULCA-NP in apple juice. 100 µM DPPH solutions in methanol were prepared and 1 ml of this solution was added to 4 ml of the LCA-NP working concentrations in apple juice. Samples were agitated and incubated for 30 min at room temperature in a dark area. Samples were vortexed for 20 s and filtered with a 0.2 µm filter. The absorbance of the resulting solution was read at 517

nm against a blank. The inhibitory percentage of DPPH was calculated according to the following equation (Chien and others 2007):

$$Scavenging\ effect\ (\%) = \left(1 - \frac{absorbance_{sample}}{absorbance_{control}}\right) \times 100 \qquad (3.4)$$

3.5.9 Minimum Inhibitory and Bactericidal Concentration

Escherichia coli O157:H7 (ATCC 43894) and *Listeria monocytogenes* (ATCC 15313) were obtained from Texas A&M University Food Microbiology Laboratory culture collection (Department of Animal Science, College Station, TX). These strain selections are representative of typical Gram-negative and Gram-positive pathogenic microorganisms commonly occurring in various food products. Both microorganisms were resuscitated in tryptic soy broth (TSB) by identical duplicate transfers and incubated aerobically for 24 h at 35ºC. The bacterial cultures were maintained on tryptic soy agar (TSA) slants at 4ºC for no more than 3 months. Transfers from slants were conducted similarly to the resuscitation method to prepare microorganisms for analysis (Figure 3.7). Pathogen isolates were maintained, revived, and handled under biosafety level (BSL) 2 containment at all times according to Texas A&M University System Institutional Biosafety Committee (IBC) policy.

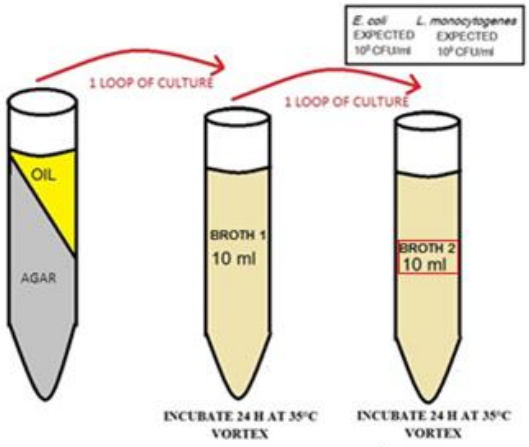

Figure 3.7: Representation of resuscitation and revival of microorganisms from TSA slant.

Minimum inhibitory concentrations (MIC) for nanoparticles and pure TC were determined using an adapted broth dilution assay (Wiegand and others 2008; Brandt and others 2010; Pendleton and others 2012; Gomes and others 2011). Overnight culture (24 h) of *E. coli* O157:H7 and *L. monocytogene*s were individually subjected to serial dilution in 9.0 ml of 0.1% (w/v) peptone water (PW) and then transferred to 9.0 ml of double strength broth (TSB for *E.coli* and TPB for *Listeria*) to obtain 5.0 $\log_{10}$ CFU/ml final concentration for use as inoculum (concentration per well on 96 well plate). *E. coli* O157:H7 and *L. monocytogenes* in double strength broth were serially diluted in 0.1% peptone water (PW) and spread on surfaces of Petri dishes containing sterile TSA and TSA-YE for enumeration of inoculum of each pathogen, respectively. Inoculated TSA and TSA-YE plates were then incubated for 24-48 h at 35°C prior to colony enumeration

(Figure 3.8). Aliquots of 100 µl of all antimicrobial solutions and solvents blanks were spread plated to ensure sterility (Hill and others 2013a; Hill and others 2013b).

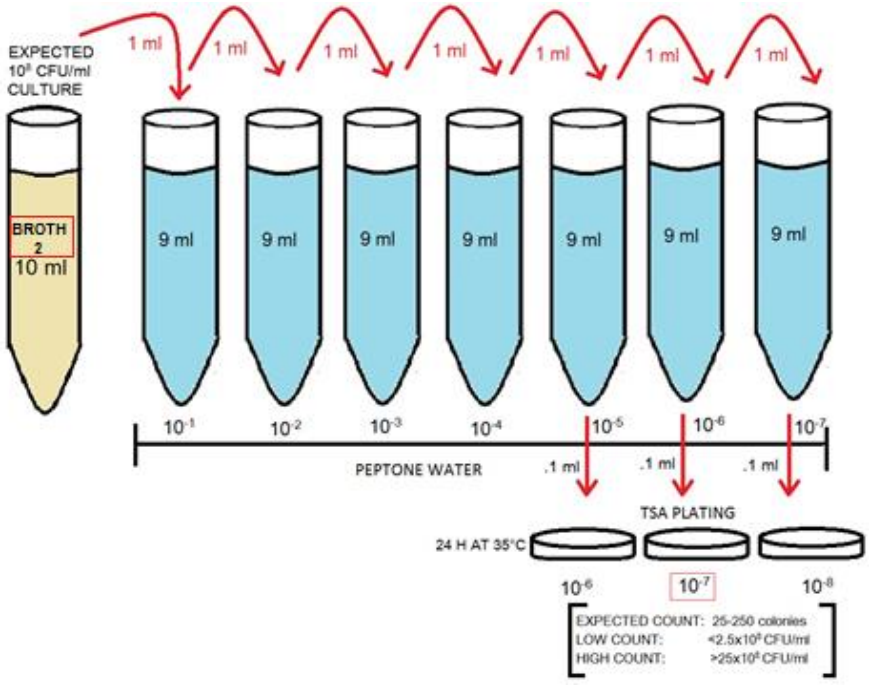

Figure 3.8. Representation of enumeration of selected microorganisms.

MIC analyses were conducted in a 96 well microliter plate (sterilized 300µl capacity, MicroWell, NUNC, Thermo-Fisher Scientific, Waltham, MA). The antimicrobial inclusion complexes were added to the wells as aqueous suspensions, while the TC was added as an aqueous microemulsion containing 1.0 g/100 g acetonitrile and 0.01 g/100 g Tween 20® (Hill and others 2013b). The concentration of LCA-NP added to the test wells ranged from 3,515 – 28,125 µg/ml (365 – 2,920 µg/ml

of TC concentration based on the entrapment efficiency (73%), while the concentration of free TC ranged from 6.25 – 2,000 µg/ml for both pathogens (Figure 3.9). Chitosan concentration ranged from 31.25 - 500 µg /L. Alginate concentration ranged from 18.75 - 600 µg /L. The test compound concentration in literature ranges from 20,000 to 20 µg/mL of nanoparticles (Kalemba and Kunicka 2003; Hill and others 2013b; Hill and others 2013a).

		1	2	3	4	5	6	7	8	9	10	11	12
TREATMENT [Add (100 µl Innoculum 5log CFU/mL + 2XTSB/TPB + (100uL Nanoparticle/Antimicrobial)]	A	LCA-NP [28125 µg/ml]	LCA-NP [14062]	LCA-NP [7031]	LCA-NP [3515]	LCA-NP [1757]	x	LCA-NP [28125]	LCA-NP [14062]	LCA-NP [7031]	LCA-NP [3515]	LCA-NP [1757]	MO + W + 2XTSB
	B	CS [500]	CS [250]	CS [125]	CS [62.5]	CS [31.2]	x	CS [500]	CS [250]	CS [125]	CS [62.5]	CS [31.2]	MO + W + 2XTSB
	C	ALG [600]	ALG [300]	ALG [150]	ALG [75]	ALG [37.5]	x	ALG [600]	ALG [300]	ALG [150]	ALG [75]	ALG [37.5]	MO + W + 2XTSB
	D	TC [1000]	TC [500]	TC [250]	TC [125]	TC [62.5]	x	TC [100]	TC [50]	TC [25]	TC [12.5]	TC [6.2]	MO + W + 2XTSB
CONTROL [Add (100uL 2XTSB/TPB) + (100uL Nanoparticle/Antimicrobial)]	E	LCA-NP [28125]	LCA-NP [14062]	LCA-NP [7031]	LCA-NP [3515]	LCA-NP [1757]	x	LCA-NP [28125]	LCA-NP [14062]	LCA-NP [7031]	LCA-NP [3515]	LCA-NP [1757]	x
	F	CS [500]	CS [250]	CS [125]	CS [62.5]	CS [31.2]	x	CS [500]	CS [250]	CS [125]	CS [62.5]	CS [31.2]	x
	G	ALG [600]	ALG [300]	ALG [150]	ALG [75]	ALG [37.5]	x	ALG [600]	ALG [300]	ALG [150]	ALG [75]	ALG [37.5]	x
	H	TC [1000]	TC [500]	TC [250]	TC [125]	TC [62.5]	x	TC [100]	TC [50]	TC [25]	TC [12.5]	TC [6.2]	x

LEGEND:

*All concentrations are [µg/ml]

LCA-NP: LOADED CHITOSAN ALGINATE NANOPARTICLES
CS: CHITOSAN
ALG: ALGINATE
TC: *TRANS*-CINNAMALDEHYDE

Figure 3.9. Example of 96 well plate setup.

200 µl of double strength antimicrobial solution was loaded into the first well of the specified row. 100 µl of sterile water was added to all remaining wells on specified row (not added to first well) and lastly 100 µl of bacterial inoculum in 2XTSB/TPB was added to all wells on specified row (added to first well) using a multichannel pipette (Brandt and others 2010; Wiegand and others 2008; Pendleton and others 2012). The first well on row (antimicrobial and inoculum) was mixed ten times with a multichannel pipette and 100 µl of this solution was added into the second well of the specified row and mixed ten times (Figure 3.8). Dilutions were completed in this manner for all remaining wells on the row. This transfer procedure continued for 10 of the 12 rows of wells (Gomes and others 2011). Along with each antimicrobial tested, sterilized water blank was used in the same fashion to ensure that the sterilized water (where nanoparticles were suspended) did not have an antimicrobial effect.

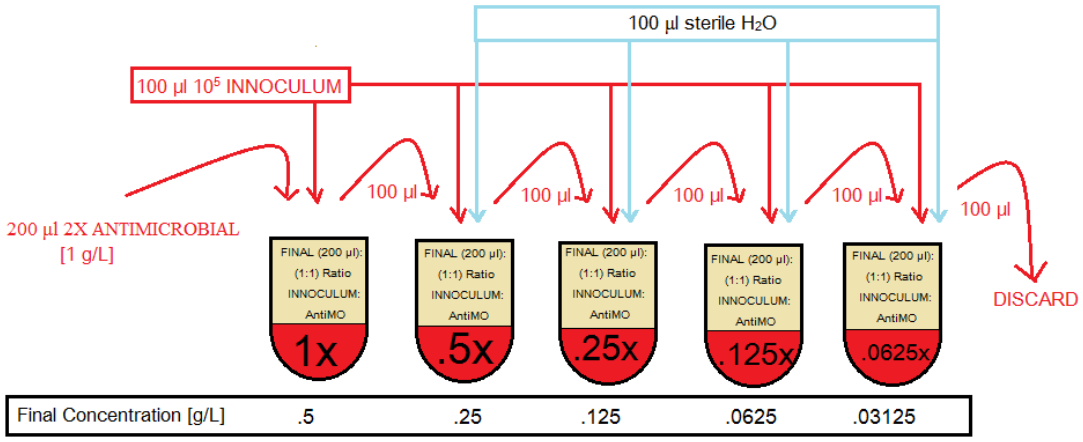

Figure 3.10. Diagram presenting the composition of sample wells with initial components, dilution factor, and final concentration. Positive controls were prepared containing inoculum and sterile distilled water.

Tween 20, free TC, and acetonitrile at test concentrations (combined and singly) to guarantee solvents and additives had no effect on optical density values at 630 nm (OD_{630}) or antimicrobial effect (Hill and others 2013a). The last column acted as a growth control. Negative controls were also prepared with antimicrobial solutions and sterile 2X broth to ensure they were not contaminated. Negative control wells were prepared in the same manner as the treatment wells. Once plates were prepared, they were covered with Mylar plate sealer (Thermo-Fisher Scientific) and OD_{630} of the wells was read (0 h) in Epoch BioTek UV/Vis range spectrophotometer (Bio-Tek® Instruments, Inc., Magellan™ software, Winooski, VT). Plates were incubated at 35ºC and after 24 h another OD_{630} was measured (24 h). Plates were normalized (baseline

adjustment) using the OD_{630} values of the negative controls with the following equations:

$$(0_{hr}OD_{630,\ Treatment}) - (0_{hr}OD_{630,\ Negative\ Control}) = 0_{hr}OD_{630,\ Normalized} \quad (3.5)$$

$$(24_{hr}OD_{630,\ Treatment}) - (24_{hr}OD_{630,\ Negative\ Control}) = 24_{hr}OD_{630,\ Normalized} \quad (3.6)$$

$$(24_{hr}OD_{630,\ Normalized}) - (0_{hr}OD_{630,\ Normalized}) = \Delta OD_{630} \quad (3.7)$$

Any antimicrobial sample well that showed ≤ 0.05 change in OD_{630} was considered ~~"in~~hibited" by the antimicrobial. The lowest concentrations of antimicrobial TC containing nanoparticles producing pathogen inhibition across triplicate identical replications (n=3) were identified as the MIC (inhibited visible growth) for nanoparticle system (Figure 3.9) (Brandt and others 2010; Hill and others 2013b; Gomes and others 2011).

To study the bactericidal activity of nanoparticle solutions after identification of MIC levels of TC-containing nanoparticles, 100 µl of solution from pathogen inhibitory wells were spread on TSA containing Petri plates for *E. coli* and TSA-YE containing Petri plates for *Listeria* (1 TSA/TSA-YE plate prepared per test well) incubated for 24 h at 35ºC. The concentrations of nanoparticles that produce ≥ 3.0 $\log_{10}$ CFU/ml reduction of the *E. coli* or *L. monocytogenes* (plate count of the inoculum minus the plate count on the TSA plate for bactericidal assay) from initial inoculum (5.0 $\log_{10}$ CFU/ml)

were classified as bactericidal. The lowest concentration of nanoparticles over all replications (n=3) were deemed the minimum bactericidal concentration (MBC) (**Figure 3.9**) (Brandt and others 2010; Hill and others 2013b; Gomes and others 2011). *E. coli* O57:H7's identity was confirmed using MacConkey-Lactose agar. *L. monocytogenes* identity was confirmed using MOX and RAPID'L.Mono™(Bio-Rad Laboratories, Inc., Hercules, CA, USA) for *L. monocytogenes*.

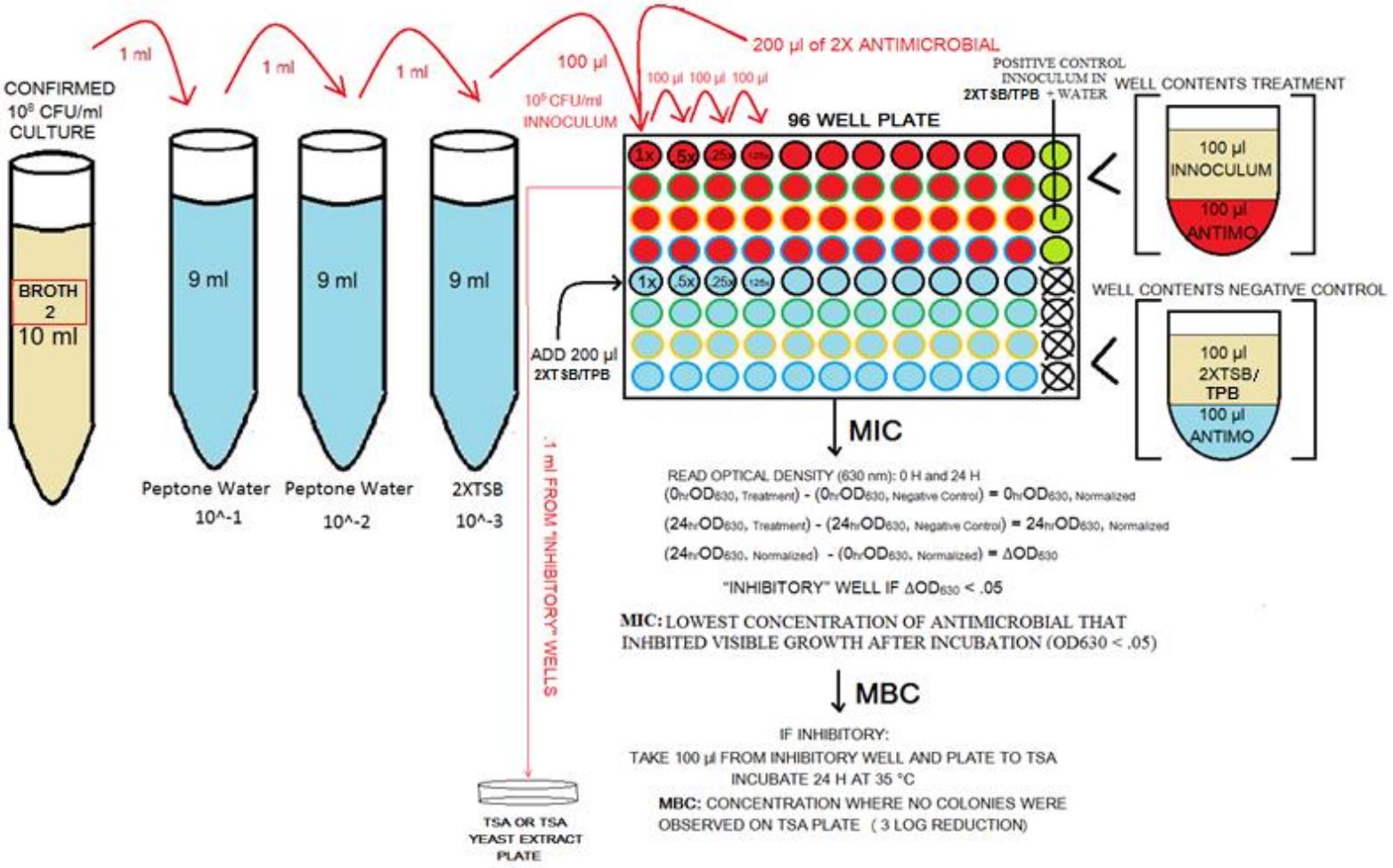

Figure 3.11. Schematic representation of MIC and MBC procedures and 96 well plate setup.

3.6 Statistical Analysis

All experiments were performed in triplicate as independent experiments and data is expressed as mean values ± the standard deviation (SD). Statistical analysis were performed using SigmaPlot v. 11 software (San Jose, CA) with p-value less than .05 considered as an indication of statistical significance. Differences between variables were tested for significance by one-way analysis of variance (ANOVA). Significantly different means ($p < 0.05$) were separated by the Tukey‘s Honestly Significant Differences (HSD) test. Linear regression and analysis of covariance with 95 % confidence interval were used when appropriate.

4. RESULTS

4.1 Introduction

Encapsulation of lipophilic compounds such as *trans*-cinnamaldehyde (TC) into aqueous-soluble nanoparticle systems (i.e. chitosan-alginate) can provide solutions to several problems in the food industry by both improving solubility and providing a controlled way to deliver and release drug payload with full potential. The ionotropic gelation polyelectrolyte complexation method (IG-PEC) is a mild nanoparticle preparation method that was optimized in this research to produce nanoparticles with the highest payload potential at the smallest size.

This chapter focuses on the characterization of loaded chitosan-alginate nanoparticles (LCA-NP) and a brief discussion and interpretation of the findings. This chapter is broken down into the following parts: (1) preliminary study results including (a) observational studies and pH testing, and (b) process parameter optimization (entrapment efficiency and particle size); and (2)characterization results using new extrapolated methodology including (c) cumulative controlled release tests, (d) differential scanning calorimetry, (e) transmission electron microscopy, (f) antioxidant capacity in apple juice, and (g) minimum inhibitory and bactericidal concentration tests.

Optimizing processing parameters of the IG-PEC method will increase the significance of characterizing polymeric nanoparticles. Optimized particle preparation and formulation will assist in future utility of post-processing and food applications such

as the stabilization of lipophilic flavoring agents, shelf life stability, antioxidant and antibacterial potential, and the reduction of unpleasant odors and tastes.

4.2 Preliminary Study

4.2.1 Observational Stability and pH Testing

Table 4.1 and Table 4.2 show the observational results of assembled nanoparticle solutions at varying mass ratios of alginate to chitosan at different pH values. Different nanoparticle samples were recorded by their visible appearance: translucence (TL), precipitation (P), aggregation (A), or opaque coloration (O). The mass ratios of alginate (AG) to chitosan (CS) of 1.5:1 and 1:1 (samples 5a and 6a; pH dispersion 5.4) yield the best observational results due to solution showing TL at 0 h (Table 4.1). However, at 24 h post synthesis, the same nanoparticle solutions showed P, A, and O suggesting that these solutions are only stable for 24 h. Table 4.2 shows nanoparticle solutions of AG:CS mass ratios of 5:1, 2:1, and 1.5:1 (samples 3b, 4b, 5b; pH dispersion 4.7) that are TL at both 0 h and 24 h post synthesis. Thus, these mass ratios were considered the most stable formulations. Examples of unstable formulations post synthesis are shown in Figure 4.1. Laboratory trials revealed that samples that were stable at 24 h post synthesis would remain stable (TL, no A, no P) in solution for up to six weeks (Figure 4.2). Samples that were unstable at 0 or 24 h post synthesis would show substantial P and A after 6 weeks of storage in solution.

Table 4.1. Observational results of varying mass ratios of alginate to chitosan (alginate: $CaCl_2$ mass ratio = 4.8:1, pH alginate = 5.3 pH, chitosan = 5.5).

Sample Number[**]	**Mass Ratio Alginate : Chitosan (AG:CS)**[1]	**0 h**	**24 h**
1a	30:1	O/P/A[*]	O/P/A
2a	7 :1	O/P/A	O/P/A
3a	5:1	O/P/A	O/P/A
4a	2:1	O/P/A	O/P/A
5a**	1.5:1	TL[*]	O/P/A
6a	1:1	TL	O/P/A
7a	1:1.5	O/P/A	O/P/A
8a	1:2	O/P/A	O/P/A
9a	1:5	O/P/A	O/P/A
10a	1:7	O/P/A	O/P/A

[*]O = opaque coloration P =precipitation A = aggregation TL =translucence

[1]Represents the mass ratio (w:w) of alginate to chitosan powder used to formulate nanoparticles.

[**]Values in red text correspond to the best working formulation (translucent and stable). Processing parameters based on parent methodology: mass ratio alginate: calcium chloride (4.8:1), mass ratio alginate: oil (50:1), stirring time (90 min), syringe size (pipette/burette tip), homogenization time (5 min), and equilibration time (24 h).

Table 4.2. Observational results of varying mass ratios of alginate to chitosan (alginate: $CaCl_2$ mass ratio = 4.8:1, pH alginate = 4.6, pH chitosan = 4.9).

Sample Number**	Mass Ratio Alginate : Chitosan (AG:CS)[1]	0 h	24 h
1b	30:1	O/P/A*	O/P/A
2b	7 :1	O/P/A	O/P/A
3b	5:1	TL*	TL
4b	2:1	TL	TL
5b	1.5:1	TL	TL
6b	1:1	TL	O/P/A
7b	1:1.5	TP	TL
8b	1:2	O/P/A	O/P/A
9b	1:5	O/P/A	O/P/A
10b	1:7	O/P/A	O/P/A

*O = opaque coloration P =precipitation A = aggregation TL =translucence

[1]Represents the mass ratio (w:w) of alginate to chitosan powder used to formulate nanoparticles.

**Values in red text correspond to the best working formulation (translucent and stable). Processing parameters based on parent methodology: mass ratio alginate: calcium chloride (4.8:1), mass ratio alginate: oil (50:1), stirring time (90 min), syringe size (pipette/burette tip), homogenization time (5 min), and equilibration time (24 h).

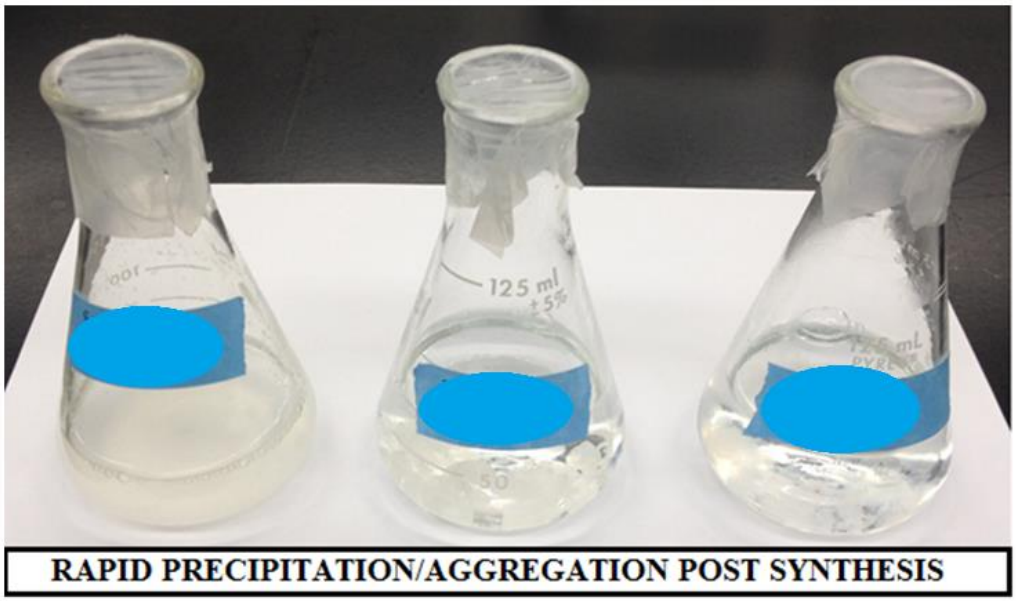

Figure 4.1. Examples of unstable formulations post synthesis (24 h); rapid precipitation (P) and aggregation (A). Disregard sample labels.

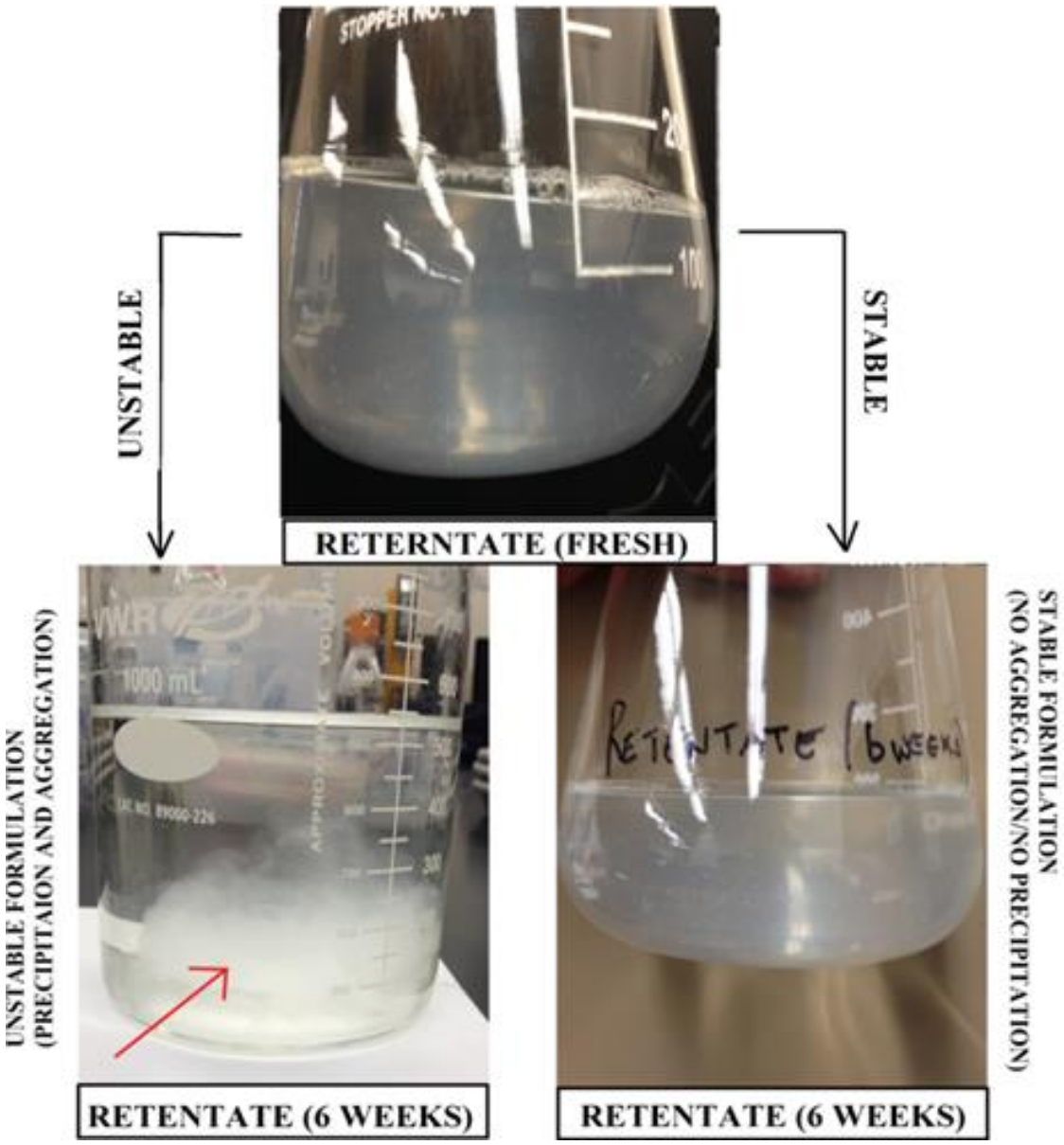

Figure 4.2. Example of fresh retentate stability after 6 weeks in solution.

The most stable mass ratio formulations (3b, 4b, 5b) were then analyzed for particle size and encapsulation efficacy (EE) (Table 4.3). From this table, it can be concluded that the best working formulation was 5b with average particle size of 294.78

nm and 60.61% EE (smallest particle size/highest EE). Average particle size was 21.4% smaller while EE% was 4.9% larger than the next best formulation (4b). All means for particle size of different treatment groups (AG:CS) were statistically significant ($p < 0.05$) while means for EE%, and physical yield percentage were significantly different only for the 5b formulation likely due to wall forming components being in stoichiometric proportion (i.e. no excess polymer forming large particle aggregates). Additionally, means for polydisperity index (PDI) were statistically significant ($p < 0.05$) for formulations 4b and 5b. There is an inverse relationship between particle size and encapsulation efficiency as AG:CS mass ratio decreased (Figure 4.3). This is likely due to water making up the bulk of the nanoparticle matrix at higher concentrations of biopolymer creating an environment that is not favorable to entrap a hydrophobic active molecule. The matrix is also permeable and porous leading to loss of entrapped TC (Singh and others 2007).

Table 4.3. Particle size, encapsulation efficiency (EE), polydisperity index (PDI), and physical yield results for nanoparticles at the three best alginate to chitosan mass ratios at pH alginate = 4.6, pH chitosan = 4.9.

Mass Ratio (AG:CS)[1]	Observations (0 h/24 h)	Particle Size * [nm]	EE%*	Yield%*	PDI
5:1 (3b)	TL/TL	648.08^{a}(28.44)	40.17^{a}(6.55)	51.25^{a}(9.58)	0.84^{a}(0.09)
2:1 (4b)	TL/TL	375.29^{b}(29.91)	57.60^{b}(5.19)	83.36^{b}(5.30)	0.69^{b}(0.03)
1.5:1 (5b)	TL/TL	294.78^{c}(26.30)	60.61^{b}(4.34)	78.86^{b}(2.93)	0.66^{b}(0.04)

*****Values given are averages of three replicate samples; standard deviations are displayed in parenthesis. Values with differing subscripts (within columns) indicate significantly different values ($p < 0.05$). Values in parenthesis are the standard deviation.

[1]Represents the mass ratio (w:w) of alginate to chitosan powder used to formulate nanoparticles. Processing parameters based on parent methodology: mass ratio alginate: calcium chloride (4.8:1), mass ratio alginate: oil (50:1), stirring time (90 min), syringe size (pipette/burette tip), homogenization time (5 min), and equilibration time (24 h).

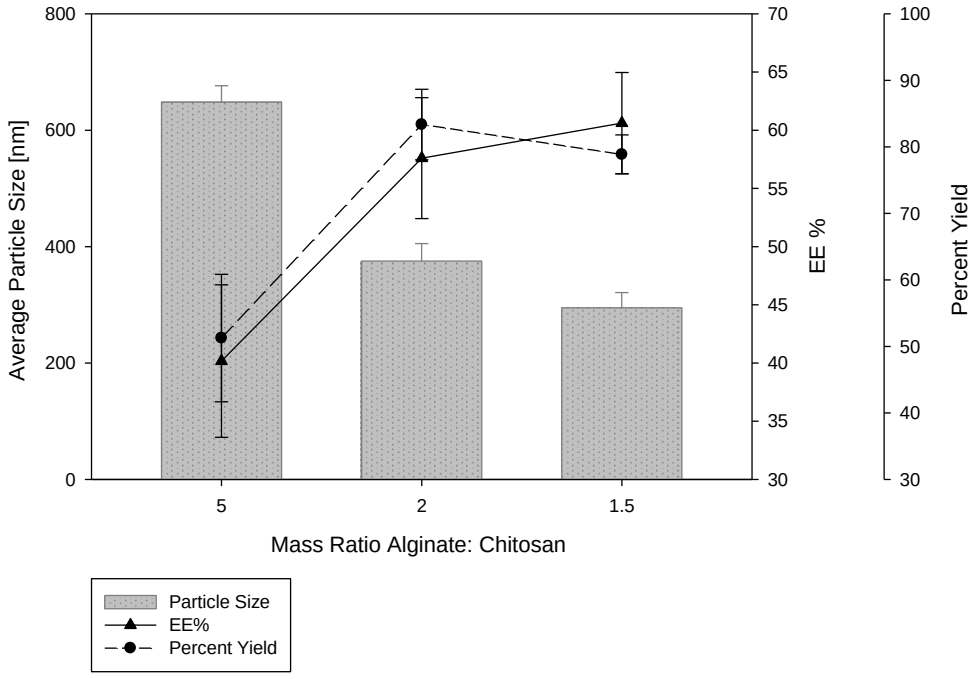

Figure 4.3. Effect of alginate to chitosan mass ratio on particle size, encapsulation efficiency, and physical percent yield at 25°C.

These results are consistent with results found throughout literature. Particle size distributions become wider as pH increases (i.e. $PDI_{pH\ 5.4}$ = .91) resulting in aggregation likely due to weaker ionic interactions (Ruo 2012). For instance, for dispersions with pH of 4.7, other studies found nanoparticles to be in the 190-300 nm in size and have 70-92% EE within AG:CS range of 1:1 to 6.3:1 to encapsulate Nisin, turmeric oil, chloramphenicol, and insulin (Zohri and others 2011; Thwala 2012; Gupta 2011; Sarmento and others 2006). In particular, Zohri and others (2011) produced 205 nm particles with 70% EE of protein with a similar mass ratio of AG:CS used in this study (AG:CS 1:1). Further increasing the pH of the dispersion saw an increase in particle size and a decrease in EE. For instance, for dispersions with pH of 5.2, Douglas and Tabrizian (2005) produced 323 nm particles with 60% EE of DNA (AG:CS 1.5:1).

On the other hand, results from studies by Sinjan and Robinson (2003) and Cegnar and Kerc (2010) directly contradict results from this study as the smallest particles were found to be in the range of 10:1 AG:CS mass ratio with average particle size of 506 nm. Particle size increased as the AG:CS mass ratio decreased to 7:1 which is the opposite effect that occurred in this study. Potential causes for this discrepancy between studies are the differences on pH which affect size and the driving forces that control spontaneous formation of nanoparticles as the ratio of AG:CS increases. Particle size significantly decreased when pH decreased from 5.5 to 4.2 for chitosan (Ruo 2012). Additionally, reports of increased EE at higher pH ranges may be due to an increase in particle size which could increase the potential drug loading volume. Differences in particle size and EE values within the same pH range can be attributed to polymer

molecular weight, polymer concentration, deacetylation of chitosan, mass ratio of polymer to calcium chloride, processing parameters (i.e. syringe size, stirring time, filtration time), and hydrophobicity of active drug to be entrapped (Li and others 2008; Gupta and others 2011).

Studies by Manish and Kulkarni (2012) and Gupta (2011) found increasing AG and CS concentrations led to increased particle size (Ruo 2012). This outcome was also seen in this study as an increase on the relative proportion of AG or CS increased particle size and ultimately decreased stability. This can be seen at a macro scale in Figure 4.4 where precipitation and aggregation were observed as polymer concentrations increased either independently or in combination. High CS concentration yielded a turbid cloudy precipitate while high AG concentrations yielded a gel like solution with high amounts of aggregation and precipitation. High concentrations of combinations of both AG and CS yielded a gel-like solution with high flocculation, aggregation, and large microstructures that appeared structurally weak. Excess chitosan changed the turbidity of the dispersion of the polyelectrolyte complex into a two phase system consisting of a clear supernatant and sediment (Cegnar and Kerc 2010). Low amounts of AG and CS produced transparent solutions meaning there was little to no nanoparticle formation.

The present study revealed that the size of loaded chitosan-alginate nanoparticles (LCA-NP) was highly dependent on the mass ratio of alginate to chitosan with a higher ratio producing larger particles. These results may ultimately prove that smaller particles were a result of functional groups being available in stoichiometric proportion (Gaumet

and others 2008). As alginate concentration increased the availability of negatively charged carboxylate groups increased. Thus, the higher electric charge on the surface of particles produced repelling forces that prevented aggregation and provided stability. However, as charge continued to increase, polymer chains became further apart producing larger and less dense particles. Blank particles (i.e. no entrapped TC) were larger in size due to adjacent polymer chains remaining further apart due to high electric charge and strong repellent forces (Appendix 2) (Mohanraj and Chen 2006; Berger and others 2004; Kong and others 2010).

Additionally, the pKa of chitosan is well known to be 6.5. Addition of alginate solution at higher pH regions would have resulted in the majority of amine groups being deprotonated and unable to become involved in ionic interaction while any that would be readily available would result in weaker interactions leading to larger particle sizes (Douglas and Tabrizian 2005). This is likely the reason for larger particles assembled at the pH dispersion of 5.4. Lowering the pH of the dispersion to 4.7 resolved the aforementioned issue by allowing stronger interactions between CS and AG leading to more compact particle formation. At lower pH regions the carboxyl groups of AG are ionized and the amine groups of CS are protonated (hydrogen ions give a high charge density) leading to more polyionic complex formation. CS chains open up at acidic pH ranges while at basic pH rages CS chains fold up and become deprotonated. Thus, fewer amino groups are exposed for crosslinking at basic pH ranges which resulted in a sparsely cross linked polymer matrix and larger particle sizes. Thus, increasing the protonation of chitosan chains allowed the formation ionic linkages with calcium

chloride resulting in small particle formation (Mohanraj and Chen 2006; Sinjan and Robinson 2003; Rajaonarivony and others 1993).

Overall, evidence suggests that increasing the amount of extended polymer chains at low pH values form smaller, more compact particles (24% smaller). It is important to note, however, that in the lower pH regions, the alginate pH may reach its pKa value of 3.5 and precipitate into alginic acid. In theory, this could lead to larger particles with less entrapment capability (Ruo 2012; Thwala 2012; Gaumet and others 2008).

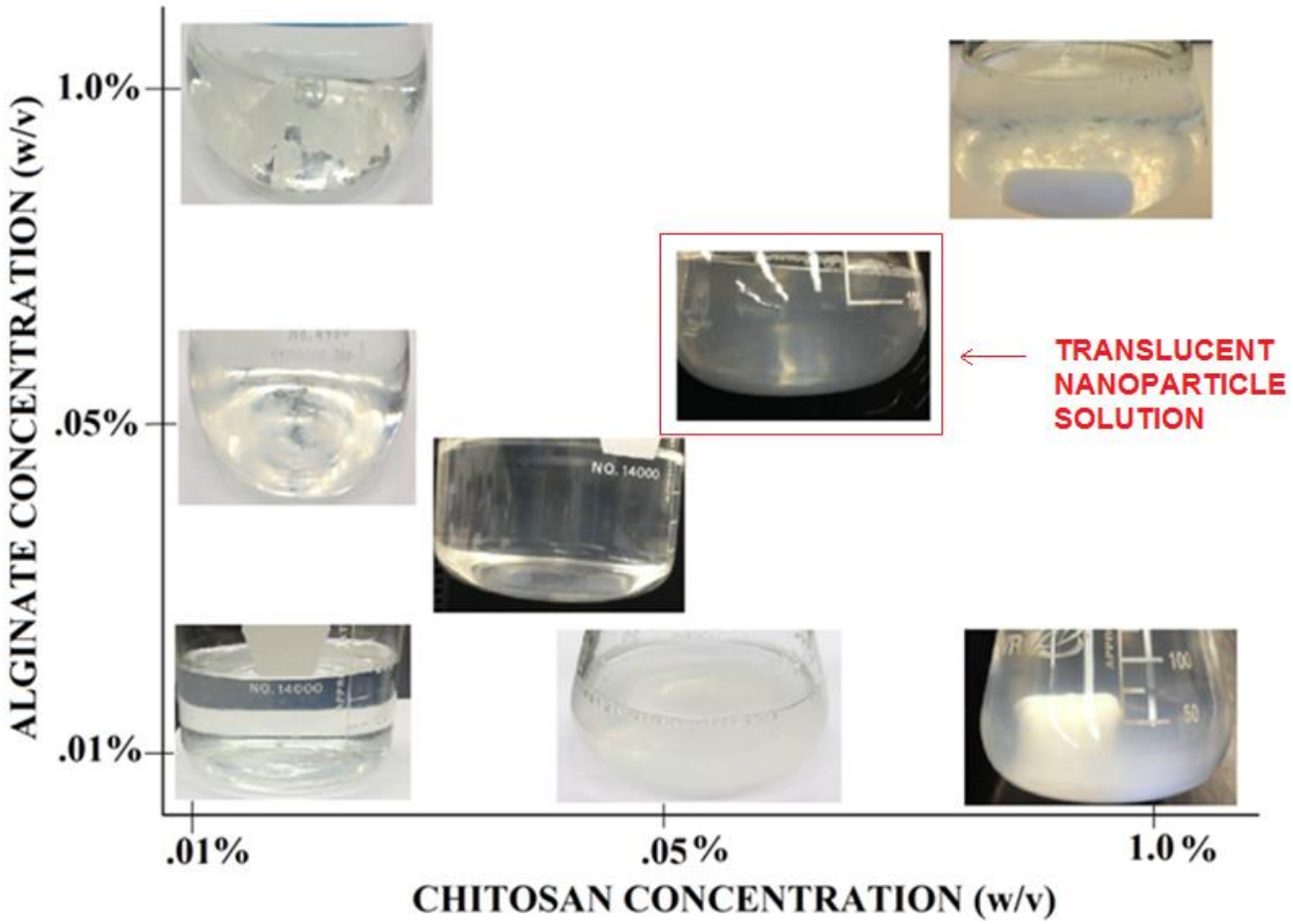

Figure 4.4. Visual representation of the effect of chitosan and alginate concentration on physical stability and appearance of nanoparticle solutions.

4.2.2 Processing Parameter Results

The preliminary observational stability and pH tests helped determine the best working formulation at a pH dispersion of 4.7 and the AG:CS mass ratio to be 1.5:1 (i.e. sample 5b). This formulation was further optimized using several processing parameters to reduce particle size and increase EE. Table 4.4 summarizes the optimized processing parameters by batch. Results elucidated that the syringe size was the processing parameter with the largest effect ($p < 0.05$) on particle size, PDI, and EE. Nanoparticles produced with an 18 gauge syringe were 19% smaller than the next best optimal batch formulation (homogenization time 15 min) and 27.7% smaller than the original parent formulation (5b). All other variables were not statistically significant ($p > 0.05$) between treatment groups (with the exception of PDI value for mass ratio alginate:oil). This result suggests that the methodology is well-designed and processing parameters only have a small impact on overall assembly of nanoparticles.

It is important to note that only one discrete processing parameter was modified and optimized per batch from the parent methodology (i.e. all other parameters held constant). The parent methodology utilized the following processing parameters: mass ratio alginate: calcium chloride (4.8:1), mass ratio alginate:oil (50:1), stirring time (90 min), syringe size (pipette/burette tip), homogenization time (5 min), and equilibration time (24 h). For example, if the mass ratio (w/w) of alginate to calcium chloride, (e.g. 1.6:1) was the parameter being improved and optimized, all other parameters would remain constant from the parent methodology (mass ratio alginate:oil (50:1); stirring

time (90 min); syringe size (pipette/burette tip); homogenization time (5 min); equilibration time (24 h). Refer to Figure 3.2 for additional clarification.

Table 4.4. Particle size, encapsulation efficiency (EE), and polydisperity index (PDI) of nanoparticles with modified methodology (alginate:chitosan mass ratio 1.5:1; pH alginate = 4.6, pH chitosan = 4.9).

Batch[**]	**Processing Parameter (Optimized)**	**Particle Size**[*]**[nm]**	**EE%**[*]	**PDI**
1	Mass Ratio Alginate: $CaCl_2$ (4.8:1)	$294.78^{a,x}$(26.30)	$60.62^{a,x}$(4.34)	$0.66^{a,x}$(0.04)
2	Mass Ratio Alginate: Oil (37.5:1)	$303.93^{a,x}$(7.79)	$65.58^{a,x}$(1.14)	$0.81^{b,x}$(.07)
3	Stirring Time (90 min)	$294.78^{a,y}$(26.30)	$60.61^{a,x}$(4.34)	$0.66^{a,x}$(0.04)
4	Syringe Size (18 gauge)	$213.01^{b,y}$(4.47)	$65.18^{a,x}$(1.48)	$0.61^{c,y}$(0.03)
5	Homogenization Time (15 min)	$263.23^{a,x}$(7.07)	$60.48^{a,x}$(2.68)	$0.67^{a,x}$(0.08)
6	Equilibration Time (24 h)	$294.78^{a,y}$(26.30)	$60.61^{a,x}$(4.34)	$0.66^{a,x}$(0.04)

[*]Values given are averages of three replicate samples; standard deviations are displayed in parenthesis. Values with differing subscripts letters within columns indicate significantly different values ($p < 0.05$). Values in parenthesis are the standard deviation.

[**]Only one parameter modified and optimized per batch. All other processing parameters held constant based on parent methodology. Constant parameters from parent methodology: mass ratio alginate: calcium chloride (4.8:1), mass ratio alginate: oil (50:1), stirring time (90 min), syringe size (pipette/burette tip), homogenization time (5 min), and equilibration time (24 h).

[a,x] Means within a column not followed by a common superscript letter are significantly different between treatment groups ([a]) and within treatment groups ([x]) ($p < 0.05$). ‗Within treatment groups' refers to a comparison of variables within the same processing parameter batch. ‗Between treatment groups' refers to comparison of two different processing parameters.

4.2.2.1 Calcium-Alginate Complex

Table 4.5 shows the results of nanoparticles synthesized with modified mass ratios of alginate to calcium chloride ($CaCl_2$) (constant AG:CS 1.5:1; sample 5b). The optimal mass ratio of AG:$CaCl_2$ was 4.8:1 due to minimal particle size and relatively high EE. No means were statistically significant ($p < 0.05$) for particle size, EE, or physical yield. AG:$CaCl_2$ mass ratio of 4.8:1 was the ratio used in the initial parent

formulation (AG:CS 1.5:1). This means no further optimization of amount of calcium chloride was needed. Particle size was 7.3% smaller while EE was 2.9% smaller than the next best AG:$CaCl_2$ mass ratio (2.4:1). Additionally, AG:$CaCl_2$ mass ratio and particle size show an inverse relationship. The AG:$CaCl_2$ mass ratio had less of a predominant effect on particle size in comparison to pH. As the alginate to calcium chloride mass ratio increased, the size distribution became wider. Lower calcium chloride concentration resulted in more compact particulate matrices (PDI Ag:$CaCl_{1.6:1}$ = .84) and more entrapped *trans*-cinnamaldehyde. As LCA-NP became larger in size, less alginate was cross linked by calcium chloride. This phenomenon was also observed in studies by Cegnar and Kerc (2010) and Thwala (2012) where high AG:$CaCl_2$ mass ratios (1.75:1 and 1.59:1) resulted in larger particles due to excess calcium ions likely encountering a higher degree of ionic interaction causing rapid gelation.

The results from this are consistent with those found in literature. Rajaonarivony and others (1993) and Sarmento and others (2006) triggered pre-gelation with a AG:$CaCl_2$ mass ratio of 5:1. Li and others (2008), Gupta (2011), and Sinjan and Robinson (2003) utilized AG:$CaCl_2$ mass ratios of 4.47:1, 4.9:1, and 5.88:1 to obtain 20-50, 230, and 282 nm particles, respectively. In fact, Sinjan and Robinson (2003) stated the optimal region of AG:$CaCl_2$ mass ratio to be between 2.85:1 and 12.5:1. Additionally, Lertsutthiwong and others (2009) found the physical yield to be in the same range as this study (70%).

Table 4.5. Particle size, encapsulation efficiency (EE), and physical yield of nanoparticles assembled with modified mass ratios of alginate to calcium chloride (alginate:chitosan mass ratio 1.5:1; pH alginate = 4.6, pH chitosan = 4.9).

Mass Ratio (AG:$CaCl_2$)[1]	Particle Size* [nm]	EE%*	%Yield*
1.6	325.11[a](7.11)	53.00[a](4.80)	61.78[a](11.12)
2.4	317.99[a](32.60)	62.48[a](4.73)	67.93[a](5.59)
4.8	294.78[a](26.60)	60.62[a](4.34)	78.86[a](2.93)

*Values given are averages of three replicate samples; standard deviations are displayed in parenthesis. Values with differing subscripts letters within columns indicate significantly different values ($p < 0.05$). Values in parenthesis are the standard deviation.

[1]Represents the mass ratio (w:w) of alginate to calcium chloride powder used to formulate nanoparticles. All other processing parameters held constant and based on parent methodology: mass ratio alginate: oil (50:1), stirring time (90 min), syringe size (pipette/burette tip), homogenization time (5 min), and equilibration time (24 h).

4.2.2.1.1 Effects of Added Calcium Chloride

Sinjan and Robinson (2003) suggested that calcium chloride is essential for nanoparticle formation because it provides alginate beads with a nucleus for nanoparticle growth. High concentrations of calcium chloride may not be essential for particle formation, but calcium chloride addition is necessary for pregel formation below AG:$CaCl_2$ mass ratios of 5:1. This statement is consistent with findings in this study as AG:$CaCl_2$ was necessary at 4.8:1 ratio to form smallest particles. There was no significant difference in lower mass ratios tested suggesting that this mass ratio is sufficient for nanoparticle production. However, results by Douglas and Tabrizian (2005) show that the absence of calcium chloride only produced marginally larger particles in comparison with the standard AG:$CaCl_2$ mass ratio of 4.5:1. Different analysis methods as well as different guluronic acid contents of alginate could be the reason for this difference. Low guluronic acid (G) content alginate is crucial to create a

nanoparticle nucleus without causing gelation. Higher G content will see a higher ionic interactions in same alginate chain form beads and result in larger particles. The effect of calcium chloride on polymeric nanoparticle formation should be further evaluated to determine if calcium chloride addition is necessary above the AG:$CaCl_2$ ratio used in this study with different G content alginates.

4.2.2.1.2 Effects of Chitosan Addition

Rajaonarivony and others (1993) found that formation of AG nanoparticles is influenced by the first compound added. If calcium chloride was not added first, the protonated amino groups of chitosan would have high affinity for the mannuronic residues of AG causing random interactions leading to large particle formation. Sinjan and Robinson (2003) confirmed that the size of chitosan-alginate nanoparticles were larger than alginate (i.e. no chitosan addition) and also suggested that particle size increases as CS and AG attach to the surface of TC. Furthermore, any increase in particle size post CS addition may indicate that a large CS concentration is localized on surface of the alginate polymer due to electrostatic interaction which may help stabilize the nanoparticle core. Respective concentrations of AG and calcium chloride allow pregel formation and small nanoparticles to form which are further strengthened by chitosan complexation.

In the pH range of this study, positively charged CS competes with calcium chloride to electrostatically interact with AG. The shielding effect of the CS counter ion can disturb the polymeric framework formed by AG and calcium chloride which will

reduce the monodisperity of LCA-NP and could significantly increase particle size (i.e. bimodal size distribution) (Ruo 2012).

4.2.2.1.3 Bimodal Size Distributions

Rajaonarivony and others (1993) explained the pregel phenomenon as a reduction of polymer size due to individual AG chains shrinking into a more compact coiled structure where the guluronic (G) regions in the same AG chain are linked by calcium ions. Ruo (2012) showed that nanoparticles form at a distinct polymer to cross linking ratio (4.8:1) which affects whether particle size follows a unimodal or bimodal distribution. This was observed in this study‘s preliminary methodology as several size distribution curves where bimodal, thus increasing average particle sizes (Appendix 2). Bimodal distributions in this study are likely due to processing difficulties at lab-scale (i.e. stirring rate and droplet rate inconsistencies) as well as the lag time before ultrafiltration and freeze drying where particles formation can be affected. Further work needs to be completed to understand bimodal size distribution occurrences.

4.2.2.2 *Trans*-Cinnamaldehyde

Table 4.5 shows the results of nanoparticles synthesized with modified mass ratios of alginate to *trans*-cinnamaldehyde (TC). The optimal mass ratio of AG:TC was 37.5:1 due to small particle size (303.93 nm) and maximum EE (65.58%). No means were statistically significant ($p < 0.05$) for particle size, EE, or physical yield. Particle size was 3% larger while EE was 7.6% greater than the next best AG:TC mass ratio (50:1). Both particle size and EE had a direct relationship with AG:TC mass ratio. The AG:TC mass ratio has a less predominant effect on particle size in comparison to pH but

just as significant of an effect on EE. Particle size and EE results were consistent with literature values. However, many studies do not divulge both the concentration of active drug incorporated and the stage of incorporation during synthesis. Thwala (2012), Gupta (2011), Sinjan and Robinson (2003), and Li and others (2008) used AG:TC concentrations of 10:1, 15:1, 15:1, and 100:1 to produce 20-230 nm particles with 83-92% EE of turmeric oil, chloramphenicol, methylene blue, and nifedipine, respectively. Manish and Kulkarni (2012) also used a polymer to drug 15:1 to achieve particle size of 230 nm and entrapment 72-92% of azelastine hydrochloride. Additional ratios (15:1 and 10:1) were tested in this study, however, resulting solutions showed white opaqueness and were considered unstable formulations.

Rajaonarivony and others (1993) found that increasing the concentration of an active drug increases the drug loading capacity. However, limitations do exist as the size of the nanoparticles could increase due to the presence of the active drug having affinity for AG and its G residues. Both scenarios were directly observed in this study as EE and particle size both increased as incorporated TC in AG solution increased. TC was added directly into AG solution in this study to avoid steric hindrance or a conformational arrangement that would lead to large particle formation through structure formation with calcium chloride (Das and others 2010). However, this could be a potential flaw in the methodology of this study, as it is difficult to completely solubilize and evenly disperse TC for entrapment in the pregel. Further work needs to be completed on the stage of TC addition in synthesis methodology.

Table 4.6. Particle size, encapsulation efficiency (EE), and physical yield percentage of nanoparticles assembled with modified mass ratios of alginate to *trans*-cinnamaldehyde (alginate to chitosan mass ratio 1.5:1; pH alginate = 4.6, pH chitosan = 4.9).

(Mass Ratio AG:TC)[1]	Particle Size*[nm]	EE%*	%Yield*
75:1	279.66[a](34.71)	57.98[a](9.28)	65.37[a](7.67)
50:1	294.78[a](26.3)	60.62[a](4.34)	78.86[a](2.93)
37.5:1	303.93[a](7.79)	65.58[a](1.14)	70.47[a](3.90)

*Values given are averages of three replicate samples; standard deviations are displayed in parenthesis. Values with differing subscripts letters within columns indicate significantly different values ($p < 0.05$).Values in parenthesis are the standard deviation.

[1]Represents the mass ratio (w:w) of alginate to *trans*-cinnamaldehyde powder used to formulate nanoparticles. All other processing parameters held constant and based on parent methodology: mass ratio alginate: calcium chloride (4.8:1), stirring time (90 min), syringe size (pipette/burette tip), homogenization time (5 min), and equilibration time (24 h).

4.2.2.3 Syringe Size, Stirring, Homogenization, and Equilibration Time

Table 4.7 (a) to Table 4.7 (d) show the results of nanoparticles synthesized with modified processing parameters. It can be concluded that the optimal syringe size is 18 gauge. Particle size was 27.7% smaller while EE was 6.9% larger in comparison to the burette/pipette tip. Means for particle size and PDI were statistically significant ($p < 0.05$) between the two tip sizes (Table 4.6 (a)). Means for entrapment efficiency were not significantly different regardless of tip size. This suggests droplet size has a larger effect on size in contrast to EE. In addition, smaller droplets at a constant rate means that less physical material (i.e. calcium chloride or chitosan) is available for complexation resulting in particles being formed with only the physical material that is present (i.e. limit excess material).

Table 4.7 (a). Particle size, entrapment efficiency (EE), polydisperity index (PDI), and physical yield percentage of nanoparticles assembled with different droplet/syringe sizes (alginate to chitosan mass ratio 1.5:1; pH alginate = 4.6, pH chitosan = 4.9).

Syringe Size [Gauge][1]	Particle Size* [nm]	EE%*	%Yield*	PDI
Burette/Pipette Tip (ID =1.50/0.6 mm)**	294.78[a](26.30)	60.62[a](5.34)	78.86[a](3.93)	0.66[a](0.04)
18 G (ID = 0.83 mm)	213.01[b](4.47)	65.18[a](1.48)	81.92[a](3.46)	0.61[b](0.03)

*Values given are averages of three replicate samples; standard deviations are displayed in parenthesis. Values with differing subscripts letters within columns indicate significantly different values ($p < 0.05$). Values in parenthesis are the standard deviation.

[1]All other processing parameters held constant and based on parent methodology: mass ratio alginate: calcium chloride (4.8:1), mass ratio alginate: oil (50:1), stirring time (90 min), homogenization time (5 min), and equilibration time (24 h).

** ‗ID' refers to internal diameter of syringe needle and pipette.

The optimal total stirring time was 90 min. Particle size was 23.3% smaller while EE was comparably larger than the next best stirring time (180 min) (Table 4.7 (b)). Means for particle size were statistically significant ($p < 0.05$) when stirring time was increased or decreased. Means for entrapment efficiency were not significantly different regardless of stirring time increase or decrease. This result likely indicates that equilibrium of polyelectrolyte complexation was achieved during this time. Shorter times possibly lead to fewer larger assembled particles while longer stirring times likely lead to aggregation of assembled particles. Additionally, no substantial change in EE is probably due to chitosan addition only affecting particle size. TC is entrapped in the ionotropic gelation step through the addition of calcium chloride. Chitosan addition only adds to the external structure to the nanoparticle which consequently increases size (Thwala 2012; Mumper and others 1994; Mohanraj and Chen 2006). Gupta (2011) results were similar to this study as 90 minutes stirring time was optimal to obtain

particles of 236 nm and 90.9% EE for entrapment of chloramphenicol. Manish and Kulkarni (2012) observed different results as stirring time was optimal at 15 min for size (245 nm) and 30 minutes for EE (91%) of azelastine hydrochloride; significantly less stirring time in comparison to this study.

Table 4.7 (b). Particle size, entrapment efficiency (EE), and physical yield percentage of nanoparticles assembled with modified stirring times (alginate to chitosan mass ratio 1.5:1; pH alginate = 4.6, pH chitosan = 4.9).

Total Stirring Time [min][1]	**Particle Size[*] [nm]**	**EE%[*]**	**%Yield[*]**
45	401.53^{a}(45.30)	58.58^{a}(7.37)	65.077^{a}(11.56)
90	294.78^{b}(26.30)	60.62^{a}(4.34)	78.86^{a}(2.93)
180	384.41^{a}(23.46)	60.16^{a}(6.13)	63.66^{a}(7.50)

[*]Values given are averages of three replicate samples; standard deviations are displayed in parenthesis. Values with differing subscripts letters within columns indicate significantly different values ($p < 0.05$). Values in parenthesis are the standard deviation.

[1]All other processing parameters held constant and based on parent methodology: mass ratio alginate: calcium chloride (4.8:1), mass ratio alginate: oil (50:1), syringe size (pipette/burette tip), homogenization time (5 min), and equilibration time (24 h).

The optimal total homogenization time was 15 min. Particle size was 10.8% smaller while EE was comparable to homogenization time of 5 min (Table 4.7 (c)). Means for particle size, EE, and PDI were not statistically significant ($p > 0.05$) regardless of homogenization time. Similar to stirring time, this suggests homogenization only affects the physical characteristic of the nanoparticles. TC loading is not effected by mechanical shearing likely due to the fact that homogenization takes place after nanoparticle formation is complete (i.e. all TC is already entrapped). Longer homogenization times were also tested (e.g. 30 and 45 min), but nanoparticle destruction

resulted. This was likely due to an overload of mechanical shearing and heat from the homogenizer shaft which lead to tearing and stretching of assembled nanoparticles reducing storage life in suspension (Ahmed and others 2012).

Table 4.7 (c). Particle size, entrapment efficiency (EE), polydisperity index (PDI), and physical yield percentage of nanoparticles assembled with modified homogenization times (alginate to chitosan mass ratio 1.5:1; pH alginate = 4.6, pH chitosan = 4.9).

Total Homogenization Time [min][1]	Particle Size* [nm]	EE%*	%Yield*	PDI
5	294.78[a](26.30)	60.62[a](4.34)	78.86[a](2.93)	0.66[a](0.04)
15	263.23[a](7.07)	60.48[a](2.68)	67.08[b](2.91)	0.67[a](0.08)

*Values given are averages of three replicate samples; standard deviations are displayed in parenthesis. Values with differing subscripts letters within columns indicate significantly different values ($p < 0.05$).

[1]Values in parenthesis are the standard deviation. All other processing parameters held constant and based on parent methodology: mass ratio alginate: calcium chloride (4.8:1), mass ratio alginate: oil (50:1), stirring time (90 min), syringe size (pipette/burette tip), and equilibration time (24 h).

Optimal equilibration time prior to ultrafiltration was 24 h. Particle size was 5.9% smaller while EE was 4.9% larger than next best equilibration time (48 h) (Table 4.7 (d)). Means for particle size were statistically significant ($p < 0.05$) for equilibration times greater than 24 h. Means for entrapment efficiency were not significantly different ($p > 0.05$) regardless of equilibration time. This likely indicates equilibrium of polyelectrolyte complexation was achieved after 12 h post CS addition. Shorter equilibration times result in fewer large particles or nanoparticles that have not completely assembled in solution. Equilibration times (e.g. filtration after 12 h) result in

a higher concentration of CS complexing with the calcium-alginate pregel forming smaller compact particles.

Table 4.7 (d). Particle size, entrapment efficiency, and physical yield percentage of nanoparticles assembled with varying equilibration times (alginate to chitosan mass ratio 1.5:1; pH alginate = 4.6, pH chitosan = 4.9).

Equilibration Time [h][1]	**Particle Size[*] [nm]**	**EE%[*]**	**%Yield[*]**
12	406.12[a](20.15)	48.03[a](9.40)	60.08[a](11.98)
24	294.78[b](26.30)	60.62[a](4.34)	78.86[a](2.93)
48	310.56[b](30.33)	57.62[a](8.74)	61.41[a](10.01)

[*]Values given are averages of three replicate samples; standard deviations are displayed in parenthesis. Values with differing subscripts letters within columns indicate significantly different values ($P < 0.05$).

[1]Values in parenthesis are the standard deviation. All other processing parameters held constant and based on parent methodology: mass ratio alginate: calcium chloride (4.8:1), mass ratio alginate: oil (50:1), stirring time (90 min), syringe size (pipette/burette tip), and homogenization time (5 min).

4.2.3 Final Methodology Results

Preparation of *trans*-cinnamaldehyde loaded chitosan-alginate nanoparticles was successfully carried out through the ionotropic gelation polyelectrolyte complexation method. The dispersion of TC in aqueous alginate with Tween 20 surfactant and calcium chloride cross linking agent created hydrogel nanoparticles. Particles were then solidified with calcium chloride as a cross linking agent followed by chitosan for structural support. This occurs as electrostatic interactions between carboxylate groups on alginate and positively charged calcium ions and protonated amine groups on chitosan. Toxic acetonitrile solvent was removed from nanoparticle solution via

evaporation at reduced pressure. The final solution was lyophilized for long term storage and ease of handling. Final design constraints of methodology are briefly displayed in Table 4.8. All values were based on optimal modified mass ratios from preliminary study (AG:CS 1.5:1; AG:$CaCl_2$ 4.8:1; AG:TC 37.5:1).

Particle size and EE were optimized with 18 gauge syringe needle, stirring times of 90 minutes, 15 minutes of high RPM homogenization, and equilibration time of 24 hours (Table 4.4). The final nanoparticle system formulated with these optimal processing parameters showed increased shelf life (9 weeks at 3°C) and translucency (TL) in solution. Average particle size was 43.6% smaller while 17.2% more *trans*-cinnamaldehyde was entrapped in comparison with the suboptimal AG:CS 1.5:1 mass ratio (Table 4.9). Means for particle size, PDI, and EE of optimal to suboptimal treatment groups were statistically significant ($p < 0.05$) while overall physical yield of nanoparticle post lyophilization was not significantly different. In conclusion, particle size was more drastically affected by processing parameters in comparison to EE within processing parameter treatment groups. Specifically, mass ratio of AG to CS, droplet size, and equilibration time had the greatest effect on particle size. However, nanoparticles formulated with all optimized processing parameters had a great effect on EE. This can be explained as a synergistic effect. No independent processing parameter had statistical significance on EE but there was statistical significance in combination ($p < 0.05$).

Table 4.8. Final design constraints for optimal nanoparticle synthesis (alginate to chitosan mass ratio 1.5:1; pH alginate = 4.6, pH chitosan = 4.9).

AG* (.06% w/v) [ml]	**$CaCl_2$ (.2% w/v) [ml]**	**TC [µg]**	**CS (.05% w/v) [ml]**	**AG [g]**	**$CaCl_2$ [g]**	**CS [g]**	**AG:TC**	**AG:$CaCl_2$**	**AG:CS**
250	15.625	4000	200	0.15	0.031	0.1	37.5	4.8	1.5

*All processing parameters based on final optimized processing: mass ratio alginate: calcium chloride (4.8:1), mass ratio alginate: oil (37.5:1), stirring time (90 min), syringe size (18 Gauge), homogenization time (15 min), and equilibration time (24 h).

Table 4.9. Effect of optimization of nanoparticles on particle size, entrapment efficiency (EE), polydisperity index (PDI), and percent yield (alginate to chitosan mass ratio 1.5:1; pH alginate = 4.6, pH chitosan = 4.9).

Sample Type	Particle Size* [nm]	EE%*	%Yield*	PDI
Suboptimal Particles[1]	294.78[a](26.30)	60.61[a](4.34)	78.86[a](2.93)	0.66[a](0.04)
Optimized Particles[2]	166.26[b](5.86)	73.24[b](3.55)	75.77[a](3.70)	0.57[b](0.03)

*****Values given are averages of three replicate samples; standard deviations are displayed in parenthesis. Values with differing subscripts (within columns) indicate significantly different values ($P < 0.05$). Values in parenthesis are the standard deviation.

[1]Suboptimal refers to particles produced with initial parent methodology: mass ratio alginate: calcium chloride (4.8:1), mass ratio alginate: oil (50:1), stirring time (90 min), syringe size (burette/pipette tip), homogenization time (5 min), equilibration time (24 h).

[2]Optimal refers to particles produced with final modified methodology. All optimized processing parameters from preliminary study are incorporated into final methodology: mass ratio alginate: calcium chloride (4.8:1), mass ratio alginate: oil (37.5:1), stirring time (90 min), syringe size (18 Gauge), homogenization time (15 min), and equilibration time (24 h).

4.3 Characterization Results

It is critical to analyze nanosystems and nanotechnologies in order to properly characterize these systems as nanoscale, homogenous, bioactive, or stable and understand structural and functional relationships. Characterization can yield substantial data for further research and design applications into food products because it will help determine nanoparticles efficacy, interactions and mechanisms involved, types of interactions that are occurring, unforeseen impacts, and undesired interactions. Ultimately, this will allow for new product research and design as well as data submission to federal authorities such as the Food and Drug Administration and the Environmental Protection Agency which could expedite the process of legally using nanoparticles as food additives.

The ionotropic pre gelation method produced chitosan-alginate nanoparticles with optimal particle size and entrapment of *trans*-cinnamaldehyde. Particle size and entrapment efficiency were successfully optimized through the manipulation of processing parameters and fundamental design constraints. Further characterization can be carried forward using the optimal nanoparticle formulations (Table 4.8). Particle size was established through the use of transmission electron microscopy. Microscopy also presented surface characteristic and morphology. Controlled release tests offered results on nanoparticle stability, burst mechanics, storage stability, and breakdown. Differential scanning calorimetry (DSC) confirmed TC in LCA-NP inclusion complexes as well as an attempt to clarify other thermal characteristics. Antioxidant and antimicrobial testing were rapid, mild testing techniques that signified potential use of LCA-NP in future food applications.

4.3.1 Cumulative Controlled Release

The temperature used for controlled release (35°C) in this study was chosen as an ideal case for microbial growth and worst case scenario for food safety (Hill and others 2013b). Release of TC from chitosan-alginate (CS-AG) inclusion complexes involved the following process: (1) diffusion of water into nanoparticles; (2) swelling and loosening of compact nanoparticle structure; (3) desorption and escape of TC entrapped at nanoparticle surface; and (4) diffusion of internalized TC through surface pores of the polysaccharide matrix (Zohri and others 2011).

Cumulative release percentage was calculated using the equation below (Das and others 2010; Xing and others 2010):

$$Cumulative\ Release\ (\%) = \frac{Released\ TC}{Total\ TC} \times 100 \qquad (4.1)$$

Figure 4.5 shows the cumulative controlled release results of TC from LCA-NP *in vitro* as a function of time. From this curve, it can be concluded that the release rate and total amount of TC release decreased after 10 h (32.5%). This is likely attributed to TC that is located in or near the external surface of nanoparticles desorping into PBS solution (i.e. possibly by weak interactive forces between CS and AG at the surface of particles) (Li and others 2008; Mohanraj and Chen 2006; Liu 2014; Wise 2000). Initial burst release may also be attributed to the charge of the polymer matrix. If the surface remains charged and hydrophilic, the polymer network (i.e. "egg box structure") will show a greater tendency for adsorption of PBS to the nanoparticle network displacing TC. Additionally, size, surface charge, pH, and hydrophobicity also play large roles in release of TC from polymeric nanoparticles (Zohri and others 2011).

Following initial burst release, another stage of controlled release was observed from 10 to 72 h with final release of 62.31%. Nanoparticles had to dissociate from the swollen state to allow internalized TC to escape. However, the rate of TC escape continued to decrease which is likely due to the formation of hydrogen bonds along the chitosan polymer chains as well as additional physical barriers from polymeric matrix. Hydrogen bonds may need to be broken before internalized TC can be released from

nanoparticles (Zohri and others 2011; Xing and others 2010; Li and others 2008). Overall, burst release was followed by more uniform release after 10 h. Thus, release rate decreases after initial burst release because internalized TC has to travel further distance and takes longer time to diffuse (Gomes and others 2011). Through extrapolation of the controlled release graph it would take approximately 115 hours to release all TC based on EE (73.24%). This value signifies the slow prolonged release of TC over time and may be attributed to the previously described mechanisms.

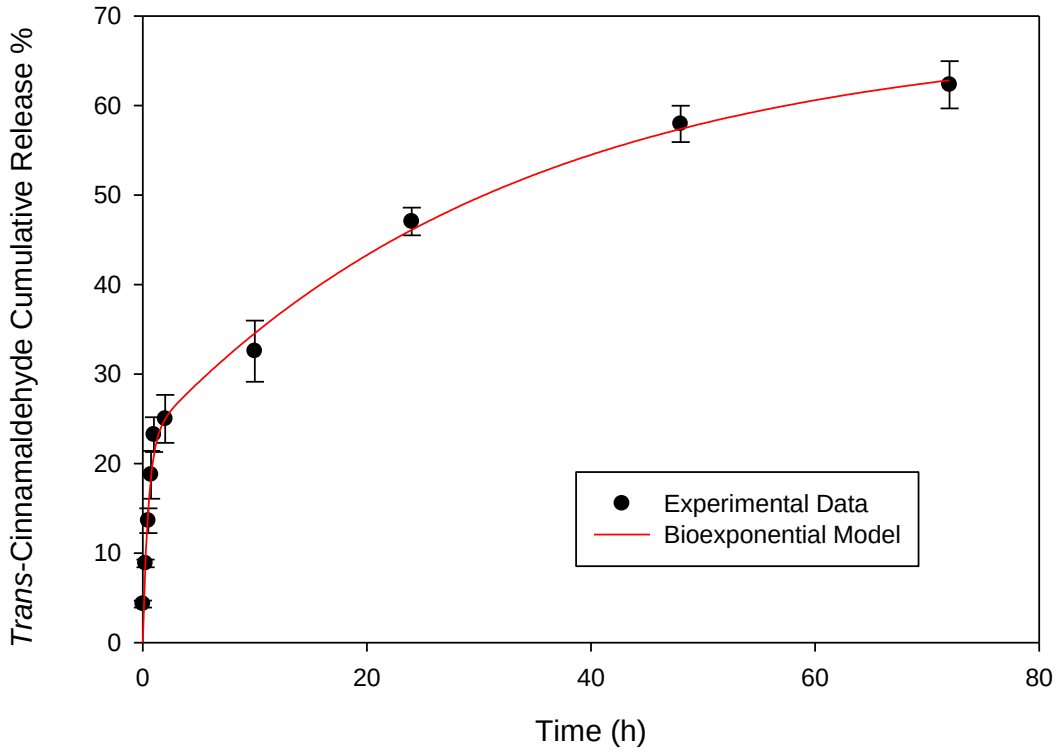

Figure 4.5. Cumulative release of *trans*-cinnamaldehyde in phosphate buffer saline at pH 7.4 and the bioexponential model at 35°C.

TC release from LCA-NP in this study best followed a bioexponential model (R^2 = .981) or power law model (R^2 = .975) (Table 4.10; Equation 4.1 and Equation 4.2) when compared to the following zero order (R^2 = .830), first order (R^2 = .906), and Higuchi models (R^2 = .791) based on the coefficient of determination (R^2) (Equation 4.3 to Equation 4.5)(Shicheng and Clive 2005):

Bioexponential: $$\frac{M_t}{M_o} = 1 - (A * \exp(-k_{1*}t) + B * \exp(-k_2 t)) \quad (4.2)$$

Power Law: $$\frac{M_t}{M_o} = kt^n \quad (4.3)$$

Zero Order: $$M_o - M_t = k_o t \quad (4.4)$$

First Order: $$M_t = M_o^{-k_1 t} \quad (4.5)$$

Higuchi: $$\frac{M_t}{M_o} = k_H t^{.5} \quad (4.6)$$

where ‗M_t‘ is the amount of TC released at time ‗t‘, ‗M_o‘ is the initial TC content, ‗n‘ is the diffusional exponent and ‗k‘ (k_o, k_1, k_2, k_H) represent the rate constant (h^{-1}) of the respective equation.

From the results, it can be concluded that the LCA-NP likely follows fickian diffusion. The bioexponential model is just a modified empirical equation that is the generalized form of the Fickian model (Equation 4.7 and Equation 4.8) employing only the first two terms (Gomes and others 2011). The fact that release follows the bioexponential model suggest that TC release consists of a rapid (burst phase) and slow function (sustained release) as previously discussed. Gomes and others (2011) and Hill and others (2013b) obtained similar results for the release of eugenol, cinnamaldehyde, and cinnamon bark extract from PLGA that followed the bioexponential model (i.e. two-term exponential model).

The value of the diffusion release coefficient was determined from the linear regression of $\log(M_t/M_o)$ versus log(t) where M_t/M_o represents the fraction of TC released at time ‗t' (amount of TC released at time ‗t'/total amount of TC in dosage form). This value (n = .303; Table 4.10) indicated that release was due to Fickian diffusion (Equation 4.6 and Equation 4.7) (Li and others 2008; Takka and others 1998; Siepmann and Peppas 2001; Nagarwal and others 2012; Shicheng and Clive 2005).

$$\frac{M_t}{M_o} = 1 - \frac{6}{\pi^2}\sum_{n=1}^{\alpha}\frac{1}{n^2}\exp(-n^2\pi^2\tau) \qquad (4.7)$$

where dimensionless time, τ, is given by:

$$\tau = \frac{Dt}{r^2} \qquad (4.8)$$

_D‘ is the diffusion coefficient of TC in the nanoparticles and _r‘ is the radius of nanoparticles. This model provides a steep initial release rate in comparison to one term exponential models (Shicheng and Clive 2005).

Release curves for different mass ratios of AG:CS (5:1, 2:1) were completed but are not shown in this study due there being no statistical significance ($p < 0.05$) between treatment groups for cumulative release after 10 h. Similar to this study, Das and others (2010) determined release of curcumin from CS-AG nanoparticles to follow the Higuchi model (i.e. modified power law; n = .5).

Results in this study are consistent with other recent studies. Thwala (2012) found tagetes oil to release in PBS (pH 7.4) in a controlled manner from CS-AG NP following initial burst effect (30%; 12 h). Zohri and others (2010) also revealed a burst release effect of Nisin from CS-AG NP (30%, 7h). Das and others (2010), Gupta and others (2011), and Nagarwal and others (2012) showed similar controlled release curves of CS-AG NP with high cumulative release of curcumin (75%), chloramphenicol (90%), and 5-fluorouracil (81%) respectively. The higher cumulative release found by the aforementioned studies could be a result of higher alginate concentrations used which would increase the degree of cross linking the alginate core.

Table 4.10. Mathematical representation of *trans*-cinnamaldehyde release kinetics.

Zero Order*	First Order*	Higuchi*	Power Law	Bioexponential Model*
$M_o - M_t = k_o t$	$M_t = M_o exp^{-k_1 t}$	$\frac{M_t}{M_o} = k_H t^{.5}$	$\frac{M_t}{M_o} = kt^n$	$\frac{M_t}{M_o} = 1 - (A * \exp(-k_{1*} t) + B * \exp(-k_2 t))$
k_o = .736 µg/h	k_1 = .012 h^{-1}	k_H = 8.53 h^{-1}	k = 17.6 h^{-1}	(A = 25.6 ; B = 31.7)*** ; k_{1*} = 1.390 h^{-1} ; k_2 = .040 h^{-1}
(R^2 = .830)**	R^2 = .906	R^2 = .791 n = .5	R^2 = .975 n = .303	R^2 = .981

* ‗k' represents rate constant; k_o = rate constant for zero order; k_1 = rate constant for first order; k_h = rate constant for Higuchi model; k_{1*},k_2 = rate constants for bioexponential model

** 'R^2' represents the coefficient of determination indicated how well experimental data fit statistical model

*** ‗A' and ‗B' represent coefficients of bioexponential model

4.3.2 Differential Scanning Calorimetry (DSC)

DSC was the thermo-analytic technique used to obtain thermal profiles, observe fusion and crystallization events, and confirm the entrapment of TC in CS-AG inclusion complexes. The thermal curves of TC, LCA-NP, and ULCA-NP are presented in Figure 4.6. Table 4.11 displays the endothermic and exothermic peaks for the respective curves. Isolated AG displayed the highest endothermic peak temperature followed by ULCA-NP, LCA-NP, and isolated CS. The highest exothermic temperature was seen for CS followed by ULCA-NP, LCA-NP, and isolated alginate. Similar results were observed by Sarmento and others (2006) for CS-AG NP with entrapped insulin. Low temperature endothermic peaks (70-80°C) were likely due to the water loss associated with hydrophilic groups while exothermic peaks (>300°C) were a result of degradation of polyelectrolytes through dehydration, decomposition, and depolymerization (e.g. decarboxylation of carboxylic groups and deteriorative oxidative reactions) (Hill and others 2013a; Sarmento and others 2006; Hedges Allan and others 1995; Teixeira and others 2013).

ULCA-NP show a broader endotherm in comparison to CS and AG, but display more narrow endothermic and exothermic regions in comparison to LCA-NP. The higher exothermic peak of ULCA-NP may represent slightly weaker electrostatic interactions. Lower temperature endothermic peaks of ULCA-NP probably represent weaker AG to calcium chloride linkages (Ruo 2012). The broadness of the LCA-NP endotherm can be explained by the complexation/coalescence (i.e. new chemical bonds) of CS to AG and can be observed through the endothermic peak at 69.67°C and the

exothermic peak at 278.5°C (Cegnar and Kerc 2010). The narrow endothermic and exothermic regions of ULCA-NP in comparison to LCA-NP are likely due to the lack of structural integrity of the nanoparticles. LCA-NP are dense and stable in comparison to hollow labile ULCA-NP (Figure 4.6).

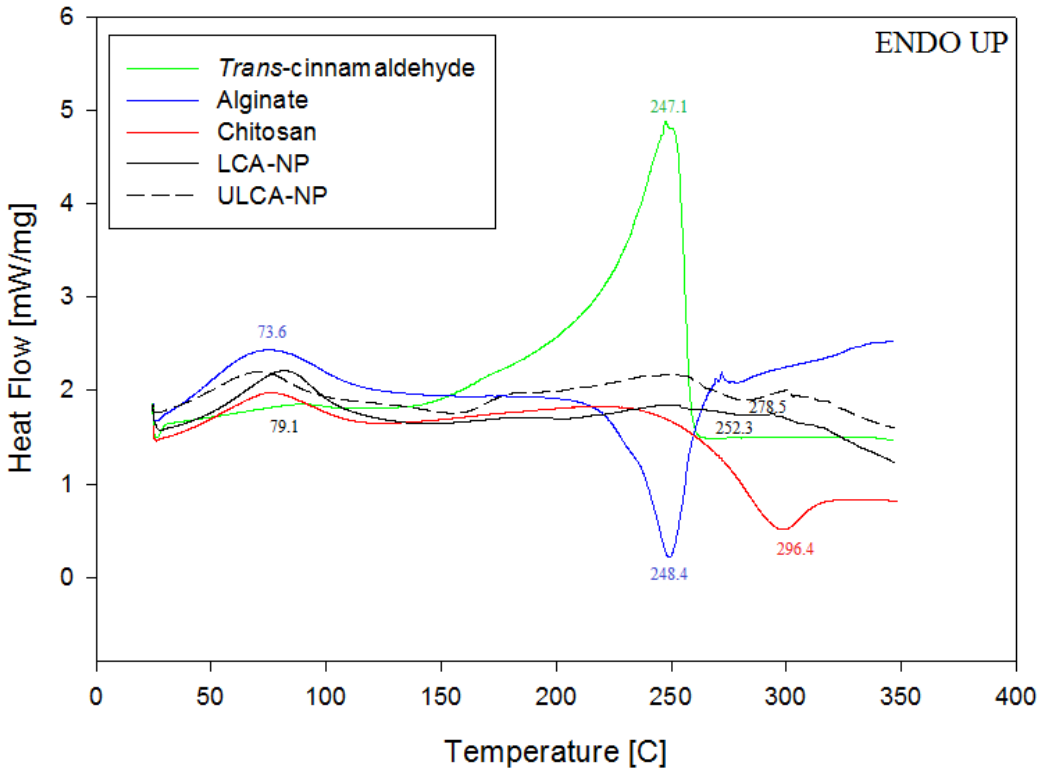

Figure 4.6. Thermograms associated with alginate, chitosan, *trans*-cinnamaldehyde, loaded nanoparticles (LCA-NP), and control nanoparticles (not loaded; ULCA-NP).

Table 4.11. Peak temperatures associated with DSC thermograms for alginate, chitosan, *trans*-cinnamaldehyde, loaded nanoparticles (LCA-NP), and control nanoparticles (ULCA-NP).

Sample	**Temperature [°C]**
	Peak
Alginate (pH 4.9)	73.6 248.2
Chitosan (pH 4.6)	71.6 296.4
Trans-Cinnamaldehyde	247.1
ULCA-NP	69.67 278.5
LCA-NP	79.1 252.3

The slight exothermic peak of LCA-NP at 252.3°C in comparison to the large exothermic peak of 278°C of ULCA-NP was possibly due to the complexation of polyelectrolytes CS and AG and the corresponding interaction between TC and the polymer mixture (Zohri and others 2010). Profile changes and peak shifts are usually a result of drug and polymer interaction (Cegnar and Kerc 2010). Results from this study compare well to a studies completed by Sarmento and others (2006), Thwala (2012), Zohri and others (2011) and Cegnar and Kerc (2010) where loaded CS-AG NP were successfully synthesized through ionic gelation. Thermograms obtained for alginate, chitosan, LCA-NP, and ULCA-NP were all comparable to the aforementioned studies (Figure 4.6).

TC showed a sharp endothermic peak at 247°C corresponding to its boiling point and potential hydrolysis and oxidation (Teixeira and others 2013; Hill and others 2013a).

Thus, its inclusion into LCA-NP was confirmed using DSC indirectly by comparing thermal stability (i.e. broad heat flow stress response) of free TC with the encapsulated TC in LCA-NP. Disappearance of the endothermic peak at 247°C indicted molecular encapsulation of TC in CS-AG inclusion complex (TC was protected within the cavity of LCA-NP) (Zhang and others 2008). This finding is consistent with Hill and others (2013a) who observed the same results with TC and eugenol entrapment in beta-cyclodextrin inclusion complexes. Similar results have also been reported in studies by Gomes and others (2011), Kamimura and others (2014), and Thwala (2012) with entrapped volatile oils.

An additional DSC study was completed on different mass ratio of AG:CS (AG:CS mass ratio of 5:1 and 2:1 are suboptimal formulations) (Figure 4.7). It appeared that increasing the concentration of CS increased the thermal stability of loaded nanoparticle formulations likely due to increased ionic interactions (i.e. AG:CS mass ratio approaches stoichiometric proportion). Sarmento and others (2006) determined that increasing CS concentration had a direct relationship with increasing the value of exothermic peaks. This was not observed in this study as there is no clear indication of this relationship. However, it can be concluded that changing the mass ratio of AG:CS resulted in different interaction between polymers with more stable complexes forming at higher CS concentrations. Optimizing process parameters also played a role in the thermal characterization. AG:CS 1.5:1 was the only mass ratio with optimized processing parameters and was the only ratio to display thermal stability (i.e. broad exothermic and endothermic peaks). Thus, this could suggest thermal stability where a

high number of polymeric complexes and ionic bonds create small compact particles increasing the stability of the formulation. It is also a possibility that more energy was required to remove higher concentrations of residual water absorbed to nanoparticles in high AG:CS mass ratios while less energy was released during breaking of ionic interactions from low AG:CS mass ratios (Ruo 2012; Zhang and others 2008). Moving forward, DSC will be useful for determining impacts of heating properties of nanostructure, tolerances of processing, temperature abuse, and temperature triggered controlled release system importance.

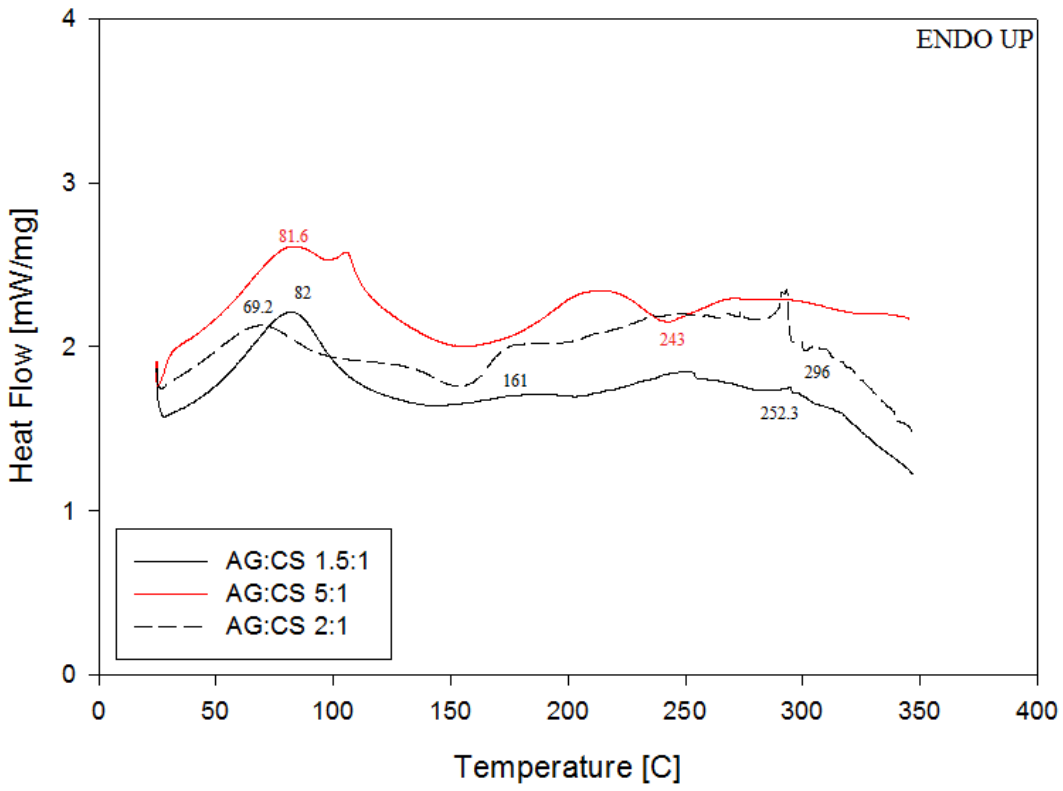

Figure 4.7. Effects of different mass ratios of at alginate to chitosan on thermal stability of *trans*-cinnamaldehyde loaded particles (LCA-NP)

4.3.3 Transmission Electron Microscopy (TEM)

Transmission electron microscopy analysis confirmed the presence and size as well as morphological information regarding shape and surface characteristics of nanoparticles. Morphology showed that LCA-NP most resembled a spherical shell and core type arrangement (i.e. spherical, distinct, and regular) (Figures 4.8 (a) - (e)). LCA-NP appeared to be smooth and surrounded by a 10-50 nm thick wall while ULCA-NP (control) were not of distinct spherical shape. Rather, they seemed to have less physical integrity and appear almost hollow. The change in morphology from UCA-NP to LCA-NP suggests the existence of amorphous products with the presence of a single compound in the complex (TC entrapment) (Hill and others 2013a; Teixeira and others 2013; Kamimura and others 2014; Zhang and others 2008). Thwala (2012) found the opposite to occur where inclusion complexes with tagete oil showed rough appearances while control particles showed a smooth appearance. Similar morphological characteristics and particle size were obtained in studies by Silva and others (2011) and Li and others (2008) where paraquat and nifedipine were successfully loaded into CS-AG NP (20-50 nm).

TEM images confirmed the size of LCA-NP. In fact, sizes of nanoparticles measured by TEM were smaller than the sizes attained from particle size analysis. Sizes seemed to be in two general regions; 10-50 nm and 100 nm. This occurrence was observed in particle size analysis as a bimodal size distribution for several sample formulation (Appendix 2). Silva and others (2011) explains this phenomena as a result of the dehydration of nanoparticles during TEM sample preparation. Additionally, dynamic

light scattering measures the hydrodynamic radius of the NP which includes the layers that form around hydrophilic particles which often leads to overestimation of particle size.

Similarly to beta-cyclodextrins complexes studied by Hill and others (2013a), there is evidence of agglomeration where large particles are attracting smaller particles. This could explain the difficulty in obtaining monodisperity during particle size analysis. There is a strong tendency to from clusters. However, this could be due to TEM‘s sample preparation method of charging particles on the grid in order to set and adhere the sample to ultimately separate into smaller particles on TEM images (Hill and others 2013a). This could explain the difficulty in obtaining monodisperity during particle size analysis. There also appears to be slight amounts of free polymer in the medium which could potentially coagulate CS and AG (Zohri and others 2011).

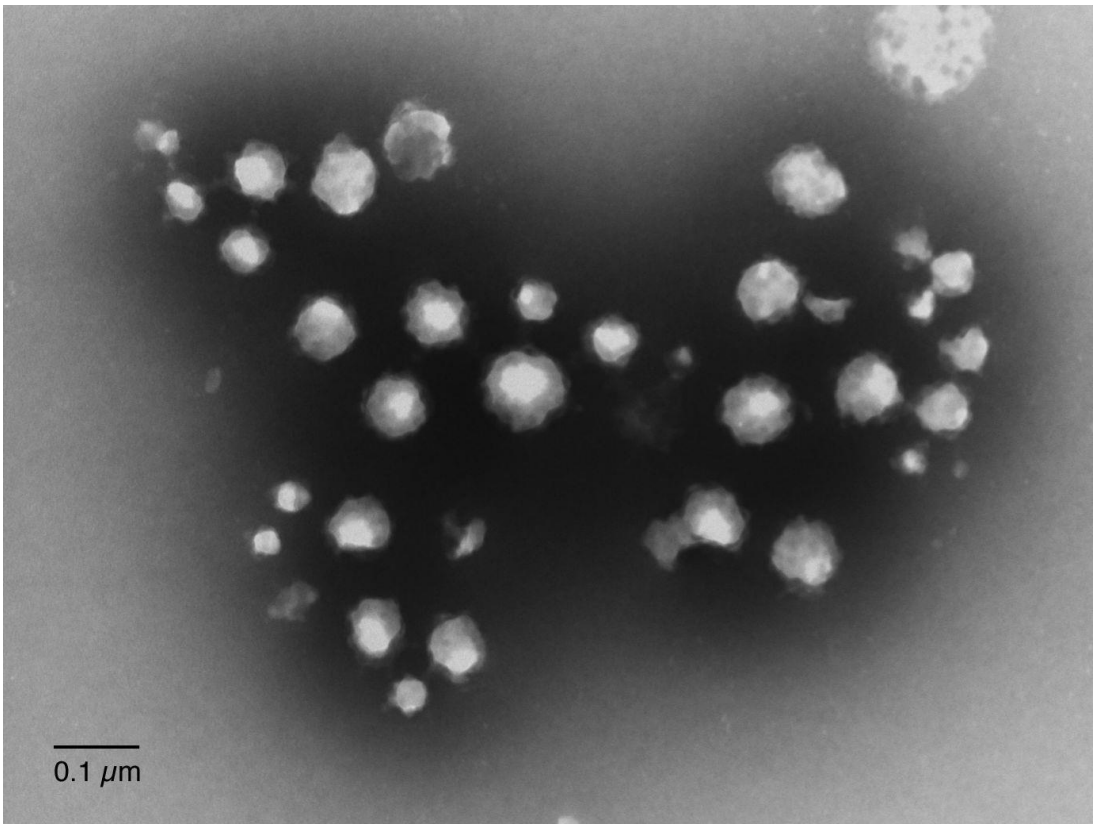

Figure 4.8 (a). Control: chitosan-alginate nanoparticles with no incorporated *trans*-cinnamaldehyde (71,000 Magnification).

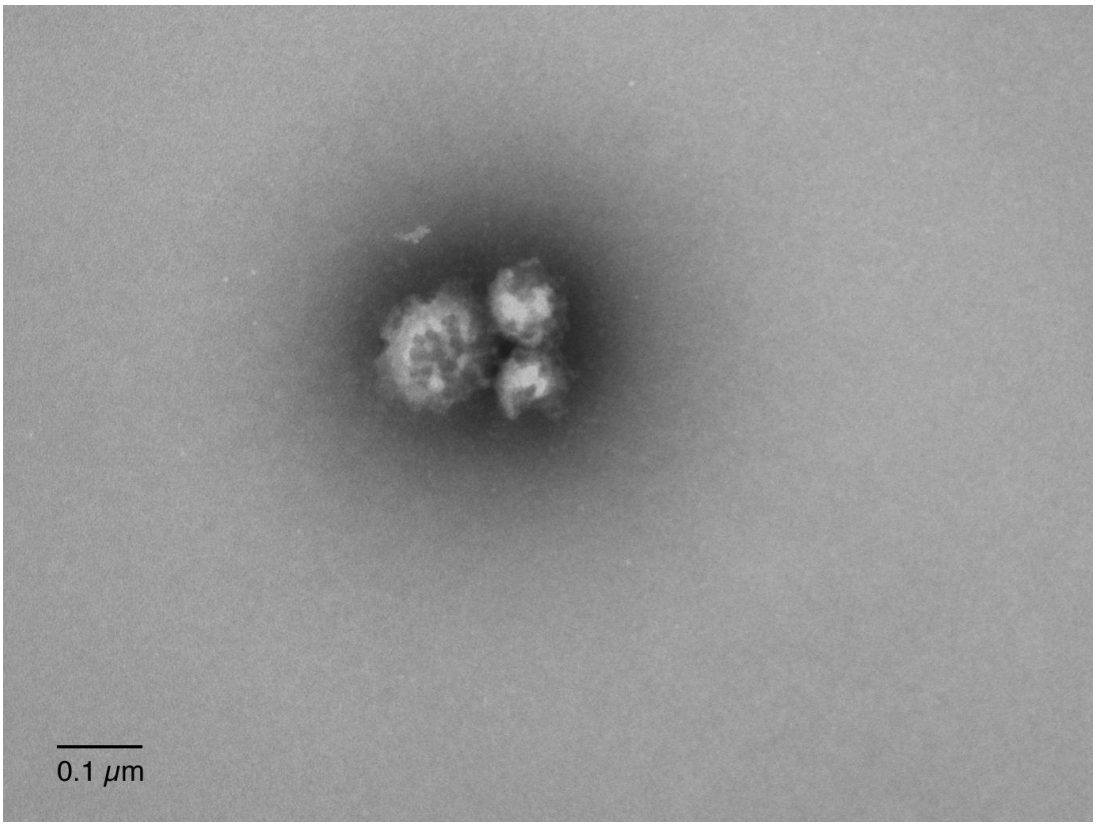

Figure 4.8 (b). Control: chitosan-alginate nanoparticles with no incorporated *trans*-cinnamaldehyde (71,000 Magnification).

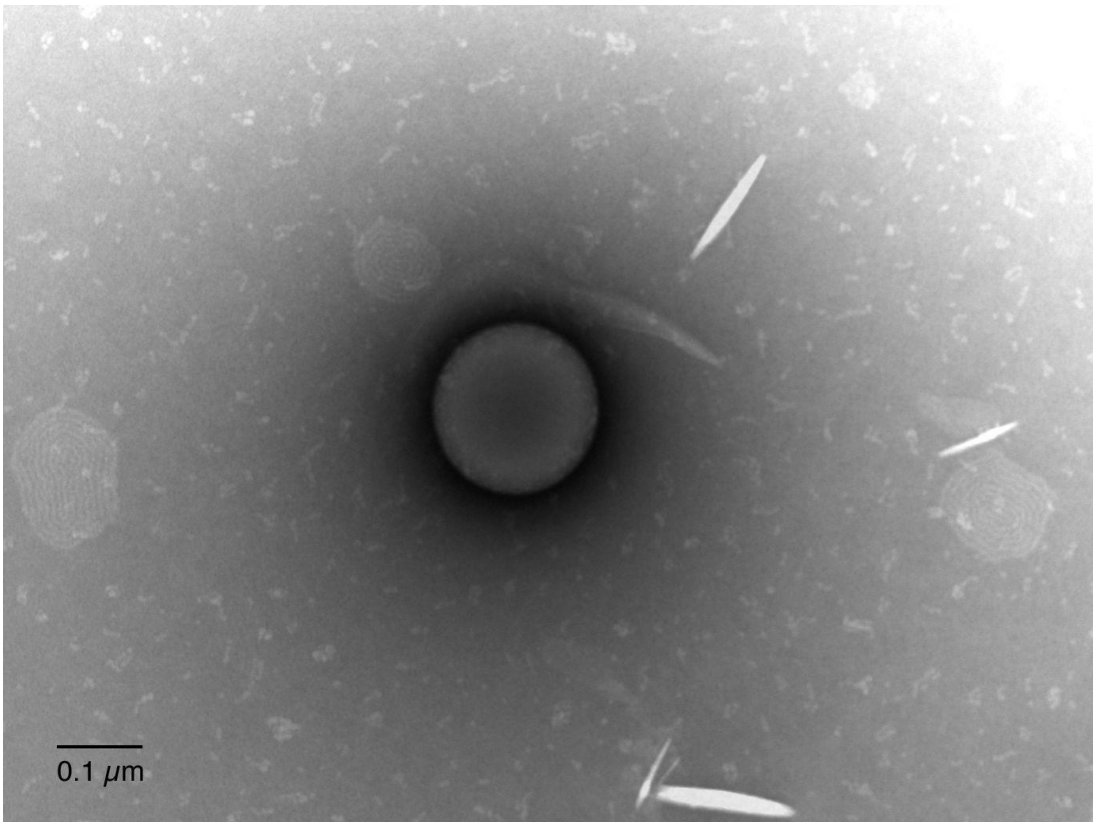

Figure 4.8 (c). Inclusion Complex: chitosan-alginate nanoparticles with incorporated *trans*-cinnamaldehyde (71,000 Magnification).

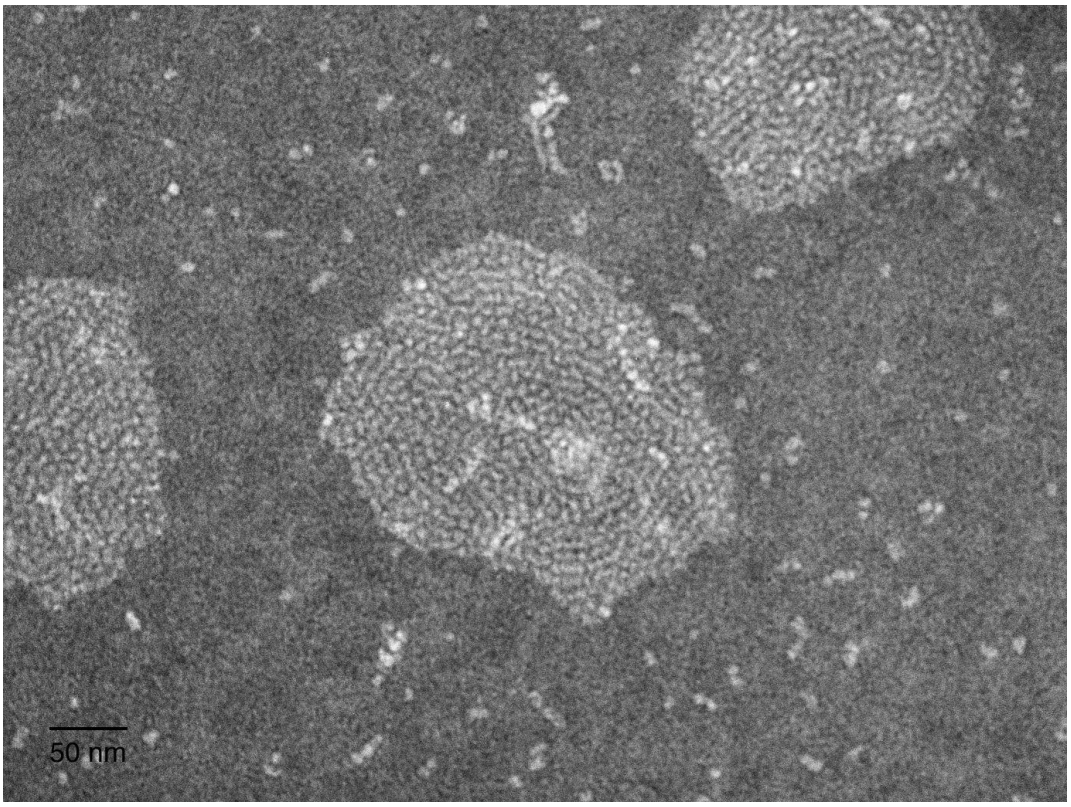

Figure 4.8 (d). Inclusion Complex: chitosan-alginate nanoparticles with incorporated *trans*-cinnamaldehyde (140,000 Magnification).

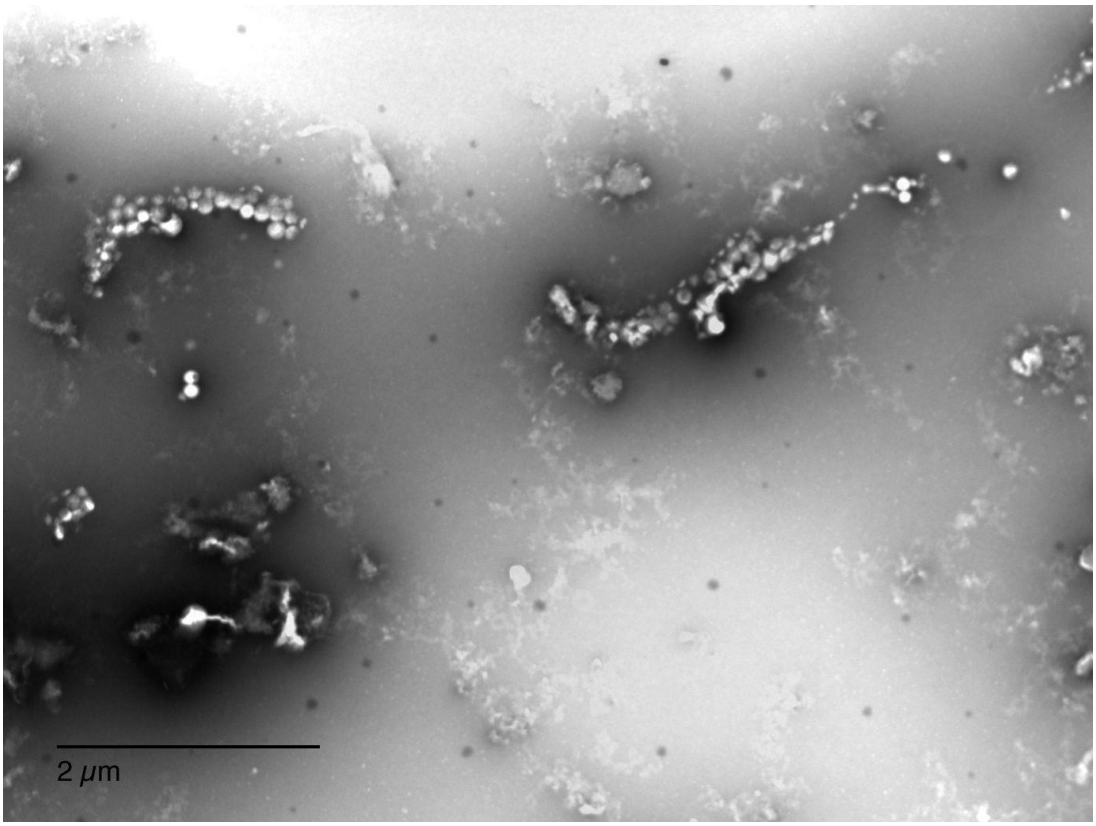

Figure 4.8 (e). Inclusion Complex: chitosan-alginate nanoparticles with incorporated *trans*-cinnamaldehyde (11,000 Magnification).

4.3.4 Antioxidant Capacity in Apple Juice

The method used to survey antioxidant capacity of LCA-NP was the 2,2-diphenyl-1-picrylhydrazyl radical scavenging test (i.e. DPPH test). The principle of this method was based on the reduction of DPPH in the presence of a hydrogen donating TC due to the formation of diphenylpicryl-hydrozine. LCA-NP reduced the color of DPPH due to its proton radical scavenging ability. Discoloration of violet DPPH to a yellow coloration clearly demonstrated the effect of nanoparticles as antioxidants. The scavenging effect (SE) applies to the antioxidant capacity of the sample.

DPPH scavenging potential of LCA-NP in apple juice is depicted in Figure 4.9. It can be concluded that: (1) scavenging ability was LCA-NP concentration dependent; (2) ULCA-NP (control) showed marginal SE; (3) inclusion complex maintained TC antioxidant activity. The final SE in apple juice was 62%. The EC_{50} value (i.e. the concentration of antioxidant required to reduce DPPH to 50% of its original concentration) was used to compare scavenging potential of LC-NP in this study to antioxidants in other studies. The EC_{50} value of LCA-NP in this study was 1 mg/ml. The following studies obtained comparable results: (1) Woranuch and Yoksan (2013) found 54% SE of eugenol loaded CS NP; (2) Teixeira and others (2013) found the SE of black pepper oleoresin loaded beta-cyclodextrins to be 68%; (3) Nallamuthu and others (2013) determined SE of thymoquinone loaded PLGA NP to be 71% at 1 mg/ml (EC_{50} = .4 mg/ml); (4) Zhang and others (2008) found SE of quercetin loaded CS NP to be 80% at 2 mg/ml (EC_{50} = 1.5 mg/ml).

LCA-NP had a higher scavenging activity in apple juice (EC_{50} = 1 mg/ml) in comparison to LCA-NP resuspended in 0.2 μm filtered water (control; EC_{50} = 1.75 mg/ml) at all polymer concentrations tested (data not shown). However, some of this effect may be attributed to the initial 9.4% increase of DPPH scavenging in apple juice compared to the control. Chien and others (2007) also observed this result as chitosan solubilized in apple juice (EC_{50} = 0.18 mg/ml) had a higher DPPH radical activity than in aqueous solution (EC_{50} = 1 mg/ml) due to apple juice‘s strong hydrogen donating capacity (Figure 4.9).

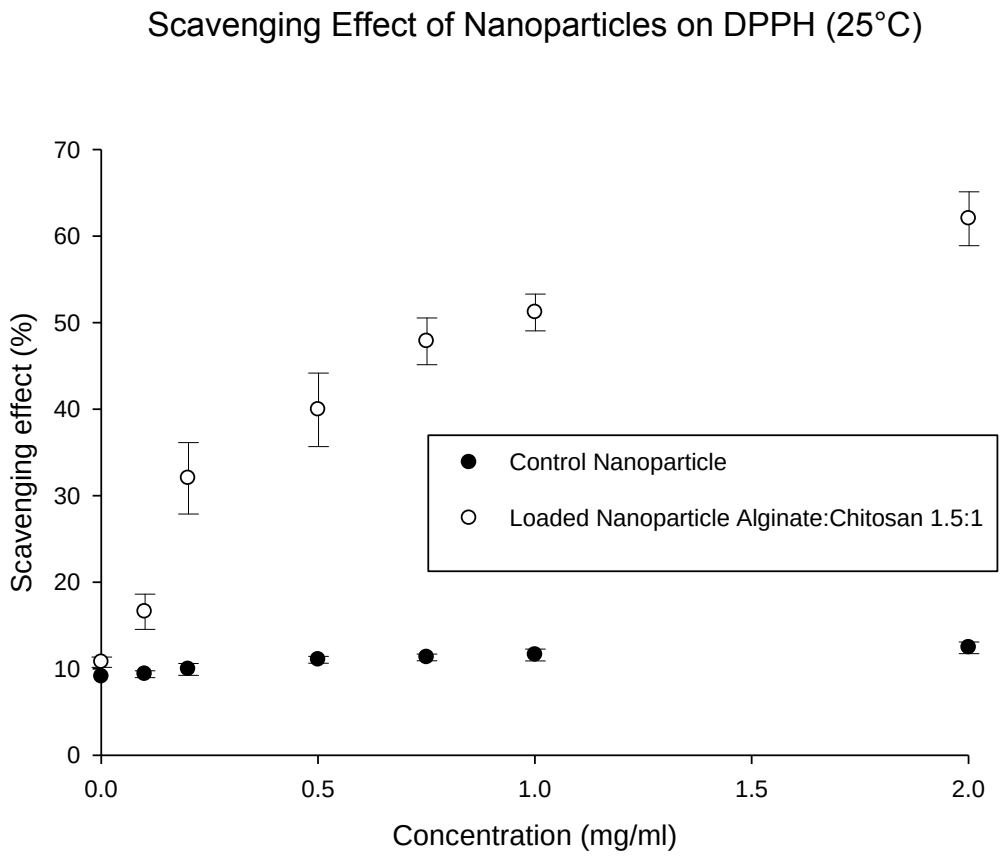

Figure 4.9. Scavenging effect of *trans*-cinnamaldehyde loaded nanoparticles and unloaded nanoparticles (control) at different concentrations in apple juice at 25°C.

ULCA-NP (control) showed limited scavenging capacities resuspended in both aqueous solution and apple juice. Scavenging effect of LCA-NP and ULCA-NP were statistically significant ($p < 0.05$). Similar results were obtained in a study by Zhang and others (2008) where quercetin was entrapped with CS; control particles showed limited

scavenging capacities while quercetin loaded nanoparticles showed increasing scavenging effects as concentration increased (EC_{50} = 1.5 mg/ml) (Figure 4.9).

The nanoparticle inclusion complex helped maintain TC antioxidant activity. As the concentration of LCA-NP increased so did the amount of TC, thus increasing concentration of antioxidant. Free TC did not show a significantly higher EC_{50} (7.7 μg/ml; Appendix 3) value in comparison to loaded TC ($p < 0.05$) based on entrapment efficiency tests (EC_{50} = 10.38 μg/ml) indicating TC was just as available to react in free form as it was in inclusion complexes. This is likely due to a large fraction of TC escaping LCA-NP in the 30 min DPPH scavenging window at the acidic pH range of apple juice. Additionally, other studies have found essential oils to release faster at pH 1.5 in comparison to pH 7.4 meaning that LCA-NP are pH sensitive and these particles could have rapid release in acidic environments such as apple juice (Li and others 2008; and Thwala 2012). Xu and others (2014) and Teixeira and others (2013) observed the same effect with curcumin loaded carrageenan nanoparticles and black pepper oleoresin loaded beta-cyclodextrins, respectively. Results confirm that TC encapsulated in LCA-NP is available for complexing DPPH and could be beneficial antioxidant delivery systems by increasing shelf life and quality of aqueous food systems such as acidic beverages.

4.3.5 Minimum Inhibitory and Bactericidal Concentration

Minimum inhibitory and bactericidal concentrations (MIC, MBC) of TC, LCA-NP, and ULCA-NP against *Escherichia coli* O157:H7 and *Listeria monocytogenes* are shown in Table 4.12 and Table 4.13, respectively. MIC values for free TC were 500

μg/ml for both *E. coli* O157:H7 and *L. monocytogenes*. MIC values for LCA-NP were 7,031.25 μg/ml for *E. coli* O157:H7 and 14,062.5 μg/ml for *L. monocytogenes*. Bactericidal effects were not observed for the majority of concentrations tested and MBCs ($\geq$3.0 $\log_{10}$ CFU/ml reduction of the pathogen) were not consistent across plate replicates (high variability). All antimicrobial compounds tested are believed to have bactericidal abilities, but at higher concentrations than those used in this study (> 28,125 μg/ml) (Hill and others 2013a). Results of the positive controls indicated complete absence of inhibition by both bacteria species (data not shown).

Table 4.12 Minimum inhibitory and bactericidal concentration against *Escherichia coli* O157:H7 for selected antimicrobial compounds.

Antimicrobial Compound	MIC[a] [μg/ml]	MBC[a] [μg/ml]
Trans-Cinnamaldehyde	500	1000
ULCA-NP	>14062.5	>28125
LCA-NP	7031.25 (730)[c]	>28125 (2920)[c]

[a] Values are the lowest concentration of unencapsulated or chitosan-alginate encapsulated essential oil for which a $\leq$0.05 OD_{630} change was observed after 24 h incubation at 35°C in tryptic soy broth.

[b] Values preceded by a higher than sign (>) means that tested concentrations were not sufficient to determine the MIC or MBC values.

[c] Values are the representative concentrations of free *trans*-cinnamaldehyde at the respective LCA-NP concentration.

[1]LCA-NP represents chitosan alginate nanoparticles loaded with *trans*-cinnamaldehyde while ULCA-NP represents nanoparticles with no incorporated *trans*-cinnamaldehyde (control).

Table 4.13. Minimum inhibitory and bactericidal concentration against *Listeria monocytogenes* for selected antimicrobial compounds.

Antimicrobial Compound	MIC[a] [μg/ml]	MBC[a] [μg/ml]
Trans-Cinnamaldehyde	500	2000
ULCA-NP[1]	>14062.5	>28125
LCA-NP[1]	14062.5 (1460)[c]	>28125 (2920)[c]

[a] Values are the lowest concentration of unencapsulated or chitosan-alginate encapsulated essential oil for which a ≤0.05 OD_{630} change was observed after 24 h incubation at 35°C in tryptic soy broth.
[b] Values preceded by a higher than sign (>) means that tested concentrations were not sufficient to determine the MIC or MBC values.
[c] Values are the representative concentrations of free *trans*-cinnamaldehyde at the respective LCA-NP concentration.
[1]LCA-NP represents chitosan alginate nanoparticles loaded with *trans*-cinnamaldehyde while ULCA-NP represents nanoparticles with no incorporated *trans*-cinnamaldehyde (control).

All antimicrobial compounds showed different degrees of inhibition against *E. coli* O157:H7 and *L. monocytogenes*. The growth of both microorganisms was inhibited by TC as well as LCA-NP; being this concentration the minimum inhibitory concentration in the broth resulting in lack of visible microorganism growth changes. At the MIC, a delay in the lag phase, a slower growth rate, and thus a lower final cell concentration of microorganism were observed (Burt 2004; Kalemba and Kunicka 2003). The concentration of TC in LCA-NP would correspond to a MIC of approximately 730 and 1,460 μg/ml of antimicrobial compound (TC) for inhibition of *E. coli* O157:H7 and *L. monocytogenes*, respectively considering loading and maximum entrapment efficiency (73.24%). This value suggests if all theoretically entrapped oil was removed, both microorganisms would be inhibited (TC concentration > 500 μg/ml). However, it is likely that not all entrapped TC escapes nanoparticles in the 24 h incubation period. The broth used for particle dissolution in this study had a pH of

approximately 7.4. Other studies have found essential oils to release from hydrophilic systems slower at pH 7.4 in comparison to acidic pH ranges meaning that LCA-NP may not have released sufficient *trans*-cinnamaldehyde for antimicrobial effects to be observed (Li and others 2008; and Thwala 2012).

Similar results to this study were obtained by Gomes and others (2011) with a combination of TC and eugenol loaded in PLGA with MIC at 10,000 and 20,000 μg/ml (corresponds to 800 and 1,600 μg/ml entrapped essential oil) for *Salmonella* spp. and *Listeria* spp., respectively. Additional studies that support this study include: (1) Hill and others (2013a) observed lower TC MIC (400 and 500 μg/ml) and MBC (1,000 and 2,000 μg/ml) for representative Gram-negative and Gram-positive microorganisms; (2) Pozzo and others (2012) found MIC of free TC against *Staphylococcus spp*. to be 800-1600 μg/ml and MBC to range from 800-6,400 μg/ml; (3) Huaiqiong and others (2013) found free TC MIC of 200 μg/ml and MBC of 900-1,400 μg/ml for *L. monocytogenes*.

MIC/MBC results indicate that *L. monocytogenes* was more tolerant to the inhibition by TC inclusion complex in comparison to *E. coli* O157:H7. It is generally accepted that Gram-positive microorganisms are more predisposed to inhibition of essential oils versus Gram-negative microorganisms due to the absence of a lipopolysaccharide outer membrane that screens entry of hydrophobic compounds into microbial cells (Kim and others 1995; Kalemba and Kunicka 2003; Hill and others 2013b; Burt 2004). *L. monocytogenes*, however, is a common exception to the statement that Gram-positive organisms are generally susceptible to inhibition by essential oils. In fact, *L. monocytogenes* has shown high tolerances to inhibition by essential oils as

confirmed by previous studies (Gomes and others 2011; Kalemba and Kunicka 2003; Kim and others 1995).

LCA-NP did not seem to enhance the antibacterial effect of TC ($p > 0.05$). In fact, results suggest that nanoparticles marginally decreased the inhibitory effect of TC because more respective TC was needed for inhibition of both microorganisms tested (Table 4.12 and Table 4.13). This is likely attributed to preparation methods and *trans*-cinnamaldehyde release mechanisms. Lyophilized nanoparticles had to be resuspended and added into test wells rapidly as not to cause burst release before addition of inoculum. This may have affected the TC release in the 24 h incubation period in broth (i.e. only adsorbed TC released corresponding to maximum release of 876 μg/ml [30%]). Again, essential oil release from hydrophilic systems has been shown to be slower at pH 7.4 in comparison to acidic values where rapid breakdown of particles and release of active drug takes place (Li and others 2008; and Thwala 2012). Increasing the initial incubation period to 48 or 72 h could help clarify results by allowing particles to break down further (i.e. sustained release function) and release additional internalized TC from loaded NP (Hill and others 2013b). Factors affecting release rate are solubilization and dissolution rate in broth medium because the release medium penetrates into particles and dissolves entrapped active molecules. This affects both the controlled release study and antimicrobial assays. Comparable results were obtained in the following studies: Hill and others (2013b) obtained a MIC value of 549.23 μg/ml for cinnamon bark loaded PLGA NP where PLGA loaded particles showed a lower MIC; Zohri and others (2010) found MIC of Nisin loaded CS-AG NP was 500 μg/ml after 72 h for *Staphylococcus*

aureus and was much lower than free Nisin (2000 μg/ml); (3) Sadeghi and others (2008) found MIC and MBC of CS NP was 2000 μg/ml against *Staphylococcus aureus* with entrapped insulin. Differences between results in this study and others reported by authors could be due to the composition of essential oils or MIC/MBC techniques employed. Also, cinnamon essential oil composition can be varied depending on where it was extracted (Pozzo and others 2012).

Different oils have different inhibition/bactericidal mechanisms (Kalemba and Kunicka 2003). In terms of essential oils, thymol and carvacrol have higher anti-listerial activity compared to eugenol and TC which was observed in this study (Huaiqiong and others 2013). TC is more polar than eugenol, thymol, and carvacrol (highest water solubility at 1.76 g/L at 20°C) and thus may be less effective in disrupting cytoplasmic membrane.

The lipophilic character of the hydrocarbon skeleton has been reported as a main reason for essential oil antimicrobial action (Kong and others 2010). Results suggest that TC and LCA-NP inhibition mechanisms (MIC) against *E. coli* O157:H7 and *L. monocytogenes* are comparable. The antimicrobial mechanisms responsible for inhibition by free TC were less available to interact with microorganisms due to its inclusion in CS-AG inclusion complex.

Shan and others (2007) described the antimicrobial mechanism of TC as follows: (1) binding to cell surface to penetrate target sites (e.g. phospholipid bilayer of cytoplasmic membrane, membrane bound enzymes); (2) inhibition of proton motive force, respiratory chain, electron flow, active transfer, and substrate oxidation; (3)

coagulation of cell contents. Additionally, uncoupling of phosphorylation, loss of metabolites, and disruption of DNA, RNA, lipid, protein, and polysaccharide synthesis take place. The hydrophilic components of TC (e.g. aldehyde group) interact with polar parts (e.g. outer membrane proteins) of the bacterial cell membrane while hydrophobic components react with lipids on the membrane and result in increased membrane permeability, disturbing enzyme systems and genetic material (Kong and others 2010; Ruengvisesh and others 2014). Subsequent damage to cell wall and cytoplasmic membrane disrupt the permeability barrier causing expansion and destabilization of the membrane thus increasing membrane fluidity, increasing ability of TC to pass through and manifest itself as leakage of various vital intracellular constituents such as ions, ATP, nucleic acid and amino acids. Finally, cell death results when there is extensive loss of cell contents, the exit of critical molecules and ions, or the initiation of the autolytic process (Kong and others 2010; Kalemba and Kunicka 2003). In addition, modes of antibacterial action are dependent on the type of microorganism and its respective cell wall structure and outer membrane arrangement.

The hydrophobic nature of TC creates challenges to deliver oil for microbial inhibition. However, encapsulation of TC could effectively distribute oil throughout media and to microbial cells while also protecting it from adverse interactions to maintain the potential for antimicrobial influence (Hill and others 2013a; Ruengvisesh and others 2014). If TC is indeed delivered to microbial cells, the hydrophobic nature of TC allows high affinity to cell membrane allowing for easy partition into cell membrane. Without this encapsulation, Hill and others (2013a) explain that TC may never come into

contact with microorganisms and may instead coalesce to limit hydrophilic and hydrophobic interactions or lose potency over time in solution (Burt 2004; Kong and others 2010). Overall, these results indicated that LCA-NP could be useful antimicrobial delivery systems with the ability to inhibit a broad spectrum of microorganisms. Further improved methodology and synthesis techniques could elucidate that these nanosystems are stable and effective preservatives for increasing shelf life of fresh or ready to eat foods. Additional testing should be carried out at increased incubation times (e.g. 48 and 72 h) and with a combination of loaded essential oils (e.g. cinnamaldehyde and thymol) (Pei and others 2009; Gomes and others 2011).

5. CONCLUSION

5.1 Conclusions

This study explored combinations of alginate (AG) and chitosan (CS) for use as entrapment matrices for the essential oil *trans*-cinnamaldehyde (TC) which is poorly soluble in aqueous media. The following conclusions were drawn based on the specific objectives of the study:

Preliminary Nanoparticles Synthesis and Formulation Study:

i. The ionotropic gelation polyelectrolyte complexation method (IG-PEC) successfully prepared nanoparticles (NP) with entrapped hydrophobic active compound at the highest payload potential at the smallest size.

ii. The best working AG to CS mass ratio was determined to be 1.5:1 at a pH dispersion of 4.7. Particle size and entrapment efficiency were further optimized at this mass ratio using an AG:$CaCl_2$ mass ratio of 4.8:1, AG:TC mass ratio 37.5:1, 18 gauge syringe needle, stirring times of 90 minutes, 15 minutes of homogenization, and equilibration time of 24 hours. Both particles size and EE of optimized LCA-NP was 166.26 nm and 73.24%, respectively.

iii. Results confirmed that AG:CS mass ratio, pH, and syringe size had the largest effect on particle size and EE.

iv. The final nanoparticle system with modified and optimized processing reduced size by 43.6% and increased entrapment efficiency by 17.2%. Optimized nanoparticles showed increased shelf life (6 weeks) and translucency in solution.

v. These results may ultimately prove that smaller particles are a result of functional groups being available in stoichiometric proportion.

Nanoparticle Characterization Study:

vi. Release tests showed TC release from LCA-NP best followed the bioexponential model.

vii. The total amount of TC released decreased after 10 h (32.5%). Following initial burst release, another stage of controlled release was observed from 10 to 72 h with final release of 62.31%.

viii. DSC confirmed TC inclusion into LCA-NP by indirectly comparing thermal stability of free TC with the encapsulated TC in LCA-NP. TC‘s sharp endothermic peak at 247°C corresponding to its boiling point disappeared in LCA-NP thermograms indicating molecular encapsulation of TC in inclusion complex. AG:CS 1.5:1 was the only mass ratio with optimized processing parameters and it was the only ratio to display thermal stability (i.e. broad heat flow stress response). Thus, this could suggest thermal stability where a high number of polymeric complexes and ionic bonds create small compact particles increasing the stability of the formulation.

ix. TEM confirmed presence and size of nanoparticles.

x. Nanoparticles most resembled a spherical shell and core type arrangement (i.e. spherical, distinct, and regular) and were in the size region of 10-100 nm. LCA-NP appeared to be smooth and surrounded by a 10-50 nm thick wall while control NP were not of distinct spherical shape. The change in morphology from

UCA-NP to LCA-NP suggests the existence of amorphous products with the presence of a single compound in the complex.

Antioxidant and Antimicrobial Nanoparticle Study:

x. DPPH scavenging ability was LCA-NP concentration dependent and inclusion complex maintained TC antioxidant activity while control NP showed only a marginal DPPH scavenging effect.

xi. The final scavenging effect of LCA-NP in apple juice was 62% (EC_{50} = 1 mg/ml) of DPPH radicals.

xii. LCA-NP had a higher scavenging activity in apple juice in comparison to LCA-NP resuspended in 0.2 μm filtered water (EC_{50} = 1.75 mg/ml) at all polymer concentrations tested.

xiii. Free TC did not show a significantly different EC_{50} (7.7 μg/ml) value in comparison to loaded TC based on entrapment efficiency tests (EC_{50} = 10.3 μg/ml) indicating TC was just as available to react in free form as it was in inclusion complexes.

xiv. Results confirm that TC encapsulated in LCA-NP is available for complexing DPPH and could be beneficial antioxidant delivery systems by increasing shelf life and quality of aqueous food systems such as acidic beverages.

xv. MIC values for free TC were 500 μg/ml for both *E. coli* O157:H7 and *L. monocytogenes*. MIC values for LCA-NP as a function of free TC were 730 μg/ml for *E. coli* O157:H7 and 1,460 μg/ml for *L. monocytogenes* considering loading and maximum entrapment efficiency (73.24%).

xvi. Bactericidal effects were not observed for the majority of concentrations tested and MBCs (> 2,920 μg/ml).

xvii. Results indicate that *L. monocytogenes* was more tolerant to the inhibition by TC inclusion complex in comparison to *E. coli* O157:H7. LCA-NP did not seem to enhance the antibacterial effect of TC.

xviii. Overall, these results suggest that LCA-NP could be useful antimicrobial delivery systems with the ability to inhibit a broad spectrum of microorganisms.

General Conclusions

xix. Optimizing processing parameters of the IG-PEC method will continue to increase the significance of characterizing polymeric nanoparticles with entrapped oil

xx. Optimized particle preparation and formulation will assist in future utility of post-processing and food applications such as the stabilization of lipophilic flavoring agents, shelf life stability, antioxidant and antibacterial potential, and the reduction of unpleasant odors and flavors.

xxi. Small size of LCA-NP are desirable because they are not visible to the human eye and cannot be detected in the mouth so they will not adversely affect texture or appearance of food products where antimicrobials are applied.

xxii. The use of CS-AG NP as carriers for essential oils and other antimicrobial compounds shows potential and could improve efficacy of drug loading and delivery due to the ability to entrap hydrophobic compounds, controlled and

sustained release, and small size (easy diffusion and movement into cytoplasm of microorganisms)

xxiii. Encapsulation of lipophilic compounds such as *trans*-cinnamaldehyde into aqueous-soluble nanoparticle systems will provide further solutions to several problems in the food industry by both improving solubility and providing a controlled way to deliver and release drug payload with full potential.

xxiv. The analysis of LCA-NP allowed proper characterization of these systems as nanoscale, bioactive, or stable and helped clarify structural and functional relationships between carrier molecule and active entrapped compound.

xxv. Antioxidant and antimicrobial testing yielded substantial data for further research and design applications into food products (e.g. acidic beverages). LCA-NP holds forth tremendous promise to provide benefits not just within food products but also surface contact materials (i.e. packaging).

xxvi. Recent technological advances in nanomaterials in parallel with the food industries ambition to discover new and alternative solutions has created a new sector in the food industry where nanotechnology has emerged as a new solution for improving quality and safety in foods. This research only attempts to substantiate these efforts to control and structure foods with greater functionality and value.

5.2 Future Considerations

Moving forward, *trans*-cinnamaldehyde loaded chitosan-alginate nanoparticle synthesis and characterization could be further improved by:

Methodology:

i. Testing different types of CS and AG (e.g. molecular weight, polymer concentration, deacetylation of chitosan, lower guluronic acid content of alginate) in initial formulation.

ii. Filtering using simple techniques such as ultracentrifugation as an alternative to tangential flow filtration. Tangential flow filtration is an expensive process and large polymers can congest filtration membranes slowing down filtration and increasing equilibration time. Ultracentrifugation could speed up nanoparticles preparation process and reduce cost.

iii. Using smaller syringe size, reduced droplet rate, and increased temperature of solution (>25°C) during calcium chloride, *trans*-cinnamaldehyde, and chitosan addition to attempt to increase pre-gel viscosity, increase ionic interactions, and speed up solubilization of polymers and oil.

iv. Changing stage of TC incorporation (e.g. add TC to $CaCl_2$ solution) to determine effects on size and entrapment.

v. Layering fully developed nanoparticles with an additional layer of *trans*-cinnamaldehyde and chitosan to alter burst release mechanics.

Thermal and Physical Characterization:

vi. Completing controlled release and antioxidant testing at a range of temperatures and pH values to determine TC release characteristics and better model release behavior.

vii. Utilizing the Ritger and Peppas (1987) or Gomes and others (2011) equations for modeling release of TC from LCA-NP.

viii. TEM and particle size analysis being performed with non-lyophilized samples.

Antioxidant and Antimicrobial Assays:

ix. Addition of LCA-NP directly to food commodity (e.g. fresh produce).

x. Testing range of temperatures in the DPPH antioxidant study to help determine if release behavior has a larger effect than observed in this study.

xi. Using a combination of loaded essential oils (e.g. cinnamaldehyde and thymol) (Pei and others 2009; Gomes and others 2011).

xii. MIC/MBC testing carried out at increased incubation times (e.g. 48 and 72 h).

xiii. Acidifying the broths used for incubation of microorganisms in order to change the release behavior of TC from NP.

xiv. Completing a controlled release test in parallel with MIC/MBC assay to determine if release behavior in antimicrobial test is similar to the PBS buffer for the NP batch tested (i.e. same amount of trans-cinnamaldehyde release).

xv. Testing controlled release tests in TSB to confirm TC release is similar to PBS.

xvi. Clarifying the mechanisms of antimicrobial activity of LCA-NP (e.g. confocal microscopy).

xvii. Determining L. *monocytogenes* stress tolerance and why tolerance increased in the presence of TC.

xviii. Further improved methodology and synthesis techniques could elucidate that these nanosystems are stable and effective preservatives and antioxidants for increasing shelf life of fresh or ready to eat foods.

REFERENCES

Abdelwahed W, Degobert G, Stainmesse S, Fessi H. 2006. Freeze-drying of Nanoparticles: Formulation, Process and Storage Considerations. Advanced Drug Delivery Reviews 58(15):1688-713.

Abdollahi S, Lotfipour F. 2012. PLGA- and PLA- Based Polymeric Nanoparticles for Antimicrobial Drug Delivery. Biomedicine International 3(1):1-11.

Abdou ES, Osheba AS, Sorour MA. 2012. Effect of Chitosan and Chitosan-Nanoparticles as Active Coating on Microbiological Characteristics of Fish Fingers. International Journal of Applied Science and Technology 2(7):158-69.

Agnihotri S, Mallikarjuna N, Aminabhavi T. 2004. Recent Advances on Chitosan-based Micro- and Nanoparticles in Drug Delivery. Journal of Controlled Release 100(1):5-28.

Ahirrao S, Gide P, Shrivastav B, Sharma P. 2013. Ionotropic Gelation: A Promising Cross Linking Technique for Hydrogels. Journal of Pharmaceutics and Nanotechnology 2(1):1-6.

Ahmed R, Gardouh R, Mamdouh M, Ghorab., S. SG, Abdel-Rahman. 2012. Effect of Viscosity, Method of Preparation and Homogenization Speed on Physical Characteristics of Solid Lipid Nanoparticles. Journal of Science and Technology 2(10):996-1006.

Al-Kaysi R, Muller A, Ahn T, Lee S, Bardeen C. 2005. Effects of Sonication on the Size and Crystallinity of Stable Zwitterionic Organic Nanoparticles Formed by Reprecipitation in Water. Langmuir 21(1):7990-4.

Anal AK, Stevens WF. 2005. Chitosan-alginate Multilayer Beads for Controlled Release of Ampicillin. International Journal of Pharmaceuticals 290:45-54.

Anderson JM, Shive MS. 1997. Biodegredation and Biocompatibility of PLA and PLGA Microspheres. Advanced Drug Delivery Reviews 28(1):5-24.

Armoon S, Golestan, Sharifzadeh. 2013. Studying the Enrichment of Ice Cream with Alginate Nanoparticles Including Fe and Zn Salts. Journal of Nanoparticles 23(1):1-5.

Astete C, Sabliov C, FW, Biris A. 2009. Ca(2+) cross-linked Alginic Acid Nanoparticles for Solubilization of Lipophilic Natural Colorants. Journal of Agricultural and Food Chemistry 57(16):7505-12.

Astruc D, Aranzaes JR, Boisselier É. 2011. Encapsulation of Vitamin C into Water Soluble Dendrimers. Google Patents.

Avgoustakis, Konstantinos. 2004. Pegylated Poly(Lactide) and Poly(Lactide-Co-Glycolide) Nanoparticles: Preparation, Properties and Possible Applications in Drug Delivery. Patras: Bentham Science Publishers.

Bajpai S, Chand N, Chaurasia V. 2012. Nano Zinc Oxide-Loaded Calcium Alginate Films with Potential Antibacterial Properties. Food and Bioprocess Technology 5(5):1871 - 81.

Bala I, Hariharan S, Kumar MN. 2004. PLGA Nanoparticles in Drug Delivery: The State of the Art. Critical reviews in therapeutic drug carrier systems 21(5):387-422.

Bansal V, Sharma P, Sharma N, Prakash O, Malviya R. 2012. Applications of Chitosan and Chitosan Derivatives in Drug Delivery. Advances in Biological Research 5(1):28-37.

Benita S. 1998. Recent Advances and Industrial Applications of Microencapsulation. In: Hıncal AA, Kaş HS, editors. Biomedical Science and Technology: Springer US. p. 17-29.

Berger J, Reist M, Mayer JM, Felt O, Peppas NA, Gurny R. 2004. Structure and Iinteractions in Covalently and Ionically Crosslinked Chitosan Hydrogels for Biomedical Applications. European journal of pharmaceutics and biopharmaceutics 57(1):19-34.

Bergin IL, Witzmann FA. 2013. Nanoparticle Toxicty by Gastrointestinal Route: Evidence and Knowledge Gaps. International Journal of Biomedical Nanoscience and Nanotechnology 3:1-2.

Berkland C, Kipper MJ, Narasimhan B, Kim KK, Pack DW. 2004. Microsphere Size, Precipitation Kinetics and Drug Distribution Control Drug Release from Biodegradable Polyanhydride Microspheres. Journal of controlled release 94(1):129-41.

Beuchat L. 1994. Antimicrobial Protperties of Spices and their Essential Oils. In: Dillon V, Board R, editors. Natural Antimicrobial systems and food preservation. Wallingford, U.K.: Cab International. p. 328.

Brandt AL, Castillo A, Harris KB, Keeton JT, Hardin MD, Taylor TM. 2010. Inhibition of Listeria Monocytogenes by Food Antimicrobials Applied Singly and in Combination. J Food Sci 75(9):M557-63.

Burt S. 2004. Essential oils: Their Antibacterial Properties and Potential Applications in Foods—a Review. International Journal of Food Microbiology 94(3):223-53.

Byun Y, Whiteside S, Darby D. 2011. α-Tocopherol-loaded Polycaprolactone (PCL) Nanoparticles as a Heat-activated Oxygen Scavenger. J Agric Food Chem 59(4):1428-31.

Caban S, Ayetkin, Sahin, Caoan Y. 2014. Nanosystems for Drug Delivery. OA Drug Design and Delivery 2(1):1-19.

Cegnar M, Kerc J. 2010. Self-assembled Polyelectrolyte Nanocomplexes of Alginate, Chitosan and Ovalbumin. Acta chimica Slovenica 57(2):431-41.

Čeppan M, Fiala R, Brezova V, Panak J, Motlikova V. 1993. Photooxidation of Cinnamaldehyde in Methanol — Product Analysis and Evolving Factor Analysis of UV Spectra. Chemicl Papers 48(1):25-30.

CFR. 2009. Code of Federal Regulations. Food Additive Permitted for Direcct Addtion to Food for Human Consumption: Synthetic Flavoring Substances and Adjuvants. Title 21, Part 172.515. p. 56-73.

Challa R, Ahuja A, Ali J, Khar RK. 2005. Cyclodextrins in Drug Delivery: An updated review. AAPS PharmSciTech 6(2):E329-E57.

Chen J, Tao X, Zhang M, Sun A, Zhao L. 2014. Properties and Stability of Blueberry Anthocyanin - Bovine Serum Albumin Nanoparticles. Journal of the Science of Food and Agriculture 94(9):1781-6.

Chia-Wen L, Chia-Wen Y, Sung-Chuan W, Kuang-Hway Y. 2009. DPPH Free-Radical Scavenging Activity, Total Phenolic Contents and Chemical Composition Analysis of Forty-Two Kinds of Essential Oils. Journal of Food & Drug Analysis 17(5):386-95.

Chien P, Sheu F, Huang W, Su M. 2007. Effect on Molecular Weight of Chitosans on their Antioxidative Activities in Apple Juice. Food Chemistry 102:1192-8.

Daemi H, Barikani M. 2012. Synthesis and Characterization of Calcium Alginate Nanoparticles, Sodium Homopolymannuronate Salt and its Calcium Nanoparticles. Scientia Iranica 19(6):2023-8.

Dandekar PP, Jain R, Patil S, Dhumal R, Tiwari D, Sharma S, Vanage G, Patravale V. 2010. Curcumin-loaded Hydrogel Nanoparticles: Application in Anti-malarial Therapy and Toxicological Evaluation. Journal of pharmaceutical sciences 99(12):4992-5010.

Das RK, Kasoju N, Bora U. 2010. Encapsulation of Curcumin in Alginate-chitosan-pluronic Composite Nanoparticles for Delivery to Cancer Cells. Nanomedicine : nanotechnology, biology, and medicine 6(1):153-60.

Davis FN. 2002. The Origin of Pegnology. Advanced Drug Delivery Reviews 54(4):457-8.

de Moura MR, Lorevice MV, Mattoso LH, Zucolotto V. 2011. Highly Stable, Edible Cellulose Films Incorporating Chitosan Nanoparticles. Journal of Food Science 76(2):N25-9.

de Moura MR, Mattoso LHC, Zucolotto V. 2012. Development of Cellulose-based Bactericidal Nanocomposites Containing Silver Nanoparticles and their use as Active Food Packaging. Journal of Food Engineering 109(3):520-4.

Dhanya A, Haridas K, Divia N, Sudheesh S. 2012. Development of Zein-Pectin Nanoparticle as Drug Carrier. International Journal of Drug Delivery 4:147-52.

Douglas KL, Tabrizian M. 2005. Effect of Experimental Parameters on the Formation of Alginate-chitosan Nanoparticles and Evaluation of their Potential Application as DNA Carrier. Journal of Biomaterials and Science 16(1):43-56.

Dudhani AR, Kosaraju SL. 2010. Bioadhesive Chitosan Nanoparticles: Preparation and Characterization. Carbohydrate Polymers 81(2):243-51.

Duncan R, Izzo L. 2005. Dendrimer Biocompatibility and Toxicity. Advances in Drug Delivery Review 57(15):2215-37.

Duncan TV. 2011. Applications of Nanotechnology in Food Packaging and Food Safety: Barrier Materials, Antimicrobials and Sensors. Journal Colloid Interface Science 363(1):1-24.

Edris E, El-Galeel A. 2010. Soluilization of Some Flavor and Fragrance Oils in Surfactant/Water System. World Applied Science Journal 8(1):86-91.

El-Baroty GS, Abd El-Baky HH, Farag RS, Saleh MA. 2010. Characterization of Antioxidant and Antimicrobial Compounds of Cinnamon and Ginger Essential Oils. African Journal of Biochemistry Research 4(6):167-74.

Escherichia coli O157:H7. FDA Investigations Summary. Silver Spring, MD.; 2013.

Esmaili M, Ghaffari SM, Moosavi-Movahedi Z, Atri MS, Sharifizadeh A, Farhadi M, Yousefi R, Chobert J-M, Haertlé T, Moosavi-Movahedi AA. 2011. Beta Casein-micelle as a Nano Vehicle for Solubility Enhancement of Curcumin; Food Industry Application. Food Science and Technology 44(10):2166-72.

Fang Z, Bhandari B. 2012. Encapsulation Techniques for Food Ingredient Systems. Food Materials Science and Engineering: Wiley-Blackwell. p. 320-48.

Fathi M, Mirlohi M, Varshosaz J, Madani G. 2013. Novel Caffeic Acid Nanocarrier: Production, Characterization, and Release Modeling. Journal of Nanomaterials 2013:9-11.

Fessi H, Puisieux F, Devissaguet JP, Ammoury N, Benita S. 1989. Nanocapsule Formation by Interfacial Polymer Deposition Following Solvent Displacement. International Journal of Pharmaceutics 55(1):R1-R4.

FoodDrinkEurope. 2013. Promoting an EU Industrial Policy for Food and Drink. Brussels.

Ford J, Woolfe J, Florence AT. 1999. Nanospheres of Cyclosporin A: Poor Oral Absorption in Dogs. International Journal of Pharmacy 183(1):3-6.

Forssell P. 2004. Starch-based Microencapsulation in: Starch in Food: Structure, Function and Applications. Boca Raton, Florida: CRC Press.

Galanakis C, Goulas V, Tsakona S, Gekas V. 2011. Predicting the Solubilization Preference of Natural Phenols to Different Solvents. 11th International Congress on Engineering and Food.

Gao W, Vecchio D, Li J. 2014. Hydrogel Containing Nanoparticle-Stabilized Liposomes for Topical Antimicrobial Delivery. American Chemcial Society Nanotechnology 8(3):2900-7.

Gaumet M, Vargas A, Gurny R, Delie F. 2008. Nanoparticles for Drug Delivery: The Need for Precision in Reporting Particle Size Parameters. European Journal of Pharmaceutics and Biopharmaceutics 69(1):1-9.

Ghosh S. 2006. Functional Coatings. Weinheim: Wiley.

Ghosh V, Mukherjee A, Chandrasekaran N. 2013. Ultrasonic Emulsification of Food-Grade Nanoemulsion Formulation and Evaluation of its Bactericidal Activity. Ultrasonics Sonochemistry 20(1):338-44.

Gomes C, Moreira GM, Castell-Perez E. 2011. Poly (DL-lactide-co-glycolide) (PLGA) Nanoparticles with Entrapped T*rans*-Cinnamaldehyde for Antimicrobial Delivery Applications. Journal of Food Science 76(2):16-24.

Gupta VK. 2011. Optimization of Process Variables for the Preparation of Chitosan Alginate Nanoparticles. International journal of pharmacy and pharmaceutical sciences 3(2):78-80.

Gupta VK, Gupta R, Mohan G. 2011. Nanoparticle Formulation Using Counterion Induced Gelification Technique: In-Vitro Chloramphenicol Release. International Journal of Pharmacy and Pharmaceutical Sciences 3:67-70.

Harte F, Venegas R. 2012. A Model for Viscoity Reduction in Polysaccharides Subjected to High-Pressure Homogenization. Journal of Texture Studies 41(1):49-61.

Hatefi A, Amsden B. 2002. Biodegradable Injectable in Situ Forming Drug Delivery Systems. Journal of Controlled Release 80:9-28.

He W, Tan Y, Tian Z, Chen L, Hu F, Wu W. 2011. Food Protein-Stabilized Nanoemulsions as Potential Delivery Systems for Poorly Water-Soluble Drugs: Preparation, in Vitro Characterization, and Pharmacokinetics in Rats. International Journal of nanomedicine 6:521-33.

Hedges Allan R, Shieh Wen J, Sikorski Christopher T. 1995. Use of Cyclodextrins for Encapsulation in the Use and Treatment of Food Products. Encapsulation and Controlled Release of Food Ingredients: American Chemical Society. p. 60-71.

Hettiarachchy N, Ravichandran M. 2012. Potential Use of Edible Nanoscale Coatings for Meat. Food Safety Magazine. p. 4-5.

Hill LE, Gomes C, Taylor TM. 2013a. Characterization of Beta-Cyclodextrin Inclusion Complexes Containing Essential Oils (Trans-Cinnamaldehyde, Eugenol, Cinnamon Bark, and Clove Bud Extracts) for Antimicrobial Delivery Applications. LWT - Food Science and Technology 51(1):86-93.

Hill LE, Taylor MT, Gomes C. 2013b. Antimicrobial Efficacy of Poly (DL-lactide-co-glycolide) (PLGA) Nanoparticles with Entrapped Cinnamon Bark Extract against

Listeria monocytogenes and Salmonella Typhimurium. Journal of Food Science 78(4):626-32.

Hirsjärvi S. 2008. Preparation and Characterization of Poly(Lactic Acid) Nanoparticles for Pharmaceutical Use. [Dissertation]. Finland: University of Helsinki. 42 p.

Holister P, Vas C, Harper T. 2003. Holister and others. 2003. Dendrimers: Technology White Papers. Cientifica. 6. online. 1. Available from Cientifica.

Honary SM, Maryam & Karami, M. 2009. The Effect of Chitosan Molecular Weight on the Properties of Alginate/Chitosan Microparticles Containing Prednisolone. Tropical Journal of Pharmaceutical Research 8(1):53-61.

Horiba. 2012. A Guidebook to Particle Size Analysis. In: Instruments HS, editor. Irvine, CA.

Huaiqiong C, Davidson P, Zhong Q. 2013. Impacts of Sample Preparation Methods on Solubility and Anti-listerial Characteristics of Eesssential Oil Components in Milk. Knoxville, TN: University of Tennessee. 36 p.

Huang Q, Given P, Guian M. 2009. Micro and Nanoencapsulation of Active Food Ingredients. Oxford University Press. 382 p.

Hyldgaard M, Mygind T, Meyer RL. 2012. Essential Oils in Food Preservation: Mode of Action, Synergies, and Interactions with Food Matrix Components. Frontiers in Microbiology 3.

Jawahar N, Meyyanathan S. 2012. Polymeric Nanoparticles for Drug Delivery and Targeting: A Comprehensive Review. International Journal of Health and Allied Science 1(4):217-23.

Jin T, Zhang H. 2008. Biodegradable Polylactic Acid Polymer with Nisin for Use in Antimicrobial Food Packaging. Journal of Food Science 73(3):M127-34.

Jong H, Borm J. 2008. Drug Delivery and Nanoparticles: Applications and hazards. International Journal of Nanomedicine 3(2):133-49.

Joshi S, Patel P, Lin S, Madan P. 2012. Development of Cross-linked Alginate Spheres by Ionotropic Gelation Technique for Controlled Release of Naproxen Orally. Asian Journal of Pharmaceutical Sciences 7(2):134-42.

Kalemba D, Kunicka A. 2003. Antibacterial and Antifungal Properties of Essential Oils. Current medicinal chemistry 10(10):813-29.

Kamimura JA, Santos EH, Hill LE, Gomes CL. 2014. Antimicrobial and Antioxidant Activities of Carvacrol Microencapsulated in Hydroxypropyl-Beta-Cyclodextrin. Food Science and Technology 57(2):701-9.

Khazaeli P, Pardakhty A, Hassanzadeh F. 2008. Formulation of Ibuprofen Beads by Ionotropic Gelation. Iranian Journal of Pharmaceutical Research 7(3):163-70.

Kim B, Kim D, Cho D, Cho S. 2003. Bactericidal Effect of TiO2 Photocatalyst on Selected Food-Borne Pathogenic Bacteria. Chemosphere 52(1):277-81.

Kim J, Marshall M, Wei C. 1995. Antibacterial Activity of Some Essential Oil Components Against Five Foodborne Pathogens. Journal of Agricultural Food Chemistry 43(11):2839-45.

Kirchner G, Bautista D, Benz K, Napolitano GE. 2009. Antimicrobial Micelles for Food Applications. Google Patents.

Kong M, Chen XG, Xing K, Park HJ. 2010. Antimicrobial Properties of Chitosan and Mode of Action: A State of the Art Review. International Journal of Food Microbiology 144(1):51-63.

Koros W, MA Y, Shimidzu T. 1996. Terminology for Membranes and Membrane Processes. Pure and Applied Chemistry 68(7):1479-89.

Koukaras EN, Papadimitriou SA, Bikiaris DN, Froudakis GE. 2012. Insight on the Formation of Chitosan Nanoparticles Through Ionotropic Gelation with Tripolyphosphate. Molecular Pharmaceutics 9(10):2856-62.

Lakkis JM. 2007. Encapsulation and Controlled Release Technologies in Food Systems, 1 ed. Iowa: Blackwell.

Leonard M, De Boisseson MR, Hubert P, Dalencon F, Dellacherie E. 2004. Hydrophobically Modified Alginate Hydrogels as Protein Carriers with Specific Controlled Release Properties. Journal of Controlled Release 98(3):395-405.

Lertsutthiwong P, Rojsitthisak P, Nimmannit U. 2009. Preparation of Turmeric Oil-loaded Chitosan-Alginate Biopolymeric Nanocapsules. Materials Science and Engineering: C 29(3):856-60.

Li P, Dai YN, Zhang JP, Wang AQ, Wei Q. 2008. Chitosan-Alginate Nanoparticles as a Novel Drug Delivery System for Nifedipine. International Journal of Biomedical science : IJBS 4(3):221-8.

Li Y, McClements DJ. 2013. Influence of Non-ionic Surfactant on Electrostatic Complexation of Protein-Coated Oil Droplets and Ionic Biopolymers (Alginate and Chitosan). Food Hydrocolloids 33(2):368-75.

Li P, Dai YN, Zhang JP, Wang AQ, Wei Q. 2008. Chitosan-Alginate Nanoparticles as a Novel Drug Delivery System for Nifedipine. International Journal of Biomedical Science 4(3):221-8.

Lin S, Kost J, Yan F, Spiro R. 2012. Hydrogels from Biopolymer Hybrid for Biomedical, Food, and Functional Food Applications. Polymers 4:997-1011.

Listeria monocytogenes Risk Assessment: I. Introduction. Spring Silver, MD.; 2003 Available from: http://www.fda.gov/Food/FoodScienceResearch/RiskSafetyAssessment/ucm184052.htm.

Liu Y. 2014. Starch-Pectin Matrices for Encapsulation of Ascorbic Acid. [Food Science and Technology Department]. Lincoln, Nebraska: University of Nebraska.

Manish K, Kulkarni G. 2012. Development and Process Optimization of Variables for Preparation of Novel Polymeric Nanoparticles Containing Azelastine Hydrochloride. Journal of Pharmacy Research 5(9).

Martelli M, Barros T, de Moura M, Mattoso L, Assis O. 2013. Effect of Chitosan Nanoparticles and Pectin Content on Mechanical Properties and Water Vapor Permeability of Banana Puree Films. Journal of Food Science 78(1):98-104.

Marthyna PS, Vaz MF, Correia TS, Cerqueira MA. 2014. Quercetin-Loaded Lecithin/Chitosan Nanoparticles for Functional Food Applications. Food and Bioprocess Technology 7(4):1149-59.

McClements D. 2009. Structural Design Principles for Improved Food Performance: Nanolaminated Biopolymer Structures in Foods. Washington DC.

McClements DJ, Rao J. 2011. Food-grade Nanoemulsions: Formulation, Fabrication, Properties, Performance, Biological Fate, and Potential Toxicity. Critical Reviews Food Science and Nutrition 51(4):285-330.

Mead PS, Slutsker L, Dietz V, McCaig LF, Bresee JS, Shapiro C, Griffin PM, Tauxe RV. 1999. Food-related Illness and Death in the United States. Emerging Infectious Diseases 5(5):607-25.

Mohanraj MJ, Chen Y. 2006. Nanoparticles: A Review. Tropical Journal of Pharmaceutical Research 5(1):561-73.

Mozafari RM, Johnson C, Demetzos C. 2008. Nanoliposomes and Their Applications in Food Nanotechnology. Journal of Liposome Research 18:309 - 27.

Mumper RJ, Huffman AS, Puolakkainen PA, Bouchard LS, Gombotz WR. 1994. Calcium-alginate Beads for the Oral Delivery of Transforming Growth Factor-β1 (TGF-β1): Stabilization of TGF-β1 by the addition of Polyacrylic Acid within Acid-Treated Beads. Journal of Controlled Release 30(3):241-51.

Nagarwal RC, Kumar R, Pandit JK. 2012. Chitosan Coated Sodium Alginate-Chitosan Nanoparticles Loaded with 5-FU for Ocular Delivery: in Vitro Characterization and in Vivo Study in Rabbit Eye. European Journal of Pharmaceutical Sciences 47(4):678-85.

Nagavarma B, AYAZ A, VASUDHA LS, SHIVAKUMAR HG. 2012. Different Techniques for Preparation of Polymeric Nanoparticles: A Review. Asian Journal of Pharmaceutical and Clinical Research 5(3):16-23.

Nallamuthu I, Parthasarathi A, Khanum F. 2013. Thymoquinone-loaded PLGA Nanoparticles: Antioxidant and Anti-Microbial Properties. International Current Pharmaceutical Journal 2(12):202-7.

NNI Supplement to the President 2013 Budget. 2012 [Accessed 2013 Feb 2013].

Tangential Flow Filtration Introduction. Pall Corporation; 2013 [Accessed 2014 June 5] Available from: http://www.pall.com/main/biopharmaceuticals/tangential-flow-filtration-introduction-51907.page.

Patel MR, San Martin-Gonzalez MF. 2012. Characterization of Ergocalciferol loaded Solid Lipid Nanoparticles. Journal of Food Science 77(1):N8-13.

Patil J, Kamalpur S, Marapur D, Kadam D. 2010. Ionotropic Gelation and Polyelectrolyte Complexation: The Novel Techniques to Design Hydrogel Particulate Sustained, Modulated Drug Delivery System: A Review. International Journal of Pharmacy and Pharmaceutical Sciences 4(2):27-32.

Patil P, Chavanke D, Wagh M. 2012. A Review on Ionottropic Gelation Method: Novel Approach for Controlled Gastroretentive Gelispheres. International Journal of Pharmacy and Pharmaceutical Sciences 4(4):27-32.

Pei RS, Zhou F, Ji BP, Xu J. 2009. Evaluation of Combined Antibacterial Effects of Eugenol, Cinnamaldehyde, Thymol, and Carvacrol against E. coli with an Improved Method. Journal of Food Science 74(7):M379-83.

Pendleton S, Story R, O'Bryan C, Crandall P, Ricke S, Goodridge L. 2012. A Membrane Filtration Method for Determining Minimum Inhibitory Concentrations of Essential Oils. Agriculture, Food and Analytical Bacteriology 2(2):88-93.

Peniche C, Argüelles-Monal W, Peniche H, Acosta N. 2003. Chitosan: An Attractive Biocompatible Polymer for Microencapsulation. Macromolecular Bioscience 3(10):511-20.

Pinto Reis C, Neufeld RJ, Ribeiro AJ, Veiga F. 2006. Nanoencapsulation I. Methods for Preparation of Drug-loaded Polymeric Nanoparticles. Nanomedicine : Nanotechnology, Biology, and Medicine 2(1):8-21.

Pozzo M, Silva Loreto É, Flores Santurio D, Hartz Alves S, Rossatto L, Castagna de Vargas A, Viegas J, da Costa M. 2012. Antibacterial Activity of Essential Oil of Cinnamon and Trans-Cinnamaldehyde against Staphylococcus spp. Isolated from Clinical Mastitis of Cattle and Goats. Acta Scientiae Veterinariae 40(4):5.

Pray L, Yaktin A. 2009. Nanotechnology in Food Products: Workshop Summary. Washington, DC: The National Academies Press.

Qi L, Xu Z, Jiang X, Hu C, Zou X. 2004. Preparation and Antibacterial Activity of Chitosan Nanoparticles. Carbohydrate Research 339(16):2693-700.

Racovita S, Vasiliu S, Popa M. 2009. Polysachhardies Based On Micro and Nanoparticles Obtained By Ionic Gelation and Their Appltcations as Drug Delivery Systems. Revue Roumaine de Chimie 54(9):709-18.

Rajaonarivony M, Vauthier C, Couarraze G, Puisieux F, Couvreur P. 1993. Development of a New Drug Carrier Made from Alginate. Journal of Pharmaceutical Sciences 82(9):912-7.

Ramaswamy V, Cresence VM, Rejitha JS, Lekshmi MU, Dharsana KS, Prasad SP, Vijila HM. 2007. Listeria-review of Epidemiology and Pathogenesis. Journal of Microbiology, Immunology, and Infection 40(1):4-13.

Rao PV, Gan SH. 2014. Cinnamon: A Multifaceted Medicinal Plant. Evidence-Based Complementary and Alternative Medicine 2014:12.

Risch SJ, Reineccius GA. 1995. Encapsulation and Controlled Release of Food Ingredients. American Chemical Society.

Ritger PL, Peppas NA. 1987. Transport of Penetrants in the Macromolecular Structure of Coals: 4. Models for Analysis of Dynamic Penetrant Transport. Fuel 66(6):815-26.

Rodriguez S, Allemann E, Fessi H, Doelker E. 2004. Physicochemical Parameters Associated with Nanoparticle Formation in the Salting-out, Emulsification-Diffusion, and Nanoprecipitation Methods. Pharmaceutical Research 21(8):1428-39.

Ruengvisesh S, Loquercio A, Castell-Perez E, Taylor M. 2014. Inhibition of Bacterial Foodborne Pathogens using Plant-Derived Antimicrobial Essential Oils in Surfactant Micelles. In: of J, editor. Journal of Microencapsulation. College Station, TX: Texas A&M University. p. 23.

Ruo L. 2012. Chitosan Particles for the Controlled Release of Proteins. [Biomedical Engineering Doctoral Dissertation]: Polytechnic University of Turin.

Sadeghi AM, Dorkoosh FA, Avadi MR, Saadat P, Rafiee-Tehrani M, Junginger HE. 2008. Preparation, Characterization and Antibacterial Activities of Chitosan, N-Trimethyl Chitosan (TMC) and N-Diethylmethyl Chitosan (DEMC) Nanoparticles Loaded with Insulin using both the Ionotropic Gelation and Polyelectrolyte Complexation Methods. International Journal of Pharmacy 355(1-2):299-306.

Safari J, Zarnegar Z. 2013. Advanced Drug Systems: Nanotechnology of health design A review. Journal of Saudi Chemical Society 18(2):85-99.

Sahoo SK, Labhasetwar V. 2003. Drug Discovery Today. 24:1113-20.

Santipanichwong R, Suphantharika M, Weiss J, McClements DJ. 2008. Core-shell Biopolymer Nanoparticles Produced by Electrostatic Deposition of Beet Pectin onto Heat-Denatured Beta-lactoglobulin Aggregates. Journal of Food Science 73(6):N23-30.

Sarmento B, Ferreira D, Veiga F, Ribeiro A. 2006. Characterization of Insulin-loaded Alginate Nanoparticles Produced by Ionotropic Pre-Gelation through DSC and FTIR Studies. Carbohydrate Polymers 66(1):1-7.

Sarmento B, Ribeiro A, Veiga F, Sampaio P, Neufeld R, Ferreira D. 2007. Alginate/chitosan Nanoparticles are Effective for Oral Insulin Delivery. Pharmaceutical Research 24(12):2198-206.

Sezer AD, Akbuga J. 1999. Release Characteristics of Chitosan Treated Alginate Beads: I. Sustained Release of a Macromolecular Drug from Chitosan Treated Alginate Beads. Journal of Microencapsulation 16(2):195-203.

Shan B, Cai YZ, Brooks JD, Corke H. 2007. Antibacterial Properties and Major Bioactive Components of Cinnamon Stick (Cinnamomum Burmannii): Activity Against Foodborne Pathogenic Bacteria. Journal of Agricultural Food Chemistry 55(14):5484-90.

Sharma OP, Bhat TK. 2009. DPPH Antioxidant Assay Revisited. Food Chemistry 113(4):1202-5.

Shicheng Y, Clive W. 2005. Drug Release from Microparticulate Systems. Microencapsulation: Informa Healthcare. p. 183-211.

Shimada K, Fujikawa K, Yahara K, Nakamura T. 1992. Antioxidative Properties of Xanthan on the Autoxidation of Soybean Oil in Cyclodextrin Emulsion. Journal of Agricultural and Food Chemistry 40(6):945-8.

Siepmann J, Peppas N. 2001. Modeling of Drug Release from Delivery Systems Based on Hydroxypropyl Methylcellulose (HPMC). Advanced drug delivery reviews 48(2):139-57.

Silva S, Cocenza DS, Grillo R, de Melo NF, Tonello PS, de Oliveira LC, Cassimiro DL, Rosa AH, Fraceto LF. 2011. Paraquat-loaded Alginate/chitosan Nanoparticles: Preparation, Characterization and Soil Sorption Studies. Journal of Hazardous Materials 190(1-3):366-74.

Silva P, Daroit DJ, Brandelli A. 2010. Food applications of liposome-encapsulated antimicrobial peptides. Trends in Food Science & Technology 21(6):284-92.

Singh G, Sumitra M, deLampasona MP, A.N. C. 2007. A Comparison of Chemical, Antioxidant and Antimicrobial Studies of Cinnamon Leaf and Bark Volatile Oils, Oleoresins and their Constituents. Food and Chemical Toxicology 45:1650-61.

Sinjan D, Robinson D. 2003. Polymer Relationships During Preparation of Chitosan–Alginate and Poly-l-lysine–alginate Nanospheres. Journal of Controlled Release 89(1):101-12.

Sonicator Ultrasonic Liquid Processors. Newtown, CT.: Hudson Fusion LLC; 2014.

Standard Sample Pans and Crimper for Pyris 6 DSC. Perkin Elmer; 2014 Available from: http://www.perkinelmer.com/catalog/family/id/standard.

Takka S, Ocak ÖH, Acartürk F. 1998. Formulation and Investigation of Nicardipine HCl–Alginate Gel Beads with Factorial Design-Based Studies. European Journal of Pharmaceutical Sciences 6(3):241-6.

Taylor T, Davidson P, Bruce B, Weiss J. 2005. Liposomal Nanocapsules in Food Science and Agriculture. Critical Reviews in Food Science and Nutrition 45(7-8):587-605.

Teixeira BN, Ozdemir N, Hill LE, Gomes CL. 2013. Synthesis and Characterization of Nano-Encapsulated Black Pepper Oleoresin using Hydroxypropyl Beta-Cyclodextrin for Antioxidant and Antimicrobial Applications. Journal of Food Science 78(12):N1913-N20.

Thies C. 1996. Microencapsulation: Methods and Industrial Applications New York: Marel Dekker.

Thwala LN. 2012. Preparation and Characterization of Alginate-chitosan Nanoparticles as a Drug Delivery System for Lipophilic Compounds: University of Johannesburg.

Tiwari R, Takhistov P. 2012. Nanotechnology Research Methods for Food and Bioproducts. Padua: Jon Wiley and Sons.

Trans-cinnamaldehyde. Vernon Hills, IL 2014 Available from: http://www.coleparmer.com/Product/trans_Cinnamaldehyde_99_50g/EW-88100-84.

Üner M, Yener G. 2007. Importance of Solid Lipid Nanoparticles (SLN) in Various Administration Routes and Future Perspectives. 2(3):289-300.

USDA Takes New Steps to Fight E. Coli, Protect the Food Supply. Designation Extends Zero Tolerance Policy for E. coli O157:H7 to Six Additional E. coli Serogroups. Washington, DC.; 2011 Available from: http://www.usda.gov/wps/portal/usda/usdahome?contentidonly=true&contentid=2011/09/0400.xml.

Wang W, Liu X, Xie Y, Zhang Ha, Yu W, Xiong Y, Xie W, Ma X. 2006. Microencapsulation Using Natural Polysaccharides for Drug Delivery and Cell Implantation. Journal of Materials Chemistry 16(32):3252-67.

Wiegand I, Hilpert K, Hancock RE. 2008. Agar and Broth Dilution Methods to Determine the Minimal Inhibitory Concentration (MIC) of Antimicrobial Substances. Nature protocols 3(2):163-75.

Wise D. 2000. Handbook of Pharmaceutical Controlled Release Technology. Boca Raton, FL: CRC Press.

Woranuch S, Yoksan R. 2013. Eugenol-loaded Chitosan Nanoparticles: II. Application in Bio-based Plastics for Active Packaging. Carbohydrate Polymers 96(2):586-92.

Xing J, Deng L, Dong A. 2010. Chitosan/alginate Nanoparticles Stabilized by Poloxamer for the Controlled Release of 5-Fluorouracil. Journal of Applied Polymer Science 117(4):2354-9.

Xu W, Jin W, Zhang C, Li Z, Lin L, Huang Q, Ye S, Li B. 2014. Curcumin Loaded and Protective System Based on Complex of κ-Carrageenan and Lysozyme. Food Research International 59(0):61-6.

Yen TB, Chang ST. 2008. Synergistic Effects of Cinnamaldehyde in Combination with Eugenol Against Wood Decay Fungi. Bioresource Technology 99(1):232-6.

Yu H, Li J, Shi K, Huang Q. 2011. Structure of Modified Epsilon-Polylysine Micelles and their Application in Improving Cellular Antioxidant Activity of Curcuminoids. Food & function 2(7):373-80.

Zhang L. 2013. Transparent Dispersions of Milk Fat-Based Solid Lipid Nanoparticles for Delivery of beta-Carotene. [Masters]. Knoxville: University of Tennessee.

Zhang Y, Yang Y, Tang K, Hu X, Zou G. 2008. Physicochemical Characterization and Antioxidant Activity of Quercetin-loaded Chitosan Nanoparticles. Journal of Applied Polymer Science 107(2):891-7.

Zohri M, Alavidjeh M, Haririan I, Ardestani M, Ebrahimi S, Sani H, Sadjadi S. 2010. A Comparative Study Between the Antibacterial Effect of Nisin and Nisin-Loaded Chitosan/Alginate Nanoparticles on the Growth of Staphylococcus Aureus in Raw and Pasteurized Milk Samples. Probiotics & Antimicrobial Protection 2(4):258-66.

Zohri M, Nomani A, Gazori T, Haririan I, Mirdamadi SS, Sadjadi SK, Ehsani MR. 2011. Characterization of Chitosan/Alginate Self-Assembled Nanoparticles as a Protein Carrier. Journal of Dispersion Science and Technology 32(4):576-82.

Zuidam N, Nedović V. 2009. Encapsulation Technologies for Active Food Ingredients and Food Processing. New York, NY: Springer.

APPENDIX 1

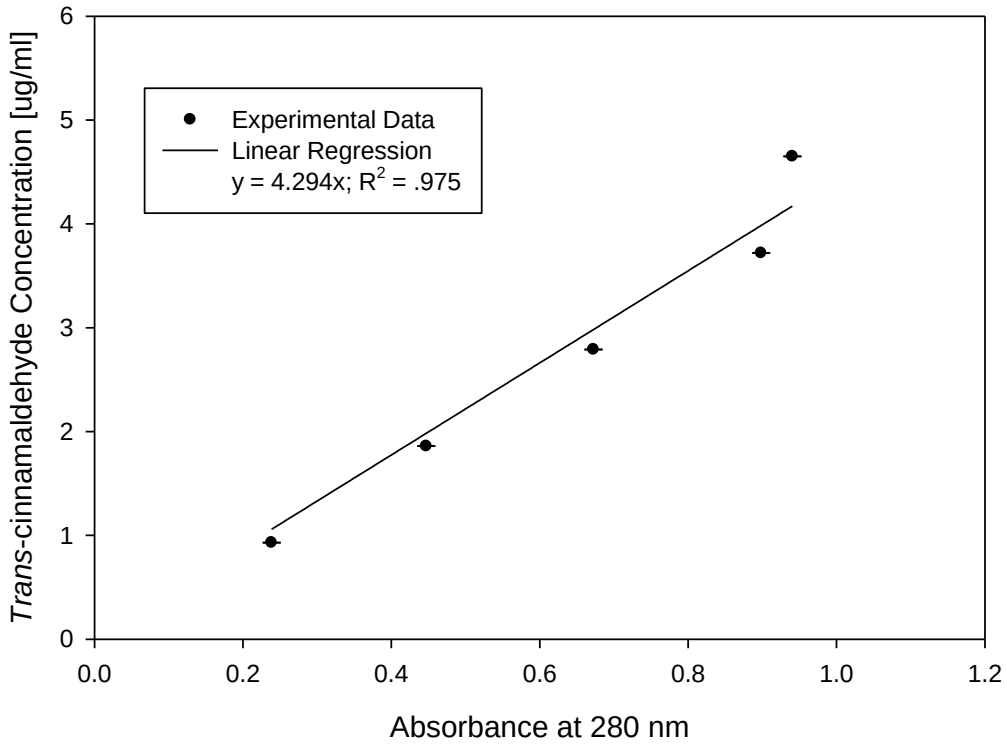

Figure 1-A. Standard calibration curve of *trans*-cinnamaldehyde for determination of encapsulation efficiency in acetonitrile. TC (0.93-4.65 µg/ml) was dissolved in acetonitrile and measured spectrophotometrically at 280 nm in triplicate to obtain absorbance (Genesys 10S UV-Vis, Thermo Scientific, Madison, WI). Regression followed equation $y = 4.294x$ ($R^2 = .975$). Samples were further diluted with acetonitrile for proper spectrophotometric readings when necessary.

APPENDIX 2

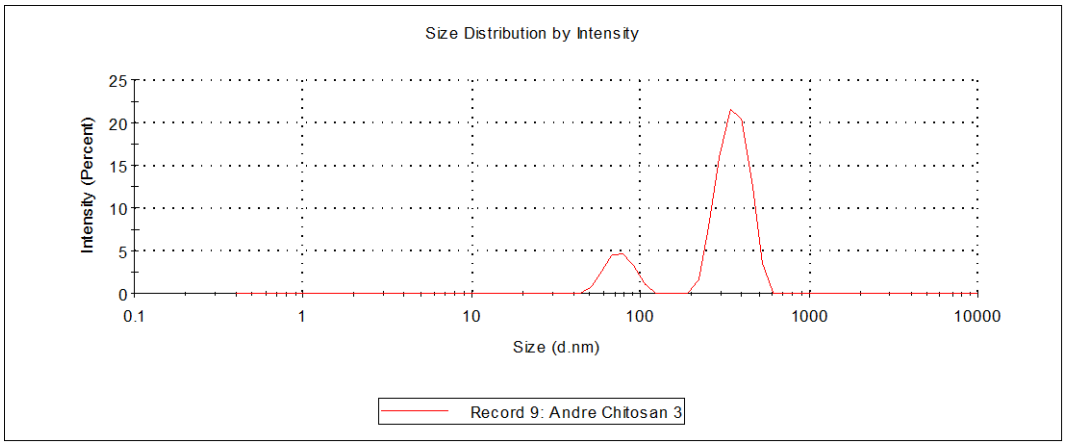

Figure 2-A. Size distribution curve for solubilized chitosan (.05% w/v). Measurements were obtained for chitosan by dynamic light scattering (DLS) in a Malvern Nanoseries ZetaSizer (Nano–ZS90, 633 nm He-Ne 200; scattering angle of 90°; refractive index of 1.590; 25 °C; 100 iterations was performed in triplicate). 2 ml of .05% (w/v) solubilized chitosan was transferred to cuvette (1 cm path length; disposable polystyrene cuvette) for analysis.

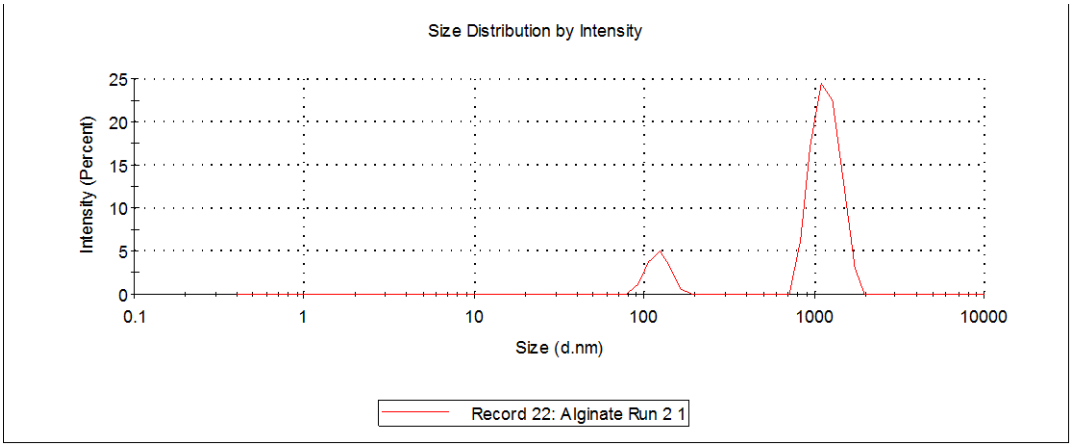

Figure 2-B. Size distribution curve for alginate (.06% w/v). Measurements were obtained for chitosan by dynamic light scattering (DLS) in a Malvern Nanoseries ZetaSizer (Nano–ZS90, 633 nm He-Ne 200; scattering angle of 90°; refractive index of 1.590; 25 °C; 100 iterations was performed in triplicate). 2 ml of .06% (w/v) solubilized alginate was transferred to cuvette (1 cm path length; disposable polystyrene cuvette) for analysis.

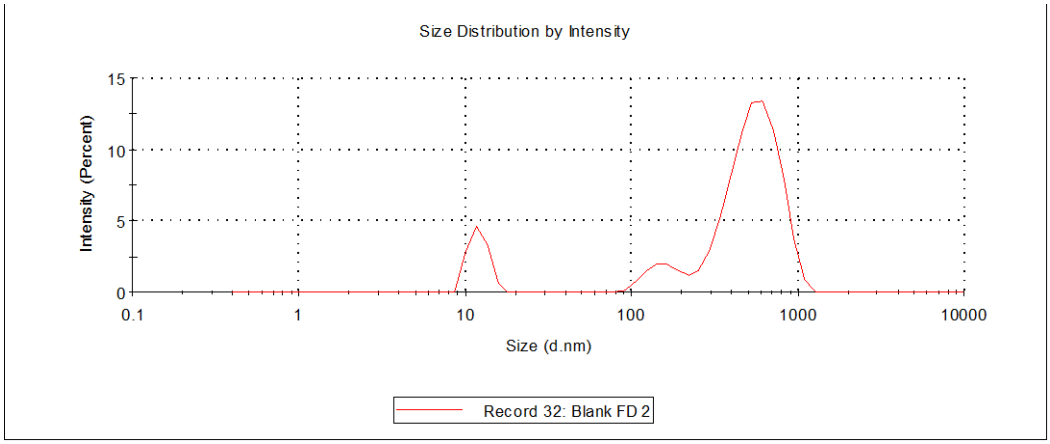

Figure 2-C. Example of bimodal size distribution curve for optimized control nanoparticles. Measurements were obtained for unloaded (control) chitosan-alginate nanoparticles (ULCA-NP) by dynamic light scattering (DLS) in a Malvern Nanoseries ZetaSizer (Nano–ZS90, 633 nm He-Ne 200; scattering angle of 90°; refractive index of 1.590; 25 °C; 100 iterations was performed in triplicate). 200 µg of resuspended lyophilized ULCA-NP in 2 ml of 0.2 µm transferred to cuvette (1 cm path length; disposable polystyrene cuvette) for analysis.

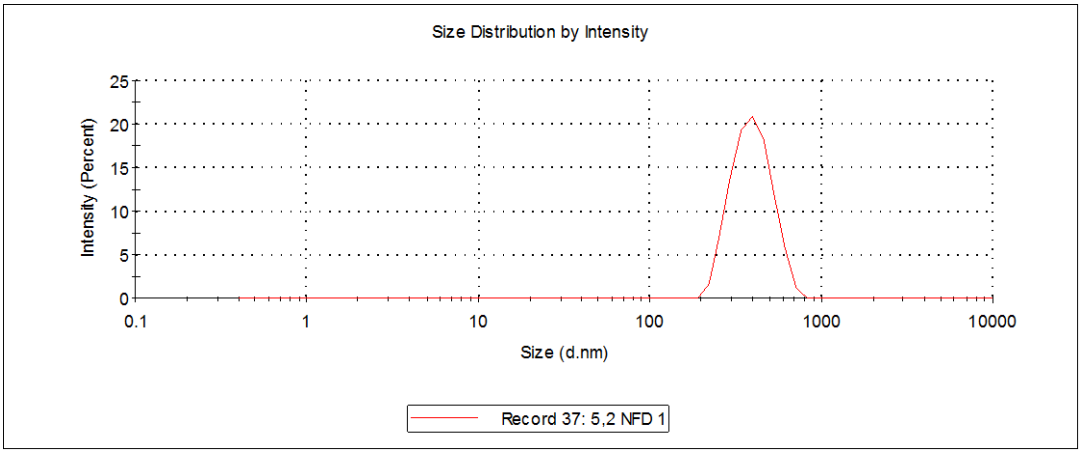

Figure 2-D. Size distribution curve for optimized control nanoparticles. Measurements were obtained for unloaded (control) chitosan-alginate nanoparticles (ULCA-NP) by dynamic light scattering (DLS) in a Malvern Nanoseries ZetaSizer (Nano–ZS90, 633 nm He-Ne 200; scattering angle of 90°; refractive index of 1.590; 25 °C; 100 iterations was performed in triplicate). 200 µg of resuspended lyophilized ULCA-NP in 2 ml of 0.2 µm transferred to cuvette (1 cm path length; disposable polystyrene cuvette) for analysis.

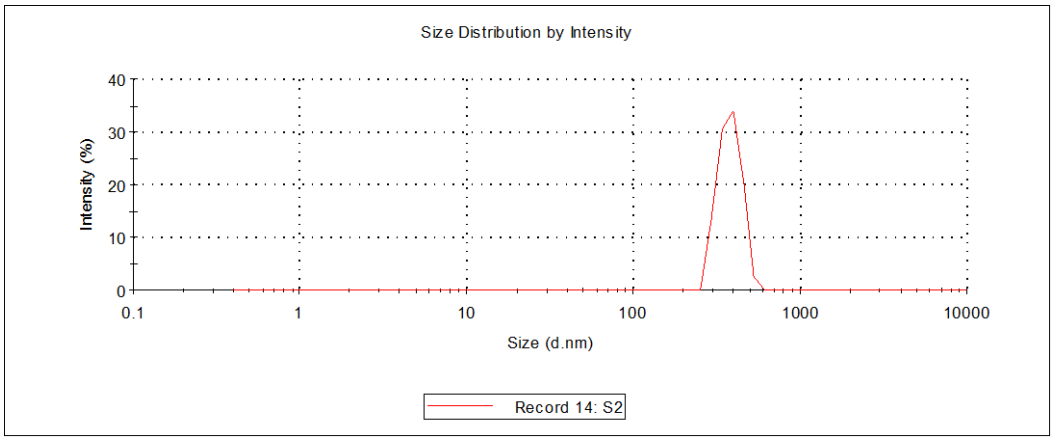

Figure 2-E. Size distribution curve for optimized *trans*-cinnamaldehyde loaded nanoparticles. Measurements were obtained for loaded chitosan-alginate nanoparticles (LCA-NP) by dynamic light scattering (DLS) in a Malvern Nanoseries ZetaSizer (Nano–ZS90, 633 nm He-Ne 200; scattering angle of 90°; refractive index of 1.590; 25 °C; 100 iterations was performed in triplicate). 200 µg of resuspended lyophilized LCA-NP in 2 ml of 0.2 µm transferred to cuvette (1 cm path length; disposable polystyrene cuvette) for analysis.

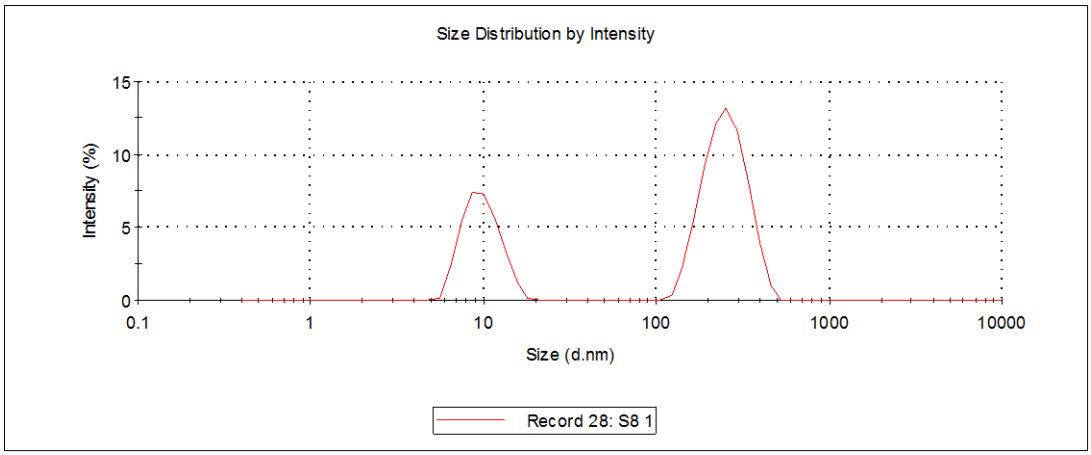

Figure 2-F. Size distribution curve for *trans*-cinnamaldehyde loaded nanoparticles showing bimodal distribution. Measurements were obtained for loaded chitosan-alginate nanoparticles (LCA-NP) by dynamic light scattering (DLS) in a Malvern Nanoseries ZetaSizer (Nano–ZS90, 633 nm He-Ne 200; scattering angle of 90°; refractive index of 1.590; 25 °C; 100 iterations was performed in triplicate). 200 µg of resuspended lyophilized LCA-NP in 2 ml of 0.2 µm transferred to cuvette (1 cm path length; disposable polystyrene cuvette) for analysis.

APPENDIX 3

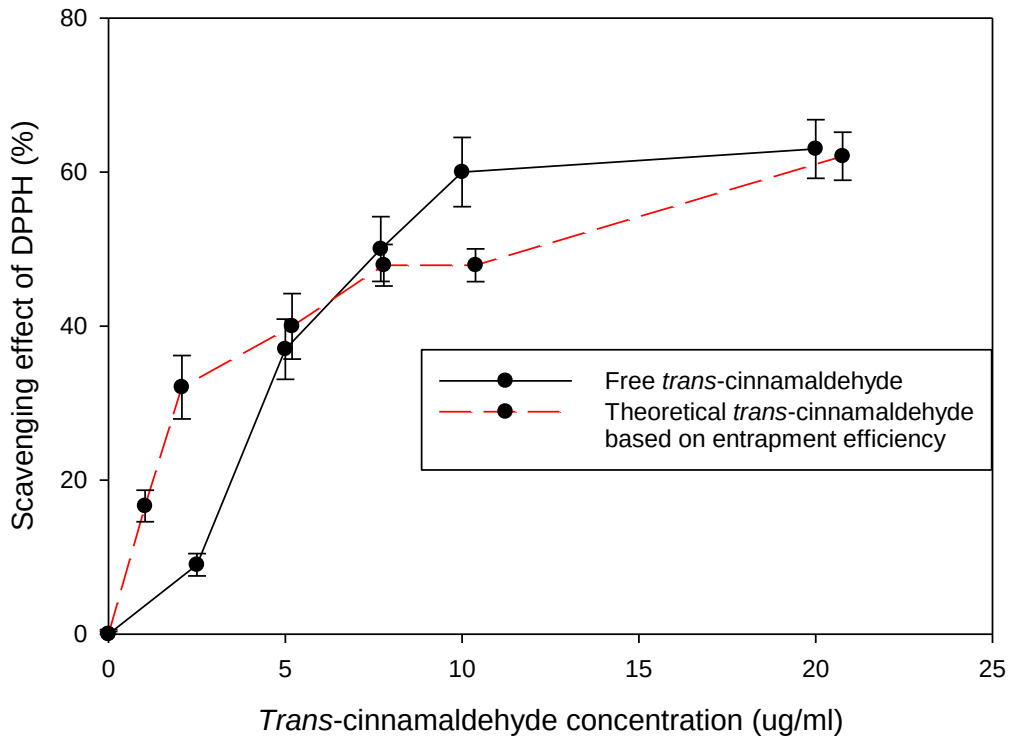

Figure 3-A. Scavenging effect of free *trans*-cinnamaldehyde versus entrapped *trans*-cinnamaldehyde (theoretical values based on maximum encapsulation efficiency). 1 ml of 100 µM DPPH solution in methanol was added to working concentrations of free *TC* (0-20 µg/ml). Samples were agitated and incubated (35°C) for 30 minutes and resulting absorbance was read at 517 nm against a blank (Genesys 10S UV-Vis, Thermo Scientific, Madison, WI).

APPENDIX 4

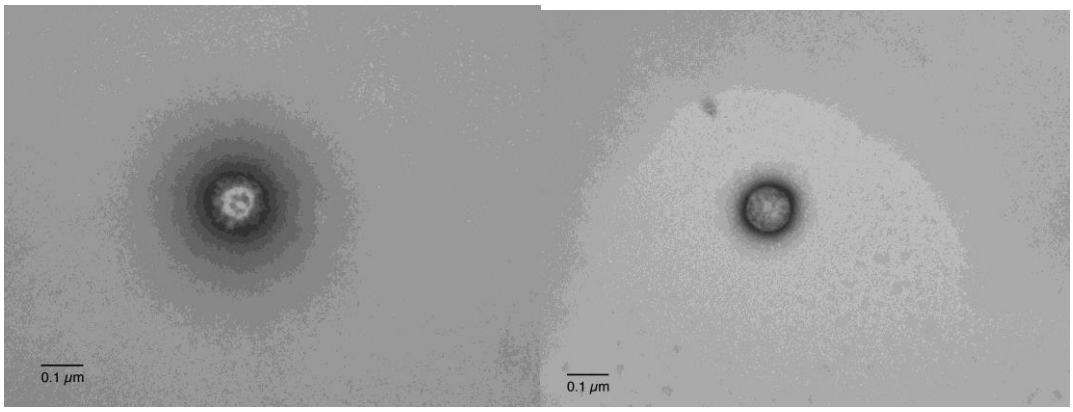

Figure 4-A: TEM images of control nanoparticles at 71,000 magnification. Surface morphology of particles was visualized using a FEI Morgagni Transmission Electron Microscope (FEI Company, Hillsboro, OR) at the School of Veterinary Medicine and Biomedical Sciences at Texas A&M University (College Station, TX) using a negative staining technique (300 mesh Cu/Ni grid filmed with carbon; 0.2% uranyl acetate).

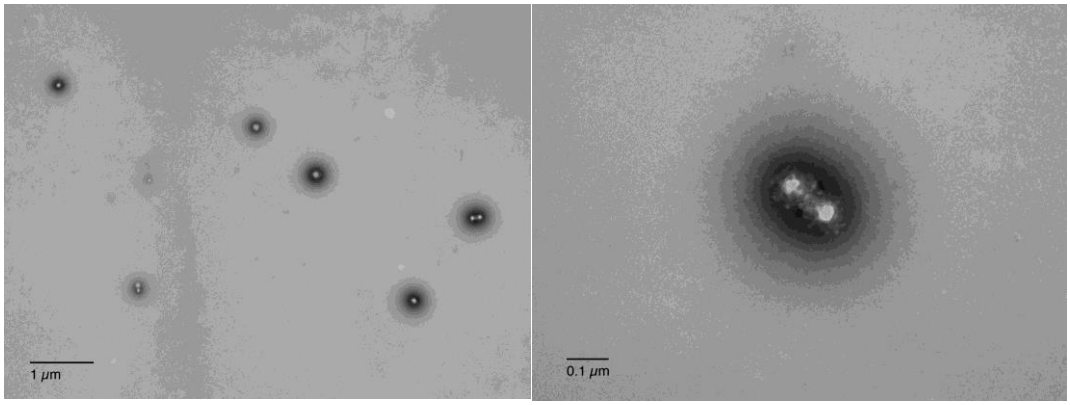

Figure 4-B: TEM images of control nanoparticles at 11,000 (left) and 71,000 (right) times magnification. Surface morphology of particles was visualized using a FEI Morgagni Transmission Electron Microscope (FEI Company, Hillsboro, OR) at the School of Veterinary Medicine and Biomedical Sciences at Texas A&M University (College Station, TX) using a negative staining technique (300 mesh Cu/Ni grid filmed with carbon; 0.2% uranyl acetate).

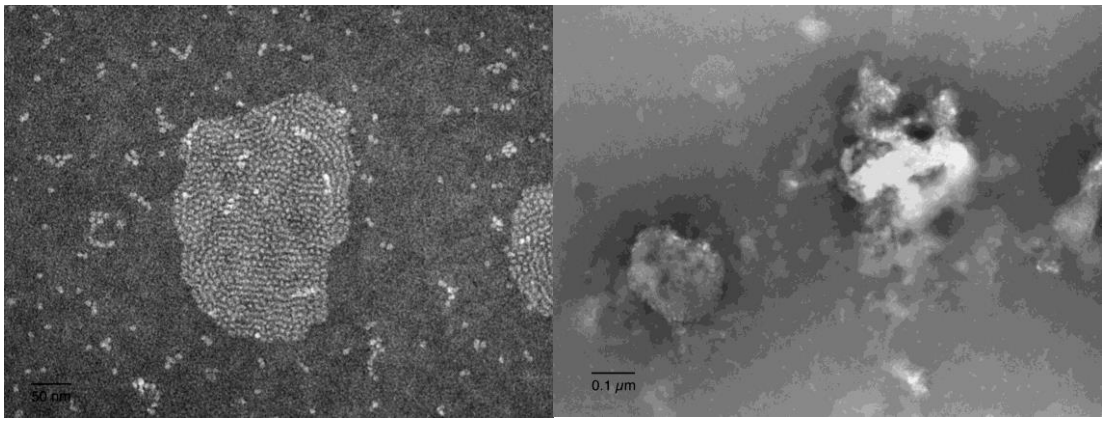

Figure 4-C: TEM images of loaded nanoparticles at 140,000 (left) and 71,000 (right) times magnification. Surface morphology of particles was visualized using a FEI Morgagni Transmission Electron Microscope (FEI Company, Hillsboro, OR) at the School of Veterinary Medicine and Biomedical Sciences at Texas A&M University (College Station, TX) using a negative staining technique (300 mesh Cu/Ni grid filmed with carbon; 0.2% uranyl acetate).

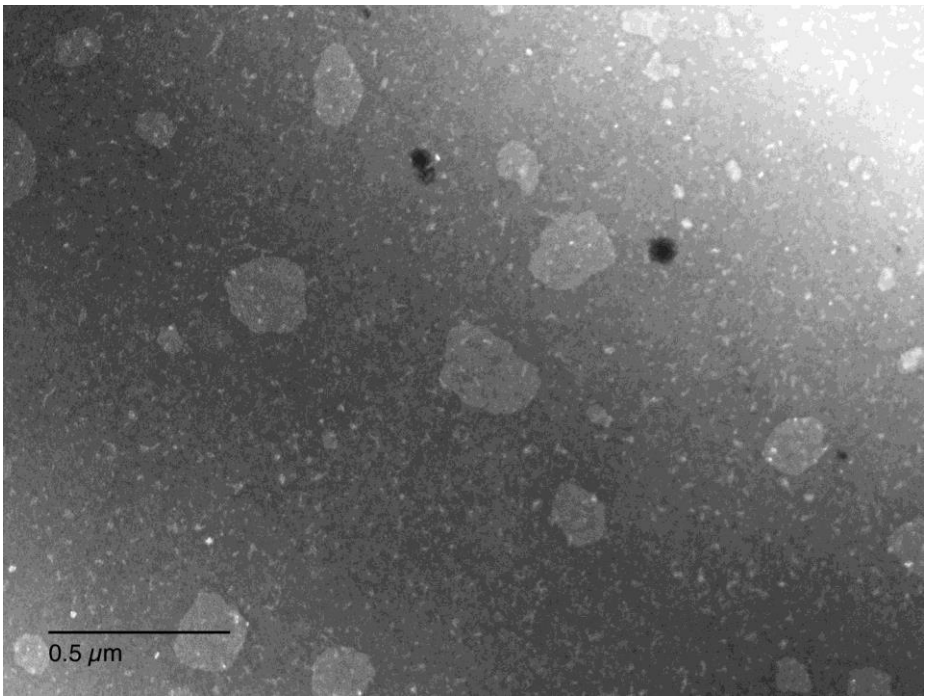

Figure 4-C: TEM images of loaded nanoparticles at 36,000 times magnification. Surface morphology of particles was visualized using a FEI Morgagni Transmission Electron Microscope (FEI Company, Hillsboro, OR) at the School of Veterinary Medicine and Biomedical Sciences at Texas A&M University (College Station, TX) using a negative staining technique (300 mesh Cu/Ni grid filmed with carbon; 0.2% uranyl acetate).

APPENDIX 5

Figure 5-A: Picture of lyophilized chitosan alginate nanoparticles. Frozen retentate was placed into a freeze dryer (Labconco Freeze Dry-5, Kansas City, MO) at -50°C under 5-7 mtorr (9.67×10^{-5} psi) for 48 -72 h to sublimate all moisture from nanoparticles.

Figure 5-B: Picture of lyophilized chitosan alginate nanoparticles. Lyophilized samples were stored in an air tight container in a freezer (-20°C) (Frigidaire FRT21) until further use.